NOBLE GAS AND RADIOCARBON CONSTRAINTS ON THE RESIDENCE TIMES OF GROUNDWATER IN AND AROUND THE CITY OF CAPE TOWN

Zita Harilall

Submitted in full fulfilment for the degree of

Master of Science

Department of Earth Science

Stellenbosch University

Supervisor: Prof Jodie Miller

March 2020

DECLARATION

I declare that ***Noble Gas and Radiocarbon Constraints on the Residence Times of Groundwater in and around the City of Cape Town*** is my own work, that it has not been submitted for any degree or examination at any other university, and that all the sources I have used or quoted have been indicated and acknowledged by complete references.

_____

Full Name: Zita Michelé Harilall Date: March 2020

ABSTRACT

The TMG Aquifer is one of the largest aquifer systems in the country and is currently targeted as a potential source of potable water for the City of Cape Town (CoCT) in times of water stress. This study has aimed to provide proper constraints on turnover time of groundwater in the aquifer system before large-scale abstraction takes place, in order to evaluate the sustainability of the resource. This study has used the $^{3}H/^{3}He$ system to date modern water (<100 years) and ^{14}C to date older groundwater (>500 years). Groundwater residence times were determined for six aquifers in the Western Cape, namely the alluvial, Witteberg, Bokkeveld, TMG, Cape Granite Suite (CGS) and Malmesbury aquifers. Noble gas and radiocarbon dating of the TMG Aquifer range from 0.3 – 44.6 and <70 – 1 626 years, respectively. Residence times calculated for the alluvial aquifer are also relatively young, ranging from 0.0 – 1 783 years. Good correlation between $^{3}H/^{3}He$ and ^{14}C ages indicate relatively short residence times for the alluvial and TMG aquifers whereas groundwater from the Witteberg (6 699 years), Bokkeveld (58.5 – 6 038 years), CGS (3.7 – 8 648 years) and Malmesbury (45.5 – 11 146 years) aquifers indicate mixing of older water bodies with modern recharge resulting in distinctly different ages derived from the two dating systems. Noble gas recharge temperatures (9.4 – 28.6°C), ^{3}H and ^{14}C activities suggest that groundwater in the region is primarily recharged at high elevations, but also that rainfall events further down the flow path at lower elevations, make substantial contributions to groundwater recharge. Evaluation of isotopic tracers and basic chemistry have led to the identification of potential proxies for residence time, namely pH, HCO_3^- concentrations and Ca/Mg ratios. These components can be used to make assumptions on groundwater residence times without the costly process of analysis. Residence times indicate short turnover times for groundwater in the TMG Aquifer (typically <130 years) which suggest that the aquifer would be susceptible to climate change. Projected reductions in precipitation and regular occurrences of droughts would likely diminish groundwater supplies in the aquifer system. If large-scale abstraction does commence, this needs to be factored into abstraction regimes as unsustainable abstraction practices could lead to groundwater depletion.

Keywords: *groundwater residence times, TMG Aquifer, tritium, radiocarbon, recharge, mixing*

ACKNOWLEDGEMENTS

Firstly, I would like to express my gratitude to my supervisor, Prof Jodie Miller. Without her guidance, assistance and patience, this dissertation would not be possible. Thank you to Dr László Palcsu and Mihaly Molnár of the Isotope Climatology and Environmental Research Centre (ICER) of the Institute for Nuclear Research for analysing all my samples, willingly receiving me for two laboratory visits and assisting with interpretation of the data.

I would like to extend my heartfelt gratitude to GEOSS South Africa (Pty) Ltd., particularly Julian Conrad, Dale Barrow, Michael Holloway, Jandré de Beer and Hendré Henn. GEOSS assisted with locating sample sites and sample collection. Additionally, I would like to thank Jan Myburgh of the AGES Group (Pty) Ltd. who allowed me to make use of their resources in order to find sampling locations. I am grateful to the farmers and home owners who so graciously allowed me to sample. I would also like to thank the South African Earth Observation Network (SAEON) for making climate data available for this study.

I would like to thank the National Research Fund (NRF), the Water Research Commission (WRC) and the Iphakade Earth Science Stewardship for providing funding without which I could not complete my Master's degree.

I would like to thank my colleagues, Jani van Gend and Jared van Rooyen. All the assistance and insight in both field work and data analysis over the past two years is highly appreciated. Thank you to Dr Andrew Watson for making himself available to provide valuable input, especially during the last stretch. Lastly, I would like to thank Yaa Agyare-Dwomoh, my friend and partner who has shared this journey with me.

I would also like to express my personal gratitude to my family for their never-ending support for the entire duration of the Master's degree.

CONTENTS

LIST OF FIGURES

LIST OF TABLES

LIST OF TERMS AND ABBREVIATIONS

A	*entrapped air (cm^3/kg)*
AWS	*automated weather station*
BP	*Before Present (Present = 1950)*
Bq/L	*Becquerel per litre*
CFB	*Cape Fold Belt*
CGS	*Cape Granite Suite*
CoCT	*City of Cape Town*
DIC	*dissolved inorganic carbon*
DOC	*dissolved organic carbon*
FRA	*fractured rock aquifer*
GSOD	*global summary of the day*
GWD	*groundwater depletion*
IC	*inorganic carbon*
mamsl	*metres above mean sea level*
n^0	*neutron*
NGT	*noble gas temperature*
p^+	*proton*
R. Kasteel	*Riebeeck Kasteel*
pMC	*percent Modern Carbon*
SAEON	*South African Earth Observation Network*
TC	*total carbon*
TMG	*Table Mountain Group*
TU	*Tritium Unit ($^3H/H \sim 10^{-18}$)*
σ	*standard deviation*
$\bar{x}$	*mean*

1 PROJECT OVERVIEW

Due to population growth and increased urbanization, the population of the City of Cape Town (CoCT) has grown rapidly over the past two decades to over 4 million residents (Battersby, 2016; Western Cape Government, 2017). As the urban population continues to steadily rise, increasing pressure is placed on the City to meet the demand for potable water as it is rapidly reaching capacity of its current water resources (Joubert et al., 2003). The CoCT relies almost exclusively on surface water to supply clean water to its residents as 95% of freshwater is sourced from a regional, integrated surface water system (City of Cape Town, 2019). The surface water is stored in a number of dams which are vulnerable to evaporative and seepage losses as well as changes in precipitation, effectively reducing water supply (Graf, 1999).

Historical rainfall data indicates that there has been a decrease in the mean annual precipitation (MAP) for Cape Town accompanied by an increase in rainfall intensity (Van Wageningen and Du Plessis, 2007; Mahlalela et al., 2019). Although climate varies naturally through time, the industrial activities of the last two centuries are having an unprecedented effect on climatic conditions and will continue to do so into the future (Benhin, 2006). It is suggested that climate change will cause increased variability in precipitation patterns as well as an increased frequency in extreme conditions (such as droughts and floods) and an increase in temperature across the country (Hewitson and Crane, 2006; Wolski et al., 2018). Studies attempting to predict the change in rainfall patterns for the intermediate future (2040 – 2100) confirmed that the western region of South Africa and its adjacent interior will receive less rainfall and have higher variability (Lumsden et al., 2009; Mahlalela et al., 2019). Predictions of decreased precipitation coupled with the looming threat of increased occurrence and severity of droughts, has led to the targeting of groundwater resources as a way to supplement the municipal supply (Joubert et al., 2003).

Groundwater – generalised as the water in pore spaces of subsurface soils and rocks or fractures in rocks beneath the Earth's surface (Shanahan, 2009) – currently makes up 16% of water usage in South Africa (DWAF, 2006). This resource is often less susceptible to

contamination and has been considered more resilient to drought (Kundzewicz and Döll, 2009). As a result, it is becoming an increasingly valuable resource for water users in the domestic and agricultural sectors of South Africa (City of Cape Town, 2019). Despite a number of aquifers systems present in the Western Cape, these aquifers often have variable chemistry and yields (Rosewarne, 2002). Groundwater in the Table Mountain Group (TMG) Aquifer, however, is considered to be some of the best quality groundwater in the country with respect to electrical conductivity (EC) and total dissolved solids (TDS) (Rosewarne, 2002). The aquifer has a large areal extent, of which approximately 37 000 km^2 outcrops at the surface in close proximity to many of the City's dams (Xu et al., 2009). As a result, the TMG Aquifer system has been targeted as an ideal source for supplementation due to its high quality and the relative ease with which it could be incorporated into dam infrastructure.

The TMG fractured rock aquifer (FRA) system is recognised as the second largest aquifer in South Africa in terms of yield and spatial extent (Weaver et al., 1999). The aquifer has low primary porosity and permeability of the aquifer (Rosewarne and Weaver, 2002), but recharge, flow and storage of groundwater are controlled by a network of fractures in the rock unit that has formed through extensive folding and faulting (De Beer, 2002a). As these highly fractured units are predominantly exposed in mountainous high-rainfall regions (Rosewarne, 2002), recharge is estimated to be as high as 15% of mean annual precipitation (Weaver et al., 1999; Watson et al., 2018). The volume of water stored in the aquifer has been estimated to be on the order of 9 x 10^8 m^3 (Xu et al., 2009). High yielding thermal springs prove there is deep-seated flow and boreholes drilled to depths of 200 m provide evidence of a shallow-seated aquifer (Weaver et al., 1999). Further isotope and chemistry work by Weaver et al. (1999) provide evidence of a medium-seated aquifer, introducing the possibility of large-scale abstraction. Despite current abstraction being only approximately 5% of potential yield (Xu et al., 2009), localised reductions of water levels in areas of the TMG Aquifer have led to concerns regarding the overestimation of its potential yield (Jolly and Kotze, 2002).

Hydrological modelling and satellite images have revealed distressing rates of groundwater depletion (GWD) across the world (Rodell et al., 2009; Famiglietti, 2014; Wada et al., 2014). GWD compromises water resources for future generations and is associated with numerous issues. Decreased base flow may cause irreversible ecological effects through the drying up of rivers and wetlands (Doell et al., 2014). The subsequent decrease in groundwater storage may result in land subsidence (Konikow and Kendy, 2005), as well as seawater intrusion which

effectively compromises the quality of remaining groundwater supplies (Aris et al., 2007). A decline in groundwater supplies may also have several indirect effects which include putting crop and other food production at risk (Doell et al., 2014). When GWD occurs, groundwater is no longer considered a renewable resource, but rather a non-renewable one (Doell at al., 2014). The majority of cases of GWD occur in arid to semi-arid regions where runoff and groundwater recharge are generally low and large amounts of water are used for crop production (Margat et al., 2006). Although abstraction from the TMG Aquifer is still relatively low, the above issues serve as a forewarning regarding the consequences of over abstraction to the CoCT which is still developing the full potential of its groundwater resources (DWAS, 2006).

Evaluation of the feasibility of large-scale abstraction from the TMG Aquifer is still underway and monitoring of exploratory boreholes has occurred for well over a decade (Woodford, 2000; Kotze, 2000). These feasibility studies on the aquifer have provided estimates of recharge rates and locations (Kotze, 2002; Hartnady and Hay, 2000; Parsons, 2002), groundwater flow paths and volumes as well as the target units for groundwater abstraction (Rosewarne and Weaver, 2002). However, despite, the research done on the mechanics of the aquifer, little research has been conducted on the groundwater residence times which remain poorly constrained. This is partly because of the difficulty in identifying suitable dating tracers in groundwater with such low TDS values.

The residence time – or 'groundwater age' – refers to the time elapsed between when water enters the saturated zone and when it was sampled at a particular site (Torgersen et al., 2013). Both stable and radioactive isotopes are often used as indicators of mean residence time. Most estimates of residence times for the TMG Aquifer have been made based on stable hydrogen and oxygen isotope systematics in springs and their relationship to the same isotopes in precipitation (Harris et al., 1999; Diamond and Harris, 2000; Harris et al., 2010; Diamond and Harris, 2019). Comparison between the two sources found that cold spring δD and $\delta^{18}O$ values are closely related to the weighted mean annual rainfall values in the area. It was concluded that recharge in cold springs are fairly rapid, effectively occurring within three years (Harris et al., 2010). This, however, does not provide quantitative estimates of residence time.

Radiocarbon (^{14}C) is widely used to date older groundwater ranging up to 50 000 years in age (Van der Plicht, 2002). ^{14}C, however, is chemically active in groundwater. Therefore, knowledge regarding the processes affecting dissolved inorganic carbon along the groundwater flow path is required in order to convert activities into ages (Clark and Fritz, 1997). However, despite this difficulty in calibrating radiocarbon ages to calendar ages, the ^{14}C activity still provides meaningful insight into mean residence times. Work done by Weaver et al. (1999) and Miller et al. (2017) indicate that the TMG is often too young to be resolved by radiocarbon as efforts to use the tracer have yielded values between 99 and 115 percent modern carbon (pMC), implying ages younger than 1950, for which radiocarbon does not provide adequate resolution (Weaver et al., 1999; Miller et al., 2017). This can be countered by the use of tritium (^{3}H) in conjunction with its daughter product, helium-3 (^{3}He), which can accurately date modern ground waters that have been recharged within the last 50 years (Solomon and Sudicky, 1991).

The aim of this study is to determine residence times for groundwater of the TMG Aquifer by using $^{3}H/^{3}He$ isotope ratios which can provide ages with a 2.5% accuracy on groundwater that has been recharged within the last 50 years. Radiocarbon will be used as a secondary tracer to constrain residence times for groundwater that has been recharged prior to 1950 (Stuiver and Polach, 1977) as well as to determine whether there has been mixing between older and younger waters. A small sample set for the Malmesbury, Cape Granite Suite (CGS), Bokkeveld, Witteberg and alluvial aquifers will be analysed for comparison as well. Constraining residence times for the TMG Aquifer in the Western Cape will assist with determining whether there is a sustainable future in large-scale abstraction from this aquifer as proper management of this resource should maximise current supply without sacrificing future supply.

Before any conclusions on the implications for sustainability of the TMG Aquifer can be drawn, a working definition of the term “sustainable” needs to be established. In the context of this project, sustainability is defined as the management and protection of groundwater resources and any related ecosystems in a manner which maximises the current supply without compromising the future integrity of the resource (Loucks and Gladwell, 1999; Maimone, 2002; Gordon, 2011). Sustainable management of groundwater resources would protect supplies from depletion as well as from any possible forms of contamination. Additionally, any ecosystems that are fed by groundwater need to be conserved, particularly wetlands and

rivers. Sustainable use is ultimately reliant on good governance of water resources (CCA, 2009). Unsustainable practices would therefore compromise the resource as well as its environmental, economic and social potential.

1.1 Problem Statement

The TMG has been delineated as having sufficient supplies to provide water to the CoCT in times of water stress. Several previous studies in localised regions of the aquifer, however, suggest that the groundwater is relatively young. Quick turnaround times of groundwater across the entire aquifer may suggest greater susceptibility to climate change and consequently, the level of abstraction that can sustainably occur. Therefore, before large-scale abstraction can commence, proper constraints on the residence time(s) of groundwater in the aquifer system are required.

Residence time is an essential descriptor of hydrology, providing evidence of groundwater recharge zones, flow pathways and storage in a single integrated measure (McGuire et al., 2005). Understanding the distribution of residence times in large watersheds may have significant implications for the predictability of groundwater transport and processes (Maxwell et al., 2016). As residence time studies are not often conducted on a regional scale, outcomes in this study could likely be applied to similar semi-arid regions around the world where water availability is a growing issue.

1.2 Study Objectives

The central aim of this study is to determine the residence time of groundwater in the TMG aquifer and how the residence time varies spatially. Context is provided by assessing the residence time of other aquifers in the region. To achieve this aim, the following objectives have been identified:

Key Objective 1: To characterise ^{3}H and ^{14}C activities of groundwater in the TMG Aquifer and its surrounding aquifer systems.

- What is the range of $^{3}H/^{3}He$ ratios and ^{14}C activities across the six aquifers?
- Is there a spatial distribution of $^{3}H/^{3}He$ ratios and ^{14}C activities and do these show a relationship to different aquifer units within the TMG?
- How do $^{3}H/^{3}He$ ratios and ^{14}C activities in the TMG compare to those of other aquifer systems?

Key Objective 2: To calculate residence times of groundwater within the TMG and its surrounding aquifers.

- How do residence times calculated from the $^{3}H/^{3}He$ and ^{14}C systems compare to one another?
- What is the analytical accuracy and precision of apparent ages?
- Is it possible to assess the residence time of groundwater from other isotopic and chemical tracers and can a residence time proxy be identified?

Key Objective 3: To evaluate the vulnerability of TMG groundwater to future climate change.

- Is it possible to distinguish groundwater mixing between different aquifer systems and how does mixing impact on residence times?
- How does the residence time of the TMG groundwater compare to various recharge estimates and what are the implications for turnover of the groundwater system?
- Based on calculated groundwater residence times, how sustainable is the TMG groundwater system and is it a viable source of long-term water security to the City of Cape Town?

1.3 Water resources in the Western Cape

1.3.1 Water Supply

Cape Town is the provincial capital of the Western Cape and home to over 4 million people (City of Cape Town, 2017). In an average year, approximately 60% of the City's water is allocated to the City and its residents whilst 30% is allocated to the agricultural sector (City of Cape Town, 2019). The municipal water supply is sourced almost entirely from surface water through the infrastructure of six major dams (Table 1, Fig. 1) (City of Cape Town, 2019). These dams are recharged by precipitation that falls in the winter season. Complete reliance on precipitation posed a serious problem for the City during the 2015 – 2017 drought (Mahlalela et al., 2019). Collective dam levels had dropped alarmingly close to 20% by 2018 and it was predicted that the city would run out of water by April of that year (Fig. 2) (DWAS, 2018). With "Day Zero" imminent, strict water restrictions were enforced. Through widespread awareness campaigns, restricted water supply and a commendable effort from the citizens of Cape Town, daily domestic water use was reduced by almost 50%. Despite falling short of the 450 ML per day target, water usage had decreased from 980 ML in 2016 to just less than 500 ML in early 2018 (City of Cape Town, 2019).

Due to sufficient rainfall in the 2018 wet season, subsequent recovery of the dam levels resulted in the indefinite postponement of Day Zero. Although recovery of the dams resulted in the restrictions being somewhat lightened, it is evident that the city can no longer rely solely on surface water supplies. Unpredictable precipitation patterns attributed to climate change means long-term water security in the region is uncertain and the City of Cape Town continues to investigate options for augmentation of the water supply (City of Cape Town, 2019).

Table 1 – The storage capacity of the six major dams servicing the City of Cape Town (from City of Cape Town, 2017).

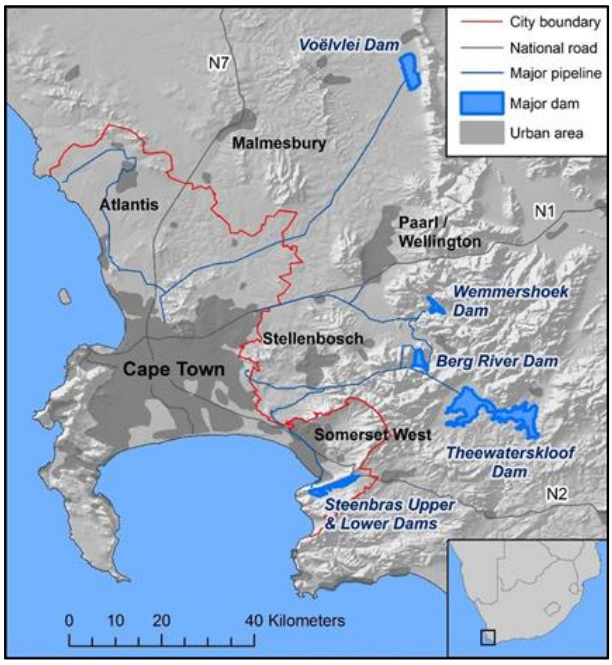

Dam	*Storage Capacity (ML)*	*% of total*
Berg River	130 010	14,5
Steenbras Lower	33 517	3,7
Steenbras Upper	31 767	3,5
Theewaterskloof	480 188	53,5
Voëlvlei	164 095	18,3
Wemmershoek	58 644	6,5
	898 221	**100**

Figure 1 – Locations of the six major dams which supply potable water to the City of Cape Town (Sinclair-Smith and Winter, 2019).

1.3.2 Water Supply Augmentation

In response to the serious crisis, a number of water augmentation initiatives are being investigated by the City of Cape Town. The first priority is to augment the municipal water supply with groundwater from the Cape Flats, Atlantis and Table Mountain Group aquifers. Groundwater abstraction from the Cape Flats Aquifer has been implemented for decades but will be expanded whilst the Atlantis and TMG aquifers are still being investigated. The City aims to collectively abstract a minimum of 100 ML per day from these aquifers (DWAS, 2018). In order to incorporate an additional 120 ML per day, the viability of a desalinization plant is being investigated through plans to implement a small-scale pilot operation at Koeberg (DWAS, 2018). As desalinization is by far the costliest option, wastewater treatment and re-use thereof appears to be a viable option that is capable of providing 70 ML/day (DWAS, 2018). The City has further confirmed that there are plans in place to increase surface water supplies by 23 Mm^3 (60 ML/day) by transferring water to the Voëlvlei Dam from the Berg River catchment (DWAS, 2018). Of the above options that are currently being investigated, groundwater abstraction remains the most cost-effective solution.

Figure 2 – Satellite imagery illustrating the storage of the Theewaterskloof Dam at A) the start of the drought in February 2015 and B) three years into the drought in January 2018. Images courtesy of Planet Labs Inc. (2018).

1.3.3 Groundwater Use

Currently, a number of towns depend solely on the TMG Aquifer for water, including Steytlerville, Jeffrey's Bay, Bredasdorp, Botrivier and Lamberts Bay whilst a number of towns are also partially dependent on this aquifer during the summer season (Lin, 2007). Published data on current (post-2015) groundwater usage from the TMG Aquifer is unavailable, however, the most recent data states that the annual usage of TMG groundwater is approximately 5.56 x 10^7 m^3, which only accounts for ~5% of estimated water stored (9.0 x 10^8 m^3) and ~4% of

entire groundwater discharge (1.3 x 10^9 m^3) of the aquifer system (DWAF, 2002; Jia, 2007). Approximately 68% of the groundwater abstracted from the TMG is used for irrigation, 20% of thermal water for holiday resorts, and only 12% is used for municipalities (Lin, 2007). Other minor users are the smaller scale farmers, homesteads and stock farms (Rosewarne, 2002; Jia, 2007).

1.4 Residence Time Determination

Groundwater residence time – or its 'idealised age' – refers to the time elapsed between when water has entered the groundwater system and when it was sampled at a specific location (Torgerson et al., 2013). The Mean Residence Time (MRT) of groundwater provides valuable insight into groundwater origin, recharge and exchange with aquifer host rocks (Kralik, 2015). Multiple environmental radioisotopes are often used to determine groundwater residence times. Recharge of groundwater occurs mainly through the addition of meteoric water which contains concentrations of environmental radioisotopes (Balek, 1988; Phillips and Castro, 2003) (Fig. 3). These isotopes enter the groundwater reservoir through recharge and once atmospherically isolated, isotopic concentrations begin to decay. Groundwater that has been recharged at a source, is subject to the interconnectedness of pore spaces, fractures and forces of dispersion, creating multipath routes between the recharge zone and discharge zone, effectively altering the true residence time (Fig. 4). The time elapsed between recharge and sampling can be resolved by the generalised radioactive decay equation (Eq. 1) (Varni and Carrera, 1998):

$$a_R = \frac{1}{\lambda}\ln\left(\frac{c_0}{c}\right) \qquad \text{(Eq. 1)}$$

where a_R is the radiometric age;

λ is the radioactive decay constant;

c_0 is the initial isotope concentration; and

c is the measured isotope concentration.

In this study, ^{3}H, ^{3}He and ^{14}C are used to determine groundwater residence times and are described below.

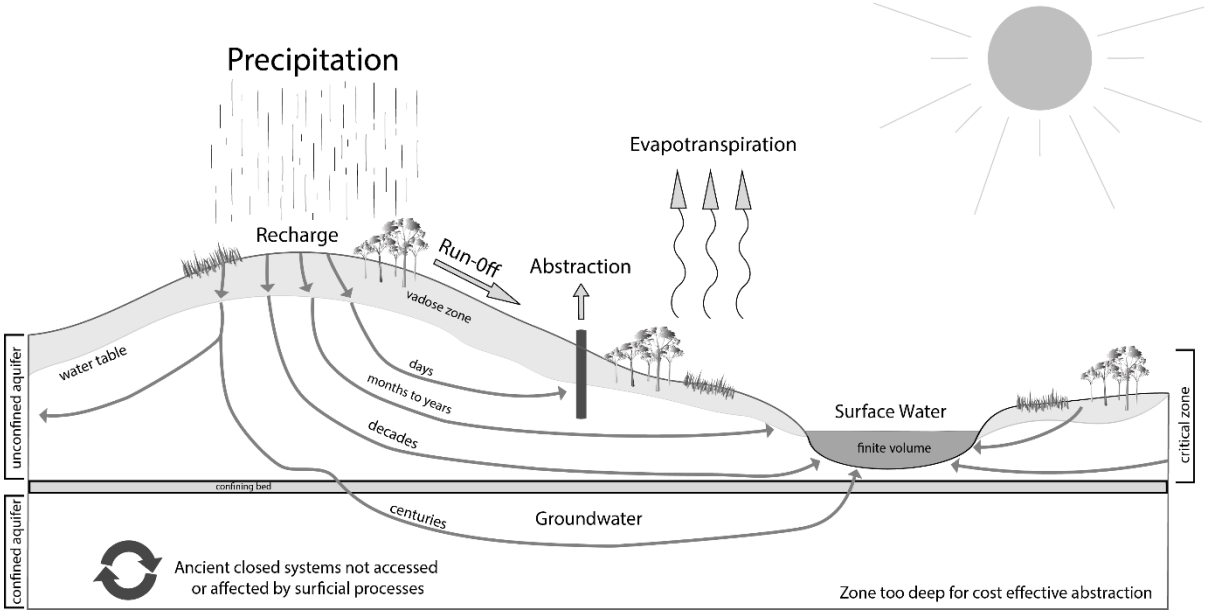

Figure 3 – Idealised groundwater flow within an unconfined and confined aquifer (Van Rooyen, unpublished work).

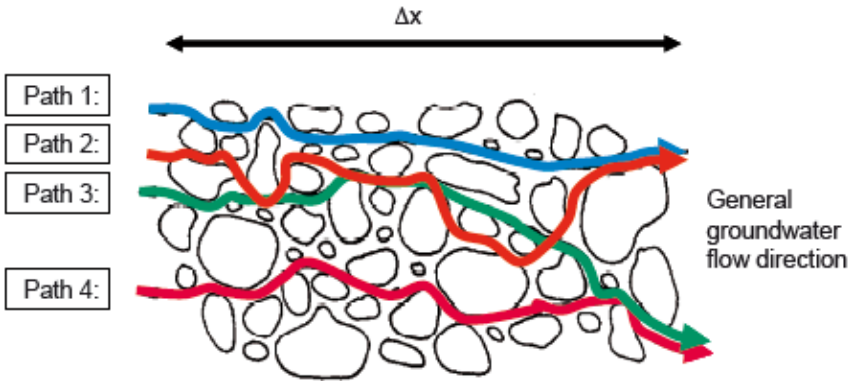

Figure 4 – Groundwater packages can flow along various paths between the point of recharge and the point of discharge (Δx), effectively altering the mean groundwater residence time (Torgerson et al., 2013).

1.4.1 Tritium and Tritogenic Helium

Tritium (^{3}H), the radioactive isotope of hydrogen, is produced in the upper atmosphere through cosmic ray bombardment of nitrogen-14 (Fontes, 1985), which can be represented by:

$$^{14}N + n^{0} \rightarrow {}^{3}H + {}^{12}C$$

Tritium is then oxidised in the atmosphere to form H_2O, which subsequently enters the natural water cycle in the form of precipitation (Fontes, 1985). ^3H concentrations are expressed in ratio to total hydrogen (H) as 'Tritium Units' (TU) where 1 TU = $^3H/H \sim 10^{-18}$ (Taylor and Roether, 1982). Natural atmospheric levels of tritium were artificially elevated due to the onset of nuclear weapons testing in the northern hemisphere in 1952 (Mook and Rozanski, 2000), resulting in 'bomb peak' levels during 1962 – 1964 (Michel, 1989). The resultant concentrations in precipitation reached levels in the range of thousands of TU whereas prior to weapons testing, natural atmospheric concentrations ranged between 2 – 8 TU (Ferronskiĭ and Poliakov, 1982; Mook and Rozanski, 2000). This clearly identifiable bomb peak concentration has been used as a valuable tracer in groundwater systems to date decadal waters that have been recharged after the onset of nuclear weapons testing, particularly in the northern hemisphere (Schlosser et al., 1988; Michel, 1989; Michel, Jurgens and Young, 2018). This anthropogenic increase, however, was significantly lower in the tropics and even more so in the southern hemisphere (Mook and Rozanski, 2000). Now that bomb peak concentrations have decayed and tritium levels have returned to background 'pre-bomb' values (Tadros et al., 2014), the use of tritium as a dating tool becomes increasingly limited.

Tritium, which has a half-life of 12.32 years (Lucas and Unterweger, 2000), decays via β^- decay to the noble gas isotope, ^3He (Kamensky, Tokarev and Tolstikhin, 1991) (Fig. 5). The presence of ^3H in groundwater is evidence for active recharge (Clark and Fritz, 1997), however due to its short half-life, ^3H is limited to dating 'young' waters as water recharged prior to 1952 has tritium concentrations close to zero (Mook and Rozanski, 2000) However, the combined measurement of both tritium and its daughter product, ^3He, provides a much more accurate dating system as it minimises the uncertainty of the input tritium concentration (Takaoka and Mizutani, 1987; Schlosser et al., 1989; Dajun and Hao, 2001). Assuming that dispersion is negligible, simultaneous measurement of both isotopes allows for the determination of the initial tritium concentration before atmospheric isolation and the onset of decay (Ekwurzel et al., 1994).

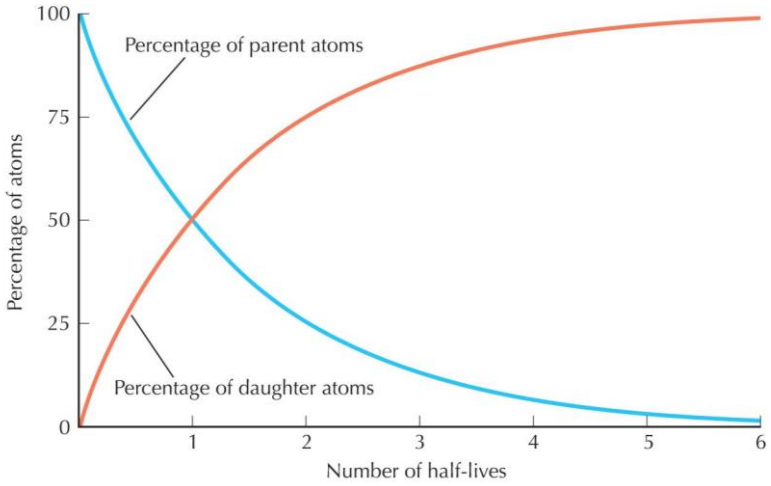

Figure 5 – In a closed system, tritium (red) decreases in an equal proportion to what tritogenic helium (blue) forms (Evolution, 2007).

Helium – which has two stable isotopes, namely ^{3}He and ^{4}He – is an excellent hydrological tracer due to its conservative nature (Gupta, Moravcik and Lau, 1994). In groundwater, helium can be derived from four main sources: the atmosphere (^{3}He/^{4}He ~ 1.38 x 10^{-6}) (Clarke et al., 1976), crust (^{3}He/^{4}He ≤ 10^{-7}), mantle (^{3}He/^{4}He ~ 10^{-5}) (Craig and Lupton, 1981) and most importantly, the decay of tritium (Kamensky, Tokarev and Tolstikhin, 1991). If dispersion is negligible, the residence time (τ) can be defined by the following equation (Tolstikhin and Kamensky, 1969):

$$\tau = \frac{1}{\lambda} * \left(1 + \frac{[\,^3He_{trit}]}{[\,^3H]}\right) \qquad \text{(Eq. 2)}$$

where λ is the decay constant (0.0556 yr^{-1}), ^3He is the concentration of tritogenic helium and ^3H is the tritium concentration (Tolstikhin and Kamensky, 1969; Beyerle et al., 1999). In order to derive an accurate age from this dating system, it is important to isolate the tritogenic helium concentration from the total helium concentration which can be expressed as (Nordstrom et al., 2005):

$$^3He_{total} = {}^3He_{eq} + {}^3He_{exc} + {}^3He_{terr} + {}^3He_{trit} \qquad \text{(Eq. 3.1)}$$

where $^3He_{eq}$ refers to solubility equilibrium concentration of the groundwater which is determined by the water temperature and the ambient pressure during recharge (Beyerle et al., 1999); $^3He_{exc}$ is the helium component attributed to excess air and $^3He_{terr}$ refers to

terrigenic component (nucleogenic and mantle ^{3}He) (Kamensky, Tokarev and Tolstikhin, 1991; Nordstrom et al., 2005). From calculation 3.1 above, the tritogenic helium component can be expressed as:

$$^3He_{trit} = {}^3He_{total} - {}^3He_{eq} - {}^3He_{terr} - {}^3He_{exc} \qquad \text{(Eq. 3.2)}$$

In order to isolate the four components, the solubility equilibrium (air-water solubility) component is first calculated by determining the solubility equilibrium temperature based on neon, argon, krypton and xenon concentrations of the water (Papp et al., 2012). The Isotope Climatology and Environmental Research Centre at the Institute for Nuclear Research, where the analyses for this study are performed, uses the closed system equilibration gas-water partitioning model of Aeshbach-Hertig et al. (1999), which requires the recharge elevation. To determine groundwater residence times, $^3He_{trit}$ is considered to be the ^{3}He component that is not accounted for by air-water solubility, excess air and terrigenic sources. ^{3}He and ^{4}He from air-water solubility are determined from recharge temperature and elevation as well as the known ^{3}He and ^{4}He concentrations in the atmosphere. As noble gas concentrations are found in fixed ratios in the atmosphere, Ne originating from excess air is the Ne component in excess of air-water solubility as Ne is only produced in the atmosphere and not from any other processes in the groundwater system (Aeshbach-Hertig et al., 1999). Any ^{4}He not accounted for by air-water solubility and excess air is assumed to be He from radiogenic sources (Hinkle, 2009). The ^{3}He/^{4}He ratios of radiogenic helium are then used to determine the ^{3}He contributed from terrigenic sources even though helium derived from the mantle is suspected to be rare in 'younger' waters (Solomon and Cook, 2000; Hinkle, 2009). Any remaining ^{3}He is assumed to be from the decay of ^{3}H. Once $^3He_{trit}$ is determined, the initial ^{3}H at the time of groundwater infiltration can be calculated as it is simply the sum of the measured ^{3}H and $^3He_{trit}$ (Hinkle, 2009).

Once all four factors have been determined, the groundwater residence time can be calculated using the standard radioactive decay equation (Eq. 2). Although the calculated value may deviate from the 'true' residence time of the groundwater as a result of tritium and/or helium diffusing into or from the aquifer (Kamensky et al., 1991), dispersion biases the calculated age towards the youngest component of mixed ground waters, which is accounted for in this study

(Schlosser et al., 1989). Due to its conservative nature and robustness, the $^{3}H/^{3}He$ dating system serves as an ideal tracer.

Uncertainty in the apparent $^{3}H/^{3}He$ (σ_T) age may arise due to lowered analytical precision of the tritium measurement (σ_{3H}) and uncertainty in the tritogenic helium contribution ($\sigma_{3Hetrit}$) (Visser et al., 2014). This uncertainty is linearly expressed through Eq. 4 (Visser et al., 2014):

$$\sigma_{\tau = \lambda^{-1}} ([^{3}H] + [^{3}He_{trit}])^{-1} (\sigma^{2}_{3Hetrit} + ([^{3}He_{trit}]/[^{3}H])^{2} \sigma^{2}_{3H})^{1/2} \quad \text{(Eq. 4)}$$

$\sigma_{3Hetrit}$ includes the uncertainty of the terrigenic component in the helium isotope ratio (if present) as well as the uncertainty in determining the recharge temperature and excess air fractionation (Ballentine and Hall, 1999).

1.4.2 Radiocarbon

^{14}C, the radioactive isotope of carbon, is naturally produced in the upper atmosphere when incident cosmic rays interact with ^{14}N through the following reaction (Mackay, 1961):

$$^{14}N + n^{0} \rightarrow {}^{14}C + p^{+}$$

Natural production of ^{14}C on earth is thought to be nearly constant (Castagnoli and Lal, 1980), and the resultant ^{14}C becomes oxidised to form ^{14}CO, and finally $^{14}CO_2$ which mixes with surrounding inactive CO_2 (Gat, Mook and Meijer, 2001). Radiocarbon is then incorporated into the cycles of living organisms in equilibrium with the atmosphere (Plummer and Glynn, 2013). Cosmogenic ^{14}C is incorporated into groundwater reservoirs during recharge where it undergoes interaction with soil CO_2 from plant root respiration and microbial degradation of soil organic matter (Plummer and Glynne, 2013). Once the dissolved inorganic carbon (DIC) becomes isolated from the atmosphere, ^{14}C begins to decay via β^{-} decay to its daughter isotope, ^{14}N (Gat, Mook and Meijer, 2001). Like tritium, ^{14}C concentrations were also anthropogenically increased in the atmosphere due to nuclear weapons testing in the northern hemisphere (Vogel, 1970), but concentrations have not yet returned to background levels due to radiocarbon's longer half-life of 5 730 ± 40 years (Godwin, 1962) (Fig. 6).

Figure 6 – Average annual atmospheric concentration of ^{14}C (fraction of modern carbon; 1.0 $F^{14}C$ = 100 pMC) since 1940, illustrating the bomb spike due to the onset of nuclear weapons testing (Ubelaker, Thomas and Olson, 2015).

The initial assumption in radiocarbon dating is that ^{14}C in the dynamic carbon reservoirs has remained unchanged over the past 50 000 years (prior to anthropogenic inputs) (Baxter and Walton, 1971). However, short-term fluctuations in ^{14}C have occurred in the past century which can be linked to solar activity (Stuiver, 1965; Damon, Long and Grey, 1966; Suess, 1967). This fluctuation is thought to be related to variation in cosmic ray flux, and as a result, a variation in ^{14}C production due to increased magnetic field strengths which is associated with sunspot activity (Baxter and Walton, 1971).

Although 5 730 is the internationally accepted half-life of radiocarbon, the Libby half-life of 5 568 years (Libby, 1955) is conventionally used to date samples (Kalin, 2000; Chiu et al., 2007). Although exceptions do exist, convention will be followed in this study. In order to determine the age (T) of a carbonaceous sample, the decay constant (λ) or half-life needs to be known as well as the measured ^{14}C concentration (^{14}A) (Torgerson et al., 2013). Assuming the initial ^{14}C concentration (point of atmospheric isolation; $^{14}_{i}A$), the age can be determined from the following equation (Gat, Mook and Meijer, 2001):

$$T = \left(\frac{5\,568}{\ln 2}\right) x \left(\frac{^{14}A}{^{14}_{i}A}\right) \qquad \text{(Eq. 5)}$$

The calculated age dates back from 1950 as the initial concentration refers to the standard activity in 1950 AD (Stuiver and Polach, 1977; Gat, Mook and Meijer, 2001). Dating of

groundwater, however, is more complicated and involves the analysis of dissolved inorganic carbon (DIC) and organic carbon (DOC) (Torgerson et al., 2013). The following calculation (Eq. 6) can be used to determine when the groundwater was atmospherically isolated (Gat, Mook and Meijer, 2001):

$$T = -8\,033 \ln \left[\frac{\left(\frac{^{14}A}{_{std}^{14}A} \right)}{\left(\frac{^{14}_{i}A}{_{std}^{14}A} \right)} \right] \qquad \text{(Eq. 6)}$$

where 8 033 is determined from $\frac{5\,568}{\ln 2}$. In this equation, the complication lies in that $_{std}^{14}A$ is not simply equal to $^{14}_{i}A$ as in Eq. 5, but instead through a number of isotopic exchange reactions (Gat, Mook and Meijer, 2001), for which various correction models exist (Ingerson and Pearson, 1964; Vogel, 1967; Fontes and Garnier, 1979).

In hydrology, ^{14}C is limited to dating groundwater older than 1950 as recently recharged waters would have ^{14}C concentrations that are not distinguishable from current atmospheric activities despite analytical sensitivity (Tamers and Scharpenseel, 1970). ^{3}H is often not present in groundwater bodies that have considerably low ^{14}C concentrations, unless considerable mixing between water bodies with significantly different ages has occurred (Mook and Rozanski, 2000). In groundwater that has undergone mixing, the obtained $^{3}H/^{3}He$ age will apply to the younger fraction of water present (Dajun and Hao, 2001).

An important factor to consider may be the contamination of the radiocarbon samples which may occur naturally or artificially and result in ages that are either too young or too old (Plummer and Glynn, 2013). The addition of ‘dead’ carbon along the flow path through the dissolution of carbonate minerals will cause an old bias whereas the overcompensation for dead carbon will result in a young bias (Plummer and Glynn, 2013). The main concern in groundwater sampling is collecting the sample from water flowing laminarly as water with a turbulent flow pattern promotes mixing with atmospheric air, effectively altering the ‘true’ radiocarbon concentration (Torgerson et al., 2013). Radiocarbon samples may also be contaminated in the laboratory through contact with compromised surfaces, equipment and personnel as research involving elevated ^{14}C contents can be detected in background samples up to decades later (Zermeño et al., 2004).

2 STUDY SITE CONTEXT

The study area is focussed within a 200 km radius of Cape Town. A summary of its physical characteristics which include its extent, climate, land cover as well as geological characteristics are presented below. Additionally, the hydrogeological characteristics which affect recharge, storage, flow and discharge from the TMG Aquifer as well as the other aquifer systems are provided.

2.1 Study area

The study site extends from Cape Town to the town of Citrusdal, some 160 km north of the City. The town is situated in the Olifants River Valley at the base of the Cedarberg Mountains. The eastern extent of the study site is approximately 16 km north of George. The greatest emphasis is placed on the Cape Winelands region, particularly in and around the towns of Stellenbosch, Franschhoek and Paarl due to the proximity of dams in the region. The study site is illustrated in Fig. 7.

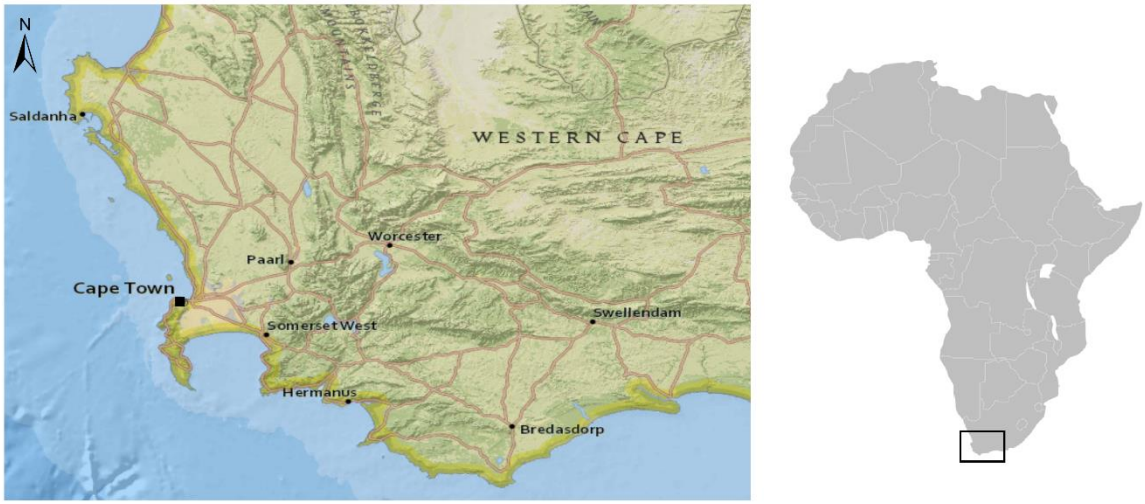

Figure 7 – The study site is focussed within a 200 km radius of Cape Town (Western Cape, South Africa).

2.2 Climate

South Africa is a water-stressed country that receives an average of 450 mm of rainfall per annum, much less than the worldwide average of 780 mm (Benhin, 2006). This average annual rainfall classifies the country's water resources as 'scarce' and 'extremely limited' (Schulze and Lynch, 2001; Behnin, 2006). Of the South African provinces, the Western Cape experiences the greatest variability in rainfall as a maximum annual average of 3 345 mm is recorded in the Jonkershoek Mountains, Stellenbosch and a minimum of 60 mm in the Tankwa Karoo (Fig. 8) (Schulze et al., 2007; Diamond, 2014). Given that the Western Cape covers a vast area and has a complex topography, the province possesses a range of climatic gradients, namely the south-north aridity gradient and an east-west rainfall seasonality gradient with summer rainfall increasing towards the east (Midgeley et al., 2005). The province is further divided into three distinct climatic regions by Van Niekerk and Joubert (2011), into the Mediterranean, South Coast and Karoo regions (Fig. 9). The City of Cape Town, located in the south-western portion of the province, is classified as having a Mediterranean-type climate characterised by cool, wet winters and warm, dry summers. The region receives an average rainfall of less than 500 mm per year (Midgeley et al., 2006; Benhin, 2006), with the majority of rain falling during the colder months of May – August. A number of the City's dams are located within or proximal to the Berg River catchment, which receives average rainfall of 600 – 1 000 mm per annum (Winter and Mgese, 2011).

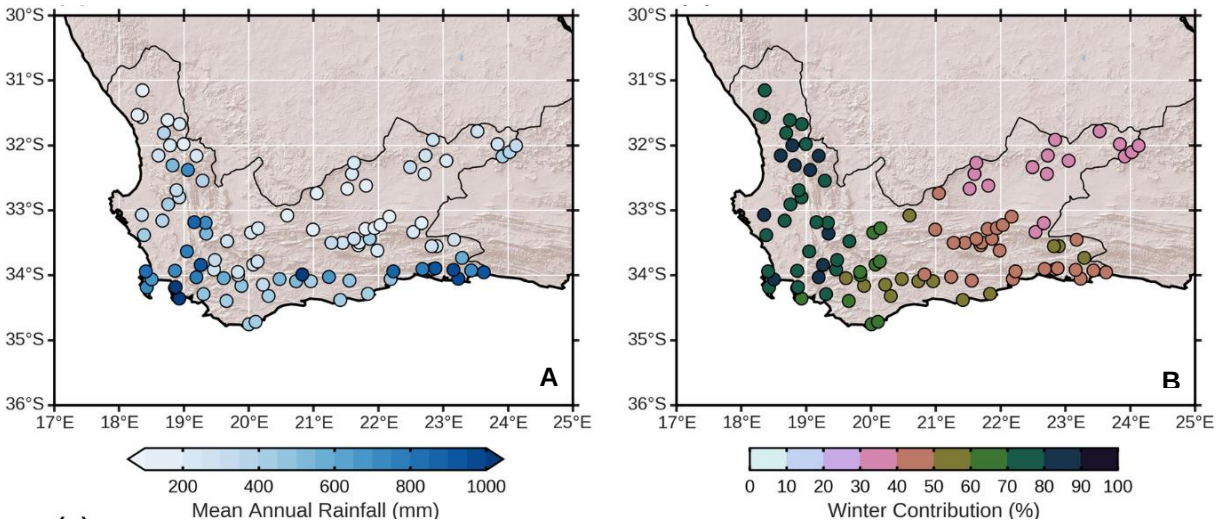

Figure 8 – A) The mean annual precipitation (mm) at SAWS stations across the Western Cape for 1979–2016; B) the mean contribution (%) of winter rainfall (June – August) to the annual rainfall total at the stations (Mahlalela, 2019).

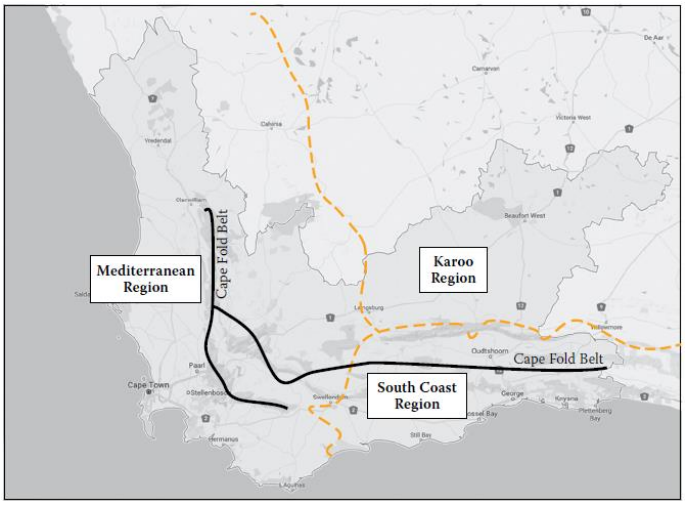

Figure 9 – The delineation of the three climatic zones in the Western Cape (dotted orange line) indicating the City of Cape Town as having a Mediterranean-type climate (Du Plessis and Schloms, 2017).

2.3 Vegetation

The study site extends over a region referred to as the Cape Floristic Region which extends along the southern and western coasts of the province (Fig. 10). Vegetation has been subdivided into two main groups, namely, the heathland fynbos (Kruger, 1979) and the Mediterranean-type shrublands which grow on more fertile soils, called renosterveld and strandveld (Boucher & Moll, 1981; Di Castri, 1981).

Fynbos is a heathland vegetation that occurs on leached acid sands which have accumulated from the in-situ weathering of granites and sandstones, or from aeolian-sourced sands (Mitchell, et al., 1986). These sands range from 0 – 70 m in depth (Boucher, 1983). The West Coast Strandveld is found on calcareous dune sands, calcretes, limestones as well as weathered granites and shales (Boucher, 1983). In contrast, renosterveld overlies shales and granites in a rainfall zone of 250 – 550 mm per year (Boucher, 1983). Strandveld dominates along the west coast of the province from a few kilometres south of Bloubergstrand all the way to St Helena Bay as well as along the False Bay Coast. Fynbos and renosterveld are much more extensive over the region (Mucina and Rutherford, 2010).

Despite the vast extent of the Cape Floristic Region, much of the endemic vegetation has been cut away in attempts to produce land for grazing and agriculture. This vegetation has been depleted to the extent that only around 14.7% of the western coastal foreland vegetation

remains in an untouched state today (Boucher, 1983). Despite the soil and climate being able to support various crops, wine grapes are dominantly cultivated in the region.

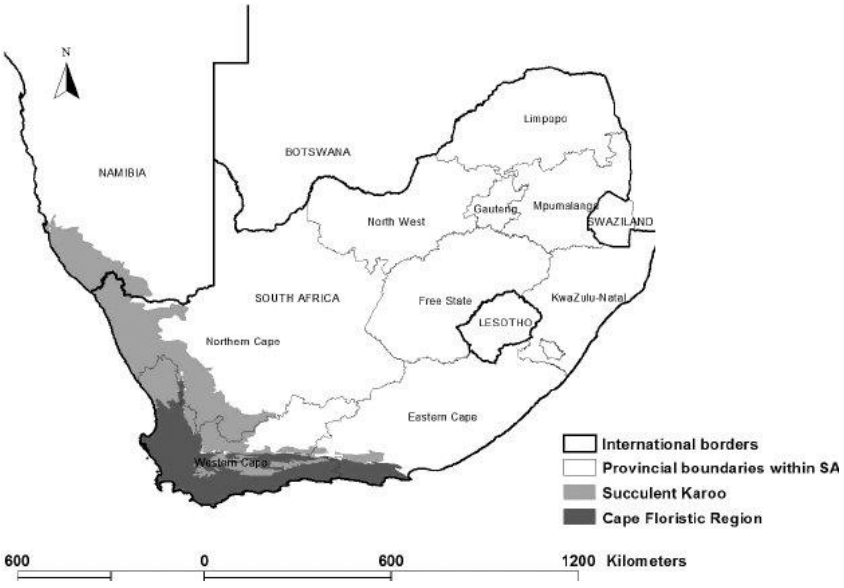

Figure 10 – The Cape Floristic region (indicated by dark grey) found along the south western coast of Southern Africa (Brownlie et al., 2005).

Grasses found along the west coast are predominantly C_3 species (> 75%). Moving eastwards, C_3 plants are progressively replaced by C_4 plants until C_4 grass species become the dominant species (> 75%) along the south coast, near Port Elizabeth (Vogel et al. 1978; Radloff, 2008). Both fynbos and renosterveld have species that follow the C_3 and C_4 photosynthetic pathways. The $\delta^{13}C$ values of C_3 and C_4 plants are supposedly very distinct as C_3 plant species tend to have values ranging from -26 to -30‰. whereas C_4 species range from -12 to -14‰ (Curtis, 2013). Mixed C_3 and C_4 habitats, however, tend to have values between -14 and -26‰ (Stock et al. 1993).

2.4 Geology

Basement rocks in the Western Cape are composed of several lightly metamorphosed groups of varied lithology (Diamond and Harris, 2019). This includes the Malmesbury Group that is predominantly found in the south-western Cape and forms part of the Saldanian Belt (Gresse et al, 2006). Intruded into the Pan-African Malmesbury Group, is the Cambrian Cape Granite Suite. The CGS is mainly found in areas of Malmesbury Group outcrop, but minor plutons are situated further east, near the town of George (Scheepers and Schoch, 2006). The Paleozoic

Cape Supergroup – composed of the Table Mountain, Bokkeveld and Witteberg Groups – unconformably overlies the basement rock and covers the vast extent of the province (Johnson, 1976). Quaternary unconsolidated alluvial sediments unconformably overlie the basement Malmesbury and CGS rocks in the Cape Flats area (Saayman and Adams, 2002) (Fig. 12). The geology is described below in order of occurrence with ages provided by the Council for Geoscience (2006).

2.4.1 Malmesbury Group (575 – 550 Ma)

The Malmesbury Group is made up predominantly of greywackes with subordinate metavolcanic rocks, conglomerates, limestone and chert units (Tankard et al., 1982). Outcrop of the Malmesbury Group is divided into three terranes (Tygerberg, Swartland and Boland), separated by two large terrane bounding north-west trending shear zones, the Colenso and Piketberg-Wellington Faults (Hartnady et al., 1974; Scheepers, 1995; Belcher and Kisters, 2003). The group, comprised of the Piketberg, Tygerberg and Porterville Formations, unconformably overlies the Swartland Group. The basal Piketberg Formation grades from conglomerates interbedded with shales at its base, into arenites and shales. This is succeeded by the Porterville Formation which contains mudstones, shales and subordinate greywackes. The final uppermost Tygerberg Formation contains mudstones, fine-grained greywackes and impure sandstones as well as a member comprised of volcanic rocks (andesites and tuff). (Buggisch et al., 2010; Belcher and Kisters, 2003). A series of deformation events and the subsequent intrusion of the Cape Granite Suite into the Malmesbury Group has resulted in low-grade metamorphism (greenschist facies) of the sedimentary rocks (Belcher and Kisters, 2003).

2.4.2 Cape Granite Suite (610 – 500 Ma)

The Cape Granite Suite (CGS) consists of plutons and batholiths intruded into the metasedimentary rocks of the Malmesbury Group (Hartnady et al., 1974; Scheepers, 1995). Three locality groupings of the batholiths are identified in the Western Cape, namely a northern group (south of the Orange River), a south-western group (near Cape Town) and an eastern group (near George) (Harris et al., 1997). In the south-western group, the granitic suite can be divided into six major batholiths, namely the Saldanha-Vredenburg, Darling, Malmesbury, Paarl-wellington, Stellenbosch-Kuils River and Peninsula batholiths (Harris et al., 1997).

Intrusions of these Precambrian-age granitic rocks are thought to have occurred in three main phases with a 120 Ma gap between the youngest and oldest intrusions (Schoch, 1972; Schoch and Burger, 1976; Scheepers., 1995). Plutons are distinguished as either A-, I- or S-type granites based on their geochemistry and petrography (Scheepers., 1995).

2.4.3 Cape Supergroup

The Cape Supergroup, mainly comprised of sandstones, quartzites and shales, can be divided into the Table Mountain, Bokkeveld and Witteberg Groups (Johnson, 1976). An impressive 1 300 km of geologic outcrop extends from the town of Nieuwoudtville in the Northern Cape southwards towards L'Agulhas on the south coast of the Western Cape. The TMG then further extends eastwards to the Eastern Cape before terminating along the coast of Port Elizabeth. Based on palaeontology and zircon dating, deposition of these Paleozoic sediments are estimated to have occurred during the time frame 510 – 350 Ma (Miller et al., 2016). The provenance of detrital zircons suggest that the sediments of the Cape Supergroup have largely been sourced from the Namaqua-Natal Metamorphic Complex (1.2 – 1.0 Ga) and Pan-African orogenic belts (650 – 500 Ma) on both the African and South American continents (Fourie et al., 2011; Vorster, 2013; Miller et al., 2016).

The Cape Fold Belt is divided into two branches which are separated by a syntaxis (De Beer, 1992), During the Cape Orogeny, deformation resulted in the low-grade metamorphism as well as the extensive folding and faulting of what is now known as the Cape Fold Belt (CFB) (De Beer, 1992). Deformation events coupled with the resistance to weathering, has resulted in the sandstones of the TMG, Bokkeveld and Witteberg Groups, outcropping in high elevation regions.

2.4.3.1 Table Mountain Group (510 – 420 Ma)

The TMG is the lowermost lithological package of the Cape Supergroup, comprised mainly of sandstone and minor mudstones (Fig. 11). The TMG is comprised of the Piekenierskloof, Graafwater, Peninsula, Pakhuis and Cederberg formations as well as the Nardouw Subgroup, which is further divided into the Goudini, Skurweberg and Rietvlei (Baviaanskloof in the Eastern Cape) Formations (Table 2) (Rust, 1967; Thamm and Johnson, 2006).

Table 2 – Summary of the stratigraphy of the Table Mountain Group and its subgroups (after Blake et al., 2010).

Group	Subgroup	Formation	Maximum thickness (m)	Lithology
Table Mountain	Nardouw	Rietvlei	280	Feldspathic quartz arenite
		Skurweberg	390	Quartz arenite
		Goudini	230	Silt sandtone, siltstone
		Cedarberg	120	Shale, siltstone
		Pakhuis	40	Diamictite, shale
		Peninsula	1800	Quartz arenite
		Graafwater	420	Impure sandstone, shale
		Piekenierskloof	900	Quartz arenite, shale, conglomerate

The basal Piekenierskloof Formation, which lies unconformably on Malmesbury Group rocks, consists of litharenites and rudites and is overlain by the semi-confining Graafwater Formation which is made up of shale/siltstone. These two units are only present in the north-south trending limb of the TMG outcrop (Thamm and Johnson, 2006). Overlying the Graafwater Formation, the Peninsula Formation is composed of quartzitic arenites. This is arguably the most significant formation as it is highly favoured for water quality and yields and is present across the entire extent of the TMG, ranging from 1 000 – 2 000 m in thickness. A thin shaley siltstone layer with an average thickness of 70 m makes up the Cedarberg Formation (Rust, 1967). As extensive as the underlying Peninsula, the Cedarberg Formation acts as a confining layer, effectively separating the lower and upper aquifers. The uppermost unit of the TMG is the Nardouw Subgroup, which is subdivided into three members (Goudini, Skurweberg, Rietvliei) of interlayered shale, sandstone, siltstone and quartzite because of its variable composition (Rust, 1967).

Figure 11 – A) TMG geological outcrop displays extensive fracturing at Table Mountain (Cape Town); and B) alternate layers of mature sandstone and siltstone which is more susceptible to weathering.

2.4.3.2 Bokkeveld Group (410 – 370 Ma)

The Bokkeveld Group, which succeeds the TMG, outcrops within the Cape Fold Belt of the Western and Eastern Cape, between the TMG and the Witteberg units. In the Western Cape, the Bokkeveld can be subdivided into two groups, namely the Ceres and Bidouw subgroups (Reid et al., 2015). The basal Ceres Subgroup (comprised of the Gydo, Gamka, Voorstehoek, Hexrivier, Tra-Tra and Boplaas formations) consists of three distinct laterally continuous, upward-coarsening successions of mudstones, siltstones and sandstones with minor calcareous lenses present in some mudstones. The Ceres Subgroup is succeeded by the Bidouw Subgroup (Waboomberg, Wuppertal, Klipbokkop, Osberg and Karoopoort formations) comprised of the fourth and fifth successions of mudstones, siltstones and sandstones (Reid et al., 2015). The cyclic deposition of sediments is interpreted to have been deposited in muddy offshore to sandy nearshore settings on a stable, storm-dominated marine shelf (Theron and Johnson, 1991; Anderson et al., 1999; Reid et al., 2015).

2.4.3.3 Witteberg (370 – 330 Ma)

The upper layers of the Bokkeveld Group grade into the sandstones of the overlying Witteberg Group. This group of sediments was deposited in the shallow marine conditions of the Agulhas Sea and is comprised mainly of quartzites, sandstones, siltstones and shales (Brundson and Booth, 2009). The Witteberg Group, which is comprised of the Weltevrede and Lake Mentz Subgroups, crops out on the inner margin of the Cape Fold Belt, cradling the Karoo (Thamm and Johnson, 2006; Cotter, 2000). It tends to form the most inland outcrops of the Cape Supergroup, and can be traced eastwards as far as Port Alfred, about 120 km beyond the Cape Fold Belt.

2.4.4 Quaternary Sediments (73 – 2 ka)

Quaternary deposits in the Western Cape extend along the south coast from Strand to Cape Town as well as along the west coast from Cape Town to far beyond the northern border of the province. Optically stimulated luminescence (OSL) dating of sand dunes along the west coast suggests five phases of active deposition with a maximum age of 73 ka and a minimum age of 4 ka (Chase and Thomas, 2007). The Cape Flats region, which is of hydrological significance, has been delineated as the low-lying sand covered region extending from Cape Town – Muizenberg, Cape Town – Kuils River and finally, Kuils River – Strand (Adelana et al.,

2010). In this area, Quaternary age sediments, range up to 50 m in thickness, blanket the TMG, CGS and Malmesbury Groups (Theron et al., 1992; Giljam, 2002; Adelana et al., 2010). Sediments are mainly sands that vary in grain size and composition but often contain bedrock fragments, calcrete pebbles and bioclastic components (Giljam, 2002). These Cenozoic sediments are referred to as the Sandveld Group and includes Quaternary sediments that were previously classified as Bredasdorp Formation sediments (Visser and Schoch, 1973; Rogers, 1982; Hendey and Dingle, 1983).

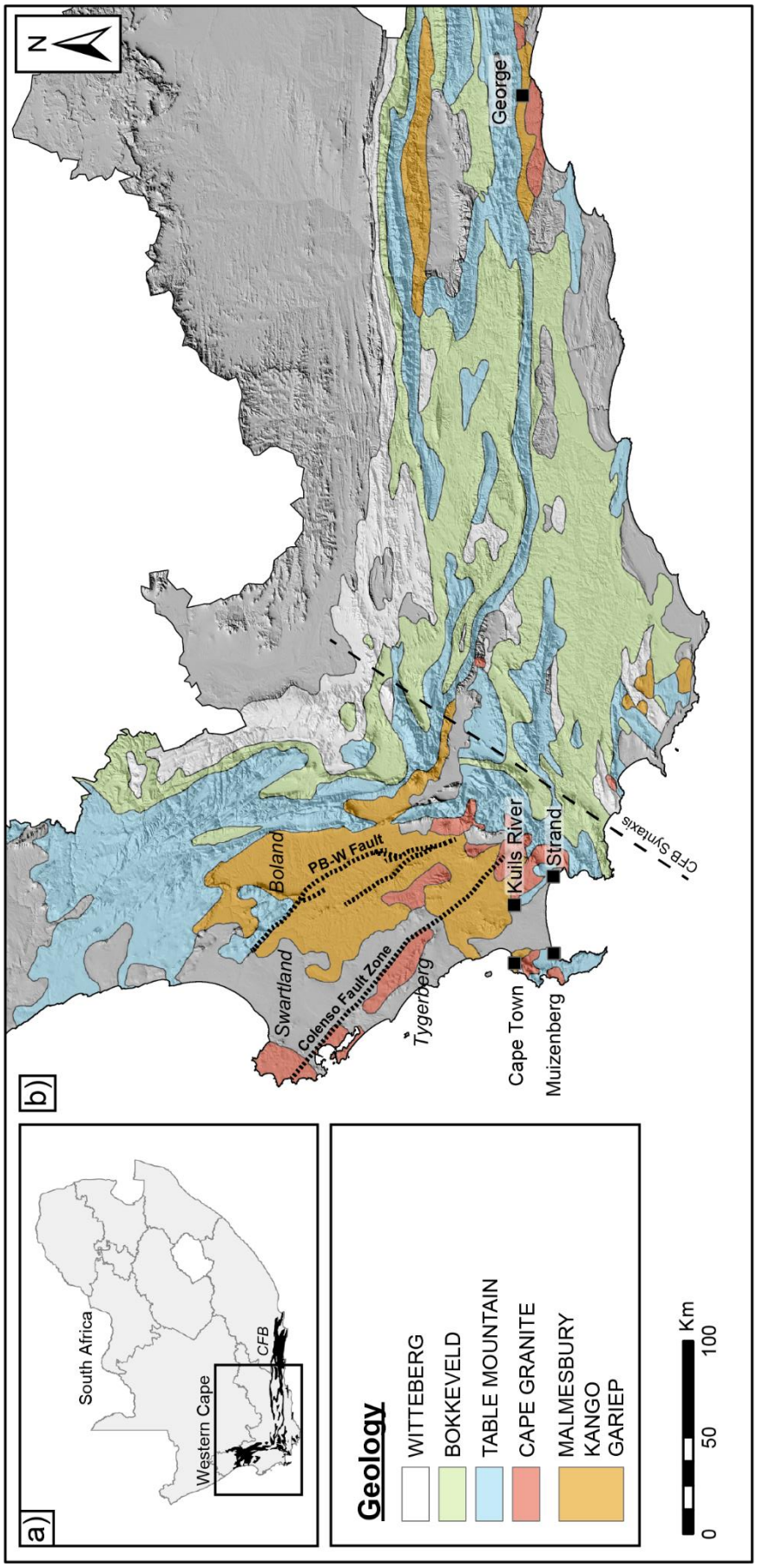

Figure 12 – Simplified geology of the Western Cape illustrating the stratigraphic units that pertain to this project.

2.5 Hydrogeology

A lithostratigraphic unit in which groundwater occurs, is called an aquifer. An aquifer is sufficiently porous and permeable, allowing for the storage and flow of significant quantities of groundwater (Lohman et al., 1972). An aquitard is an impermeable unit which often contains water but does not allow for the transmission of water (Walton, 1990). An aquiclude, on the other hand, is an impermeable unit that neither stores nor transmits water (Maxey, 1964; Freeze and Cherry; 1979). Aquifers usually have great areal extent and store vast amounts of water. When a number of aquifer units are separated by semi- and impermeable units, it is referred to as an aquifer system (Fig. 13) (Todd, 1959; Wilson, 1983).

The aquifer units found in the study area are summarised in Table 3 and are discussed in this section. The Witteberg, Bokkeveld and CGS Aquifers (also simply referred to as a granitic aquifer in this study) are only briefly discussed as these aquifers have not been investigated as viable units for containing considerable amounts of water and have little available literature to review. Studies on the TMG Aquifer are much more extensive resulting in a detailed discussion on the aquifer.

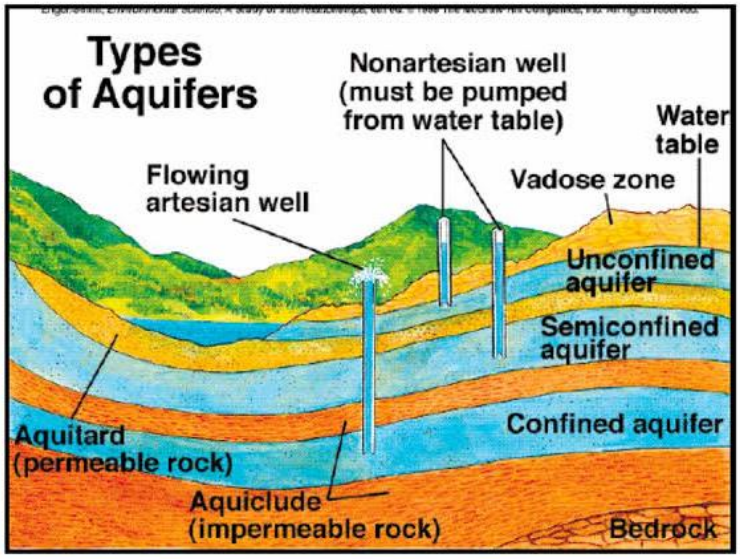

Figure 13 – Types of aquifer units (Enger and Smith, 1995)

Table 3 – Simplified hydrogeology of aquifer units within the study site with special division within the TMG Aquifer system (after Blake et al., 2010).

Stratigraphy					**Hydrostratigraphy**		
Age (Ma)	*Supergroup*	*Group*	*Formation*	*Description*	*Superunit*	*Unit*	*Subunit*
2 - 0		Sandveld/Bredasdorp	Various	Alluvium		Quaternary Aquifer	
Major unconformity							
510 - 330	Cape	Witteberg	Various	Sandstone, siltstone and shale		Aquitard	
		Bokkeveld	Various	Shales and minor sandstone		Gydo Mega-aquitard	
		Table Mountain	Rietvlei	Feldspathic sandstone; minor shale	Table Mountain Superaquifer	Nardouw Aquifer	Rietvlei Subaquifer
							Verlorenvalley Mini-aquitard
			Skurweberg	Thickly bedded quartzite			Skurweberg Subaquifer
			Goudini	Reddish brown quartzitic sandstone		Winterhoek Mega-aquitard	Goudini Meso-aquitard
			Cedarberg	Dark grey shale and siltstone			Cedarberg Meso-aquitard
			Pakhuis	Diamictite and quartz sandstone			Pakhuis Mini-aquitard
			Peninsula	Thickly bedded quartzite		Peninsula Aquifer	Platteklip Subaquifer
							Leeukop Subaquifer
Major unconformity							
610 - 500		Cape Granite Suite		Granite		Basement Aquicludes	
575 - 550		Malmesbury		Metasediments			

2.5.1 Malmesbury Aquifer

On a regional scale, the Malmesbury Group is classified as an aquiclude due to the impervious nature of its host rock (Conrad et al., 2019). The high component of clay and micaceous minerals significantly hinders groundwater flow within the metasediments (Münch and Conrad, 2007). Groundwater within the Malmesbury Group is generally associated with and fracturing and faulting as groundwater flows along foliation planes, bedding (where preserved), faults and fractures (Colvin and Saayman, 2007; Münch and Conrad, 2007). Studies in the Verlorenveli Valley (near Elands Bay) suggest that the Malmesbury Aquifer in the region is recharged by the TMG Aquifer (Watson et al., 2018). The fractured rock aquifer tends to be confined to semi-confined, making it much less vulnerable to contamination (Colvin and Saayman, 2007). Groundwater quality of the aquifer is quite variable as EC values range from less than 1000 to over 10 000 µS/cm (Conrad et al., 2019). Elevated TDS values of groundwater in the aquifer generally limits the usability of the water (Colvin and Saayman, 2007). Previously, the Malmesbury Group has been classified as a low-yielding aquifer as yields from boreholes drilled into the aquifer are typically within the range of 0.1 to 0.5 L/s (Conrad et al., 2019). Boreholes drilled along fault-related fracture zones inferred from the Wellington – Piketberg Fault and Shear Zone, however, has resulted in much higher yielding boreholes (Conrad et al., 2019)

2.5.2 Cape Granite Aquifer

Granitic rocks typically do not store or transmit groundwater as they are aquicludes. The Cape Granite Suite, however, is weathered and fractured, resulting in a fractured crystalline aquifer with generally low hydraulic conductivity (0.06 m/d) (Conrad et al., 2019). As the composition of granitic rocks vary, diverse forms of weathering take place, effectively altering the hydrology of the resultant aquifer (Wu, 2009). EC values in the Cape Granite Aquifer ranges from 40 to ~1 100 µS/cm (Agyare-Dwomoh, 2020). Very little literature on the Cape Granite Aquifer exists, making it difficult to provide context on the aquifer.

2.5.3 TMG Aquifer

2.5.3.1 Hydrostratigraphy

The Table Mountain Group Aquifer system can be divided into three main units: the Peninsula Aquifer, Nardouw Aquifer and the Winterhoek Mega-aquitard which separates the two (Kotze, 2002a) (Table 3). Two minor hydrostratigraphic units, the basal Piekenierskloof Aquifer and the overlying Graafwater Aquitard, which underlie the Peninsula Aquifer, are not laterally continuous and predominantly found in the western branch of the Cape Fold Belt (De Beer, 1992). The Skurweberg Formation – a subaquifer of the Nardouw Aquifer – and the Peninsula Formation are thought to have sufficient overall thickness and massive thick-bedded zones which could possibly support large-scale groundwater abstraction (Rosewarne and Weaver, 2002, Netili, 2007). The delineation of these aquifers and aquitards is purely based on hydrological lithologies, despite the fact that each rock type possesses unique hydrological characteristics in terms of porosity, permeability and trasmissivity (Xu et al., 2009).

2.5.3.2 Aquifer Characteristics

The medium to coarse grain size coupled with the relative purity of the quartz arenites lead to the enhanced quality of TMG groundwater (De Beer, 2002b). Groundwater is considered to be of excellent quality as it is characterised by low electrical conductivity (EC) ($\bar{x}$ = 100 – 300 µS/cm), low total dissolved solids (TDS) as well as low alkalinities (<50 mg/L) (Brown et al., 2003; Miller et al., 2017; Turner, 2018). Despite low ionic content, groundwater is typically characterised as Na-Cl type water (Wu, 2008). The pH of the groundwater is fairly acidic, reaching values as low as 5 which can be corrosive to borehole infrastructure (Netili, 2007). Groundwater within the aquifer often contains elevated iron contents resulting in biofouling which causes clogging of infrastructure (Jolly, 2002; Robey et al., 2014).

The bulk storativity of the two main aquifer units of the TMG – the Peninsula and Nardouw Aquifers – has been estimated at 10^{-2} or 10^{-3} (Rosewarne, 2002). Conservative storage yield models based on the average porosity of the sandstones estimate the volume of groundwater released for 1 m unit head decline to be 6.9 and 1.1 Mm^3 for the Peninsula and Skurweberg aquifers, respectively (Blake et al., 2010). Despite the difficulty in constraining groundwater storage of the TMG Aquifer system, the volume stored is estimated to be on the order of 9 x 10^8 m^3 (Xu et al., 2009). Both these aquifer units are fractured rock aquifers that have low

primary porosity. An intricate network of fissures, joints and fractures largely controls the flow of groundwater within the TMG (Xu et al., 2009). Knowledge on the interconnectivity of these fracture networks is also crucial to how easily groundwater can be abstracted from the aquifer.

The TMG Aquifer ranges between 50 – 2000 m in depth and water tends to be under artesian flow, emanating as cold springs in many locations (Diamond and Harris, 2000). Boreholes drilled deeper than 200 m into the aquifer generally have dramatically higher yields than shallow boreholes. This is most likely related to a stress-generated confining zone within the uniformly quartzitic rock. Borehole yields in excess of 5 l/s are common in the TMG (Netili, 2007; Hartnady and Hay, 2002b).

The hydrogeological characteristics of the TMG Aquifer are heterogeneous. As a result, water table depth, infiltration, storage and transmission vary across the aquifer due to lithology and structural/tectonic controls (Netili, 2007; Pietersen and Parsons, 2007; Thamm and Johnson, 2006; Rosewarne, 2002). It is suspected that fracturing in certain areas within the TMG may extend to several hundred meters below the surface. This fracture network is assumed to be even more extensive at greater depths, which may result in rainwater contributing to deep groundwater flow. This is evidenced by the hot springs that circulate at depths (Meyer, 2002).

11 major thermal springs are present throughout the Western Cape (Fig. 14) (Brown et al., 2003; Xu et al., 2009). These hot springs reach temperatures as high as 64°C as the water is circulated at depths of at least 2 000 m below ground level (Diamond and Harris, 2000; Brown et al., 2003). These springs emanate from Peninsula Aquifer and are thought to be linked to either the contact between the over- or underlying aquitard, the impermeable fault zone, or where the Peninsula is hydraulically connected to the Nardouw due to faulting (Brown et al., 2003). The contact zone between the TMG and the Bokkeveld Groups is also thought to provide a mixing conduit for older water at deeper depths and groundwater that has been more recently recharged (Weaver et al., 1999).

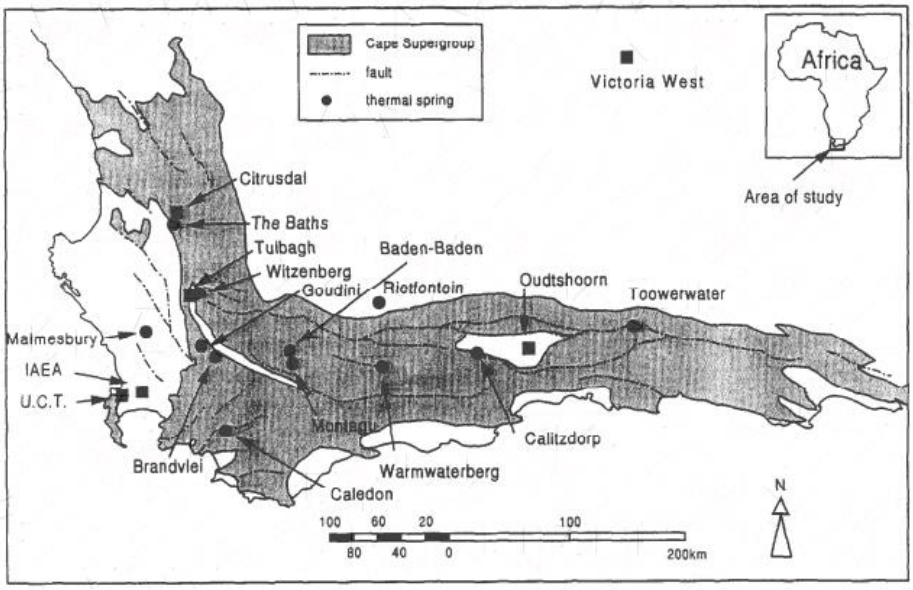

Figure 14 – 11 thermal springs in relation to the Cape Supergroup; large faults in the Western Cape are also displayed (Diamond and Harris, 2000).

2.5.3.3 Recharge and Discharge

Groundwater recharge generally occurs through the infiltration of precipitation within the higher elevated areas (maximum elevation of ~2 300m) of the Cape Fold Belt (CFB) in the hinterland to the City of Cape Town which extends to the north and east around the CFB syntaxis (Fig. 12) (Diamond, 2014; Xu et al., 2009). Depleted isotopic signatures of stable hydrogen and oxygen further substantiates that precipitation of the TMG Aquifer occurs at high altitudes (Diamond and Harris, 2000). Recharge from precipitation at the water table varies seasonally. This is due to seasonal variation in evapotranspiration, which can intercept infiltrating precipitation (Netili, 2007). Research shows that recharge in this aquifer is also influence by snowmelt to some extent. This, however, is only present in catchments with elevations higher than 1 000 m (Wu and Xu, 2005).

Various methods to determine recharge within the TMG found infiltration into the aquifer ranged from 0 – 57% of mean annual precipitation (MAP) (Parsons, 2002; Watson et al., 2018). Low recharge estimates were obtained in low lying regions which receive less rainfall and have reasonably thick soil cover whereas higher recharge estimates were calculated in mountainous regions with exposed rock (Hartnady and Hay, 2002a; Parsons, 2002). It has been recognised that recharge to the Peninsula and Nardouw Formations occurs at different rates (Kotze, 2000). Geology of the Peninsula Aquifer is generally located at higher elevations which receive higher volumes of precipitation. This coupled with the highly weathered and

fractured nature of the brittle sandstones, results in the Peninsula Aquifer receiving higher amounts of recharge (Shand, 2004). In contrast to the Peninsula Aquifer, the Nardouw Aquifer is characterised by a lower fracture frequency and more ductile nature due to the presence of thicker shale layers (Kotze, 2002a). The Nardouw Formation generally outcrops at lower elevations and receives much less direct recharge. Despite this, a considerable amount of indirect recharge is estimated to be sourced from the Peninsula Aquifer via fractures connecting the two aquifers (Watson et al., 2018). Due to the favourable outcrop and nature of the rocks, recharge is relatively high, reaching average rates of up to 15% of MAP for the superaquifer (Meyer, 2002).

Groundwater flows along the fracture network toward lower lying or discharge areas. Discharge from the TMG Aquifer is usually in the form of seep zones, wetlands, seasonal low flow and perennial cold springs in cases of shallow circulating groundwaters or thermal hot springs for groundwater circulating at depth (Netili, 2007). Where shallow water-bearing fractures intersect the surface, groundwater discharges as springs. Flow rates are likely to be fast and storage limited (Le Maitre et al., 2002). Discharge from deeper sources occur along the contact between the TMG and the relatively impermeable shales (e.g. Nardouw-Cedarberg contact) as well as between the faulted contact with the basement rocks (Malmesbury, Cape Granite Suite). These deep flow systems are likely to be higher yielding, with greater storage volume in the fractures and faults (Le Maitre et al., 2002).

2.5.4 Bokkeveld Aquifer

Much like the Witteberg Aquifer, the Bokkeveld Group forms a secondary fractured aquifer. The Bokkeveld shales which extend over much of the central Klein Karoo, experience low recharge volumes, typically less than 6 mm per annum (Le Maitre et al., 2009). Recharge in certain regions of the Bokkeveld Aquifer are thought to be from the fractures connecting the Bokkeveld to the TMG (De Beer, 2002b). The contact between the Bokkeveld and the TMG Groups is a zone of high hydraulic conductivity and provides a mixing conduit for deep-seated older groundwater and water that has been more recently recharged (Weaver et al., 1999). Boreholes drilled into the sandstone-poor portion of the Bokkeveld Aquifer are generally low-yielding as yields are typically less than 1 L/s. The sandstone-rich Ceres Subgroup, however, possesses formations with higher yields (5 L/s) and permeabilities (Meyer, 2002; Le Maitre et al., 2009). EC is generally variable and ranges between 300 and 4 000 µS/cm for the Ceres

Subgroup whereas groundwater EC of the Bidouw Subgroup is often in excess of 4 000 µS/cm (Netili, 2007). Groundwater in the Bokkeveld Aquifer is typically classified as Na-Cl-type (Netili, 2007).

2.5.5 Witteberg Aquifer

The Witteberg Group has low primary permeability and porosity and is generally considered an aquitard. The Witteberg forms a secondary fractured aquifer and groundwater flow and storage are controlled through fracture and fault systems; these open fractures can store reasonably large volumes of water however they only constitute a small portion of the total rock volume (Le Maitre et al., 2009). Analysis of borehole yields drilled into various units of the aquifer found that 30% of boreholes yield less than 0.5 L/s whereas only 26% yield more than 5 L/s (Meyer, 2001; Netili, 2007). Shale units within the Witteberg Aquifer typically possess brackish groundwater with EC values between 2 000 and 7 000 µS/cm, whereas groundwater within the sandstone units are generally of better quality and have EC values ranging from 700 – 1 500 µS/cm (Netili, 2007).

2.5.6 Alluvial Aquifer

The main alluvial aquifer of interest within the study site is the Cape Flats Aquifer (CFA) (Fig. 15). The CFA covers an area of approximately 630 km^2 and is composed of unconsolidated coarse-grained materials, such as sand and gravel, with areas dominated by silt and clay lenses (Harris et al., 1999; Adelana et al., 2006). The alluvium is typically horizontally stratified and several lithostratigraphic units can be recognised (Adelana and Xu, 2006). The aquifer material is well sorted and rounded resulting in hydraulic conductivities of 30 – 40 m/d in the central region and 15 – 50 m/d in the eastern area (Gerber, 1981). Groundwater typically flows in a semi-radial pattern from the higher lying basement in the northeast (near Durbanville), towards Table Bay to the northwest and the False Bay coast to the south (Hay et al., 2015). Groundwater recharge is estimated to be in the range of 16 – 37% of MAP (Adelana et al., 2010), however, it is estimated that 28 x 10^6 m^3 of groundwater is lost to the sea through seepage (Tredoux, et al., 1980).

The CFA is predominantly unconfined with a generally shallow water table (average depth 3.75 m below surface) (Harris et al., 1999). It is likely that rivers and wetlands are hydraulically connected to the relatively shallow aquifer (Hay et al., 2015), however there is no

hydrogeological link to any other aquifer, except to the talus/scree material along the foot of the mountains in the west (Wright & Conrad, 1995). The groundwater chemistry of the aquifer is quite variable as groundwater collected from the aquifer ranges from freshwater to brackish (Aza-Gnandji et al., 2013). The Cape Flats is a low-lying region and therefore, difficult to drain, which could lead to possible soil salinization (Adelana et al., 2006).

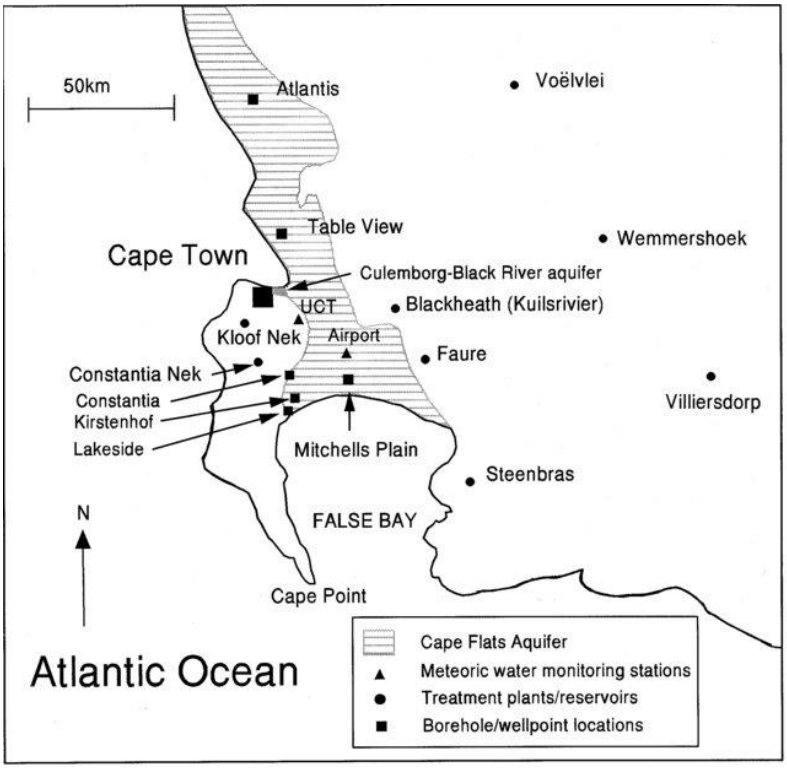

Figure 15 – The Cape Flats Aquifer in relation to the City of Cape Town and a few dams which supply municipal water (Harris et al., 1999).

3 METHODOLOGY

A detailed approach regarding the sampling procedures and analytical techniques that have been used in this study, are given in the sections below. As it is imperative that the groundwater not be exposed to the atmosphere for any of the isotope tracers used in this study, only capped boreholes and springs were sampled for this project. Atmospheric contamination during sampling is the biggest concern during sampling hence limitations to the sampling protocol are addressed as well.

3.1 Sample Sites

Sampling was primarily focused within a 200 km range from Cape Town and comprised of three campaigns during 2018 – 2019 which concluded in May 2019. Sampling was focused on boreholes drilled into the TMG as the primary target. However, for comparability, groundwater samples were taken from boreholes, well points and springs in the Malmesbury, Cape Granite Suite, TMG, Bokkeveld, Witteberg Groups as well as from Quaternary sediments. Collectively, 150 samples were taken from 73 sites across the Western Cape (Fig. 16). This can further be divided into 28 noble gas, 59 tritium and 64 radiocarbon samples. $\delta^{13}C$ was collected from sites where radiocarbon was sampled.

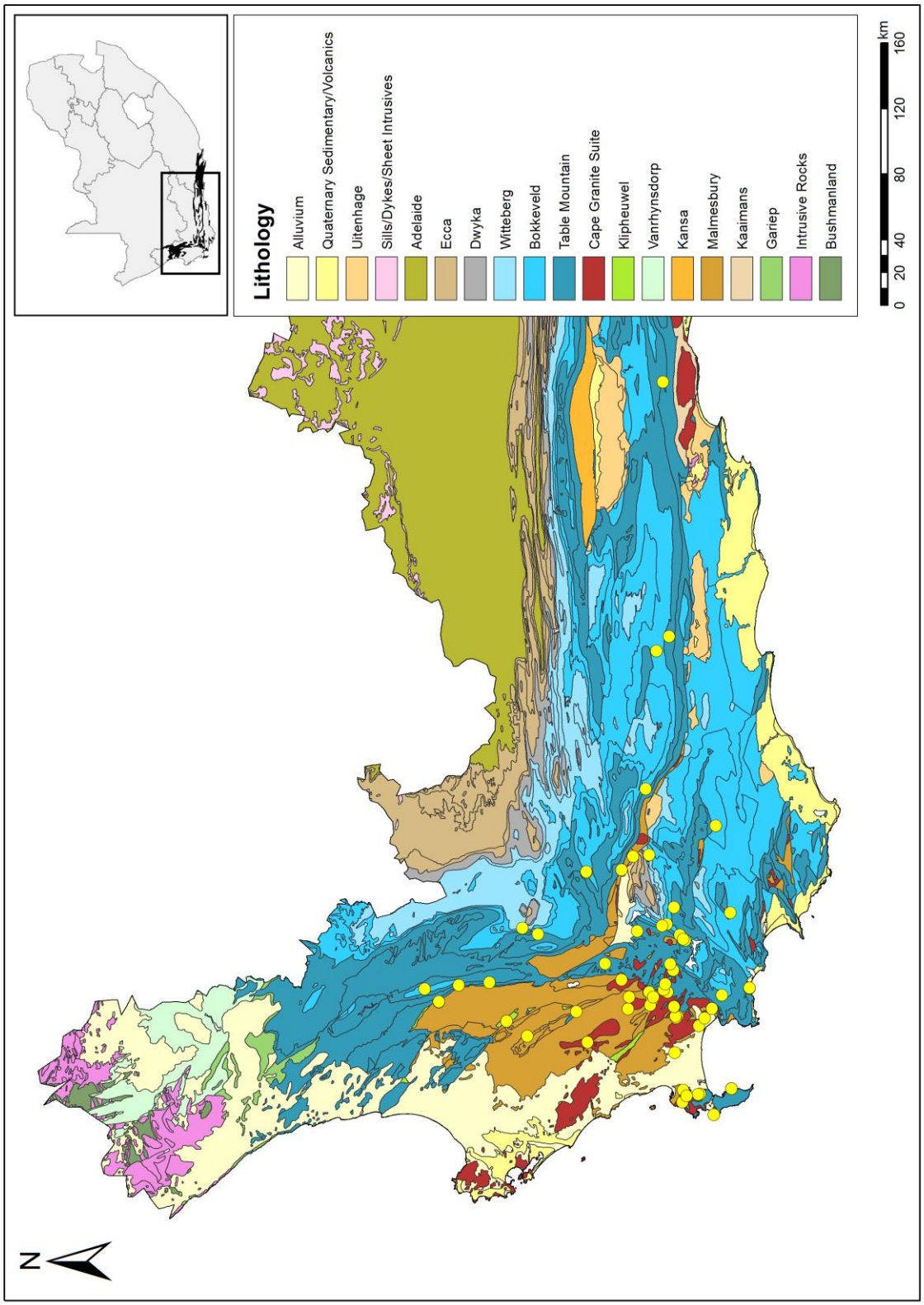

Figure 16 – Simplified geological map including sample collection sites (yellow) across the Western Cape, South Africa.

3.2 Sampling Protocol

3.2.1 Tritium and Tritogenic Helium

With sampling for noble gases, it is essential that all air is excluded from the collection system. The collection system consists of a piece of copper tubing (1 m or 0.4 m), with a 9.8 mm diameter and 1.2 mm wall thickness, two aluminium clamps and a mounting rack. The clamps are placed on either end of the tube and mounted in the mounting rack (Fig. 17). The clamps are tightened such that they hold tight to the copper tube, keeping it in position, but do not compress the copper tube.

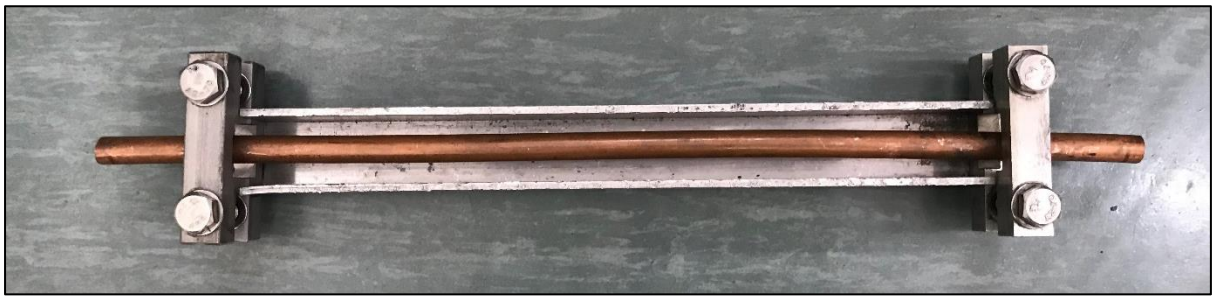

Figure 17 – 40 cm copper tube (in which the noble gas will be collected) placed in the metal mounting rack, secured on either end with aluminium clamps.

After the borehole has been purged to ensure that fresh groundwater is being accessed, it is suggested that the pressure be adequately lowered during sampling to prevent tiny bubbles in the flow stream that may accompany turbulent flow. One end of the copper tube is then attached to the water source and the water to be sampled is allowed to run through the copper tube. The copper tube is repeatedly tapped to ensure that all air bubbles exit the tube. Thereafter, the clamp on the free end of the copper tube is tightened such that it is flush with the washers in the clamps and no water or air can penetrate the tube. The tube is now sealed at the free end with the water backing up inside the tube (Fig. 18). The clamp at the end of the tube connected to the water source is then tightened in the same way such that the copper tube is now sealed with the tube between the two clamps filled with water and no air bubbles are present (Fig. 19). 0.4 m copper tubes are collected in duplicate whereas 1 m copper tubes only require a single sample. In addition to the copper tubes, 500 ml of groundwater is also collected in an HDPE bottle to determine tritium activity (Fig. 20).

Figure 18 – A) After the copper pipe is attached to the water source; B) the clamp at the free end of the copper tube is tightened first allowing the water to back up inside the tube.

Figure 19 – A) The clamp nearest to the water source is clamped last resulting in a copper tube filled with water that has not been exposed to air; B) example of a copper tube sample crimped between aluminium clamps.

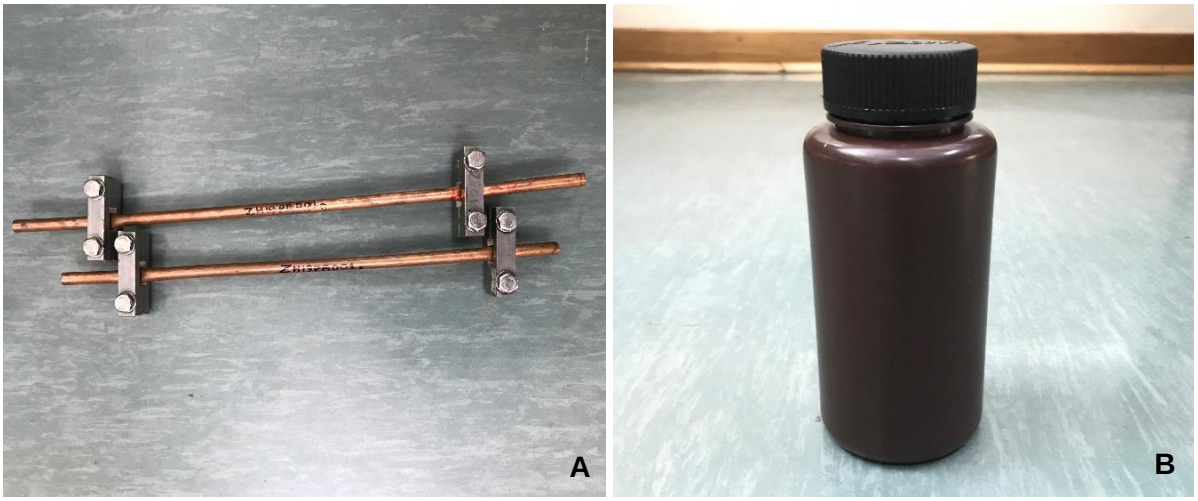

Figure 20 – Samples required for the analysis of $^{3}H/^{3}He$ ratios; A) two copper tubes for noble gas concentrations and B) a 500 ml HDPE bottle for tritium activity.

In order to isolate the groundwater from the atmosphere before sample collection, an outlet device was designed (Fig. 21). The outlet device is comprised of three main components: an inlet connection, a hose and an outlet tap. The inlet connection should be able to connect to as many borehole pipes as possible. Adapters of varying sizes can be attached to this end. A ball-valve tap is attached at this end to ensure that the water pressure can be adjusted. Then, a hose just wide enough to house the copper tube should be incorporated. Finally, a tap at the outlet end of the device is able to allow water to exit the device. It is important to note that once the copper tube gets sealed off at the free end, pressure will begin to build inside the device. To prevent the copper tube from shooting out of the hose, pressure can be alleviated by opening the outlet. As the main function of this device is to be airtight, it is crucial that all components are screwed in properly and tightened.

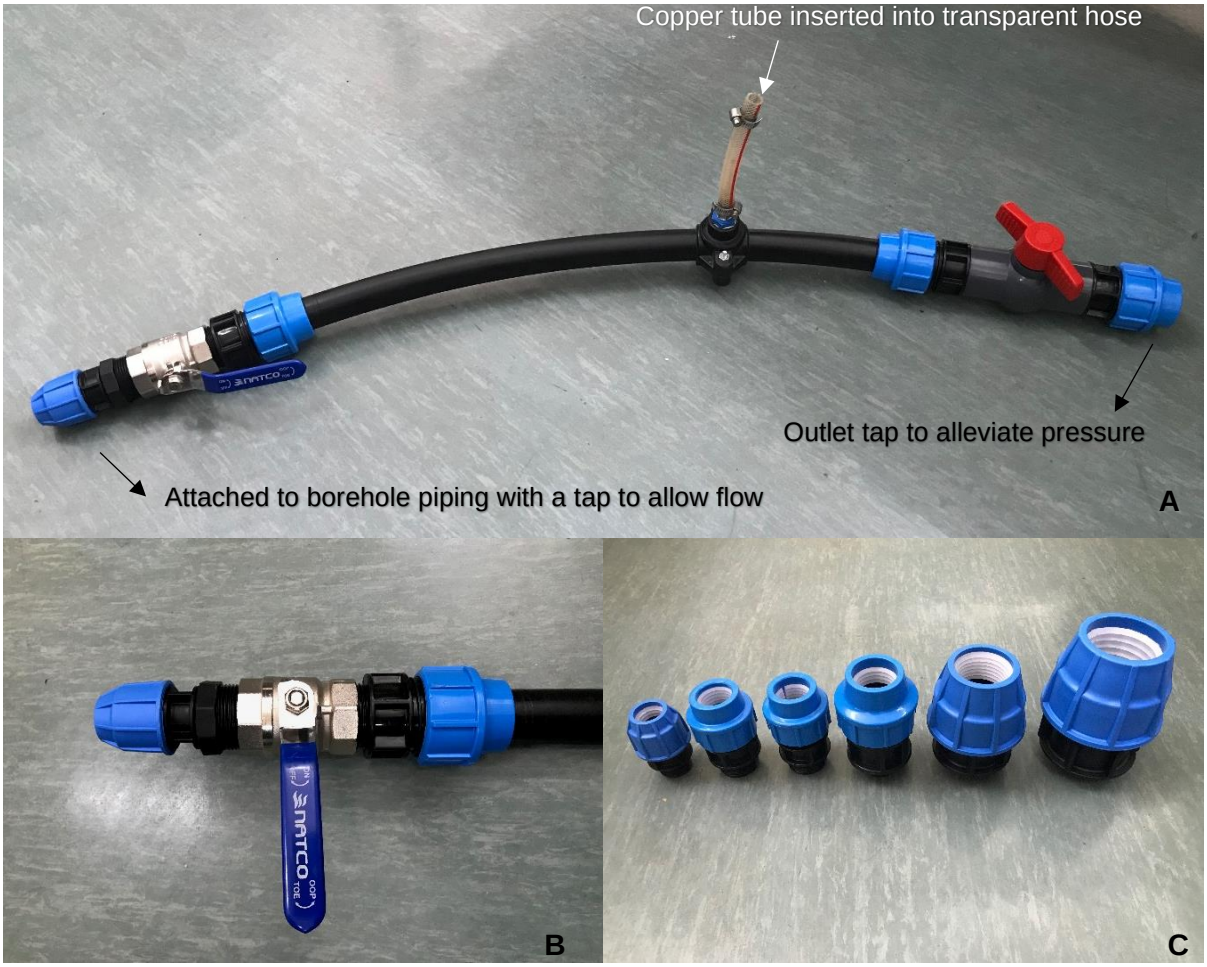

Figure 21 – A) – Explanation of the mechanisms of the refined outlet device fashioned for this project; B)) end of the outlet device that is able to attach to the borehole; C) multiple bushings can be attached to externally or internally threaded borehole pipes, it can also be accommodated to smooth piping as well.

3.2.2 Radiocarbon

Groundwater samples for radiocarbon dating were collected in a 500 ml opaque HDPE bottle. Before collection, the borehole is “purged” by allowing the pump to run for a sufficient amount of time to ensure that sample is directly from the aquifer rather than stagnant water in the piping. The bottle is then rinsed with the groundwater ensuring the inside of the bottle has been thoroughly flushed. When collecting the sample, it is important to ensure that the water enters the bottle with laminar flow to prevent atmospheric exchange. The contents are allowed to fill the sampling bottle 2 – 3 times over, then filled to the brim and sealed.

3.2.3 δ^{13}C-DIC

Samples for $\delta^{13}C$ are collected in 50 ml centrifuge tubes. The tubes are first rinsed with the water to be sampled and subsequently filtered with a 0.45 µm cellulose acetate filter before sample collection. It is important to exclude any air bubbles from the tube during collection.

3.3 Sampling Limitations

After extensive field work, it is apparent that there is a need for regulation in borehole infrastructure on a national level. Despite the fact that national legislation is in place which requires regular monitoring of groundwater levels and chemistry of licensed boreholes, it is not generally enforced. Many boreholes did not have a sampling tap or basic outlet from which to sample the groundwater as often the first ‘take-off’ point would be either after filtration or treatment or after a long run of black agricultural pipe (Fig. 22). This resulted in great effort being undertaken to disconnect infrastructure, or often resulting in no sample being collected. Industrial boreholes have also posed problems during sampling as the dimensions of the piping are often too large to attach the outlet device and the water pressure in the pipes are very high. Where possible, a thin pipe was screwed into the pressure gauge opening and then attached to the outlet device (Fig. 23). Despite the fact that it takes the outlet device some time to fill up, it continues to isolate the groundwater from the atmosphere before sampling. The borehole is always adequately purged before attaching the piping.

Figure 22 – Borehole infrastructure has no easily accessible outlet from which to collect a sample resulting in connections having to be removed.

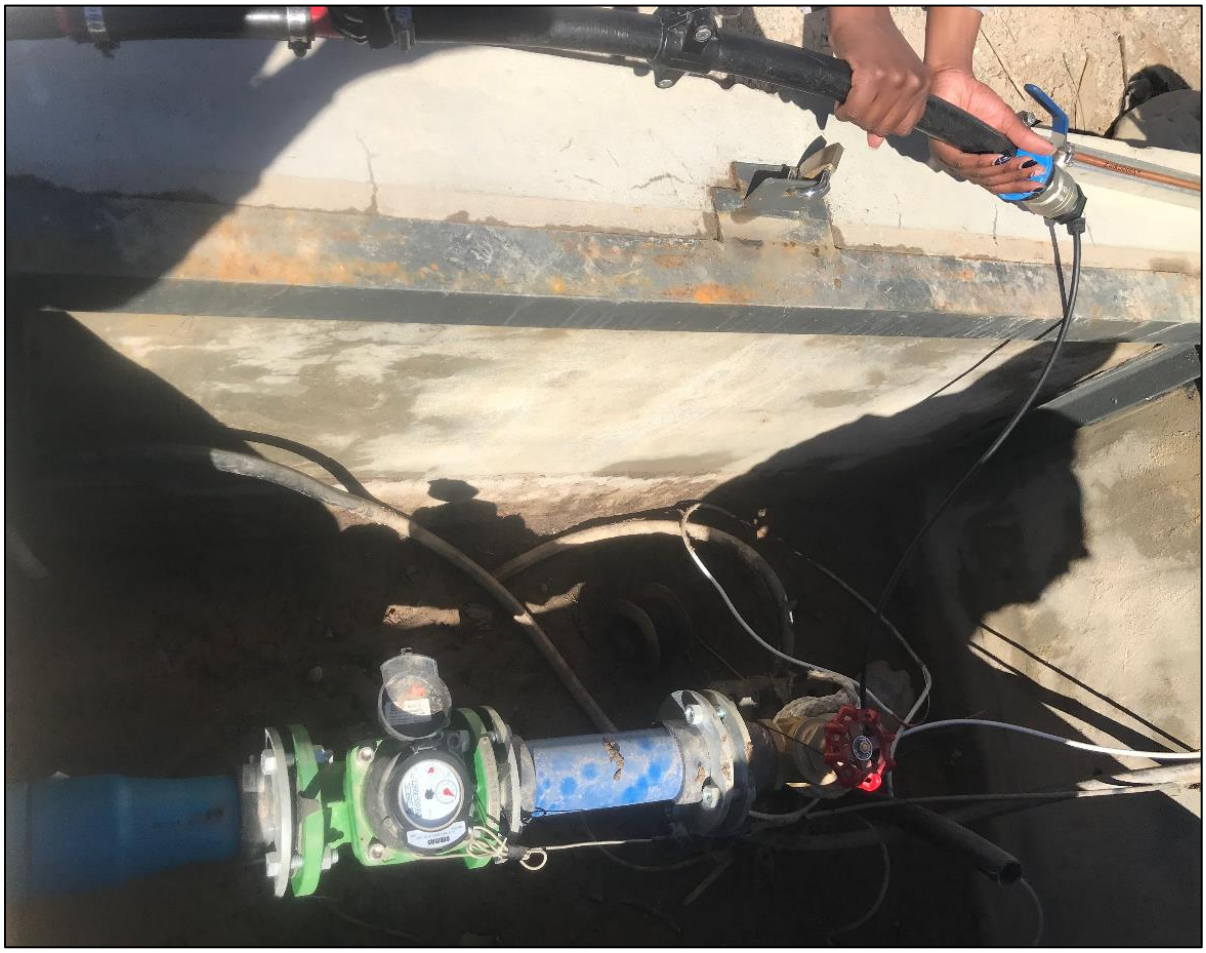

Figure 23 – A thin pipe connects the outlet device to the borehole through the pressure gauge opening.

3.4 Analytical Techniques

3.4.1 EC, pH, Alkalinity

EC, pH and alkalinity were analysed on the day of sample collection at the Department of Soil Sciences at Stellenbosch University. EC was analysed on a Eutech Con700 and pH was measured on a Eutech pH700. Alkalinity is measured on a Metrohm 702 SM Titrino. Both before and after 10 ml of sample is titrated with 0.01 M of HCl acid until buffering capacity is reached, pH readings of the sample are taken. Once samples have reached buffering capacity, the volume of acid used for titration is returned. Values are plugged into Equation 7 below to determine alkalinity:

$$Alkalinity\ \left(\frac{mg}{L}\right) = \frac{Vol\ of\ titrant\ x\ Normality\ of\ acid}{Vol\ of\ sample}\ x\ 50\ 000 \qquad \text{(Eq. 7)}$$

3.4.2 Tritium and Tritogenic Helium

Tritium and helium isotope ratios are analysed at the Isotope Climatology and Environmental Research Centre (ICER) of the Institute for Nuclear Research in Debrecen, Hungary. Concentrations and isotope ratios of He as well as Ar, Kr, Ne and Xe are measured using a noble gas mass spectrometric system comprised of a cryogenic preparation line and a VG5400 noble gas mass spectrometer (MS) following the set-up outlined by Papp et al. (2012) (Fig. 24). Dissolved gases in the groundwater samples are extracted from the copper tube on a preparation vacuum line by means of a cryogenic cold system consisting of two cold traps and a getter trap. Ar and other chemically active gases (N_2, CO_2, etc.) are adsorbed in an empty trap at 25 K. Subsequently, Ne and He are adsorbed in a charcoal trap at 10 K. He is desorbed at 42 K and Ne at 90 K. These temperature controls allow for the two gases to be admitted to the mass spectrometer separately (Papp et al., 2012). Once He enters the mass spectrometer, the magnet in the MS chamber separates ^{3}He into a SEM (secondary electron multiplier) and ^{4}He into the Faraday Cup. The heavier noble gasses are then released from the stainless-steel trap and measured simultaneously in the VG5400 noble gas mass spectrometer. Fast calibrations with known air aliquots of He, Ne and air are performed

between analyses by the VG5400 mass spectrometer. $^{3}He/^{4}He$ ratios are expressed as R/R_a values where R represents the measured $^{3}He/^{4}He$ ratio of a sample in ratio to R_a, the $^{3}He/^{4}He$ ratio of the atmosphere. Consequently, R/R_a values tending to 1 indicate samples with $^{3}He/^{4}He$ samples with concentrations similar to that of the atmosphere. The VG5400 has an analytical uncertainty of 1% for He and Ar concentrations, 2% for Ne, Kr and Xe and 2,5% for $^{3}He/^{4}He$ ratios.

Tritium analysis is conducted on a Helix SFT mass spectrometer with a sensitivity of 0.02 TU. Tritium is measured through the ^{3}He ingrowth method with ^{4}He isotope dilution (further discussed in Papp et al., 2012). The sample is first distilled into glass flasks, then degassed via vacuum pumping to ensure the removal of dissolved gasses. The sample is then stored in metal bulbs for a certain period of time to allow ^{3}He to accumulate in the water through tritium decay. Finally, the helium fraction that has formed is admitted to the noble gas mass spectrometer to measure the ^{3}He activity. The tritium concentration of the sample is calculated using the measurement of helium isotopes.

Figure 24 – Helix SFT mass spectrometer which separates ^{3}He into a SEM (left arm) and ^{4}He into the Faraday Cup (collector on middle right of figure).

3.4.3 Radiocarbon

Radiocarbon activity is measured using the EnvironMICADAS accelerated mass spectrometer (AMS) at the Isotope Climatology and Environmental Research Centre (ICER) of the Institute

for Nuclear Research in Debrecen, Hungary. Radiocarbon is analysed through the graphitization of the dissolved inorganic carbon in the sample and the subsequent mass spectrometric analysis of the graphite. At ICER, the preparation of water samples is dependent on carbon content as low dissolved carbonate content (LDC) samples are prepared differently than high dissolved carbonate content (HDC) (Molnár et al., 2013). Before sample preparation, the carbon content per sample was determined by the following equation:

*Carbon content (mg) = Measured alkalinity (HCO_3, CO_3) * 0.6 *12 / molar mass of HCO_3 * 0.500 L*

3.4.3.1 Low dissolved carbonate content (LDC) samples (< 0.5 mg C)

LDC samples can be treated in one of two ways. In the first method, up to 500 ml of water is transferred to a 1 000 ml flask and then closed with a dry-ice trap attached to the top of the flask. The entire sample is quickly removed via vacuum pumping. 5 ml of 85% phosphoric acid is injected into the sample and magnetically stirred. CO_2 produced from the sample can then be admitted to the combustion line. In the second method, 0.5 g of 40 M NaOH is added to each 500 ml sample in order to increase its pH to ± 11. 6 – 7 ml of $BaCl_2$ is added to the solution in order to precipitate $BaCO_3$ and $BaSO_4$ (Fig. 25). The precipitate that has collected is rinsed in order to achieve a neutral pH. The precipitate is then centrifuged for 2 minutes at 3 600 rpm and dried. This precipitate is then transferred to a flask and treated with phosphoric acid. The resultant CO_2 can be admitted to the combustion line.

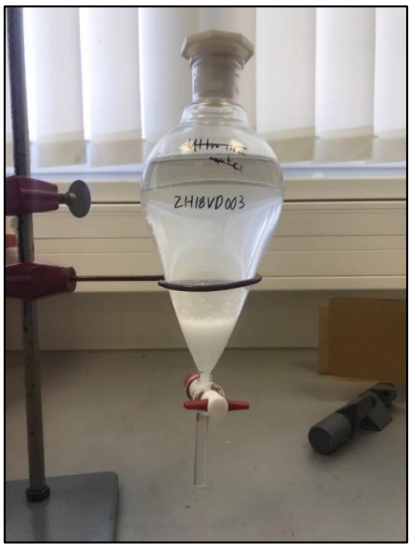

Figure 25 – $BaCO_3$ and $BaSO_4$ forming a white precipitate from groundwater sample ZH18VD003.

3.4.3.2 High dissolved carbonate content (HDC) samples (> 0.5 mg C)

10 – 20 ml of HDC sample is transferred to a closed 70 ml reaction cell already containing 3 ml of 85% phosphoric acid and subsequently heated at 75°C for one hour in order to facilitate the liberation of CO_2 gas from the dissolved carbon. The CO_2 is then separated from water at -78ºC and finally trapped at cryogenic temperature. The CO_2 gas – obtained by the various preparation methods described above – is transferred to a sealed quartz tube containing 10 mg titanium hydride, 60 mg zinc and 4.5 mg of powdered iron in order to be graphitized. This test tube is heated for three hours at 500°C to liberate hydrogen followed by five hours at 550°C in an oven to facilitate graphitization. A “magazine” containing 22 target holders, each containing a graphite sample, is then admitted to the AMS. ^{12}C, ^{13}C and ^{14}C are measured simultaneously. Groundwater samples are analysed with two standards, a blank standard and a known carbon concentration standard. Analysis is repeated and average values based on the two runs are used for calculations. Statistics are also automatically run during analysis to remove any outliers. Radiocarbon activities are reported as percent of Modern Carbon (pMC) and modern samples have an uncertainty of < 3% (Molnár et al, 2013).

3.4.4 $\delta^{13}C$-DIC

Prior to analyses, $\delta^{13}C$ samples were stored at 4°C until analysis could take place. $\delta^{13}C$ analyses are conducted on a Gas Bench II (Thermo Finnigan) Delta Plus XL at the University of Lausanne, Switzerland. For groundwater samples, the sample block is kept at room temperature (15°C). 10 drops of 85% H_3PO_4 is added to an empty vial which is then sealed. Sample vials are purged to allow air in the vial to be replaced with helium. Once purging is complete, groundwater samples are added to the vial via a clean syringe. Samples with EC values greater than 80 µS/cm require dilution with distilled water but no less than 0.3 ml of sample can be used for analysis. CO_2, which is produced in a reaction between DIC in water and H_3PO_4, is analysed. Sample sequences are analysed against standards of Carra Marble ($\delta^{13}C$ = 2.05% VPDB). $\delta^{13}C$ of DIC is reported against the standard of VPDB (Vienna Pee Dee Belemnite) in parts per mille (‰).

3.4.5 Total Carbon

Groundwater samples were measured for total carbon (TC), total inorganic carbon (TIC), total organic carbon (TOC) and non-particulate organic carbon (NPOC) using the LiquiTOC system at the University of Lausanne, Switzerland. High EC samples are diluted with distilled water, due to instrument sensitivity. The dilution factor for samples with EC values between 500 and 1 000 µS/cm is 2x, and 5x for samples with EC values >1 000 µS/cm. 20 ml of sample is placed in a glass vial, covered with foil and refrigerated until analysis can take place. Analysis is conducted through the oxidation of carbon at 750°C and the subsequent detection of CO_2 by an NDIR (non-dispersive infrared) photometer with a detection limit of 0.5 ppm.

3.5 Assigning Samples to Aquifer Type

Before any results can be reported, classification of samples into their respective aquifers is imperative in order to make deductions about the different aquifer. Samples were classified following the methods outlined by Agyare-Dwomoh (2020) and Costaras (2019). Samples were initially classified by the geological group/formation provided by the property owners/managers. This approach was coupled with the use of borehole coordinates and depths overlain on geological outcrop shapefiles, courtesy of the Council for Geoscience. These assumptions were then confirmed through the characterisation of ^{222}Rn and $^{87}Sr/^{86}Sr$ ratios in groundwater. Each aquifer has distinctive ranges for each of the isotopic tracers (Agyare-Dwomoh, 2020; Costaras, 2019).

^{222}Rn is derived from the decay of U- and Th-bearing minerals in rocks and as a result, tends to have higher concentrations in granite-hosted aquifers like that of the Cape Granite Suite (CGS). Although granitic rocks often do not store or transmit water, the Cape Granite Suite has been extensively fractured, resulting in the formation of a low-yielding aquifer. The study by Agyare-Dwomoh (2020) found that radon concentrations in the CGS reached levels of 370 Bq/L whereas concentrations in sandstone units were significantly lower. The TMG and Bokkeveld Aquifers had average radon concentrations of 35 (1σ = 39) and 48 (1σ = 52) Bq/L, respectively; a single Witteberg Aquifer sample was measured at 12 Bq/L. Radon concentrations in the alluvial aquifers were highly variable and ranged from 3 – 653 Bq/L ($\bar{x}$ = 127). Groundwater from the Malmesbury Aquifer had an average radon concentration of 70 Bq/L (σ = 53).

^{87}Sr, which is formed through the decay of ^{87}Rb, is present in most silicate minerals and can be used to track the interaction of groundwater with the aquifer host and the mixing of ground and surface water. Costaras (2019) found that groundwater from the TMG Aquifer had $^{87}Sr/^{86}Sr$ ratios clustering at approximately 0.71000 whereas the CGS had values ranging from 0.72500 – 0.73000. Groundwater sampled from the Malmesbury Aquifer had ratios between 0.71500 – 0.73000. Although similar to that of the CGS, the Malmesbury samples have distinctly different groundwater chemistries.

In both studies by Agyare-Dwomoh (2020) and Costaras (2019), basic cations and anions provided insight into classification as most of the aquifers tend to have distinctive basic chemistry (Appendix I). The TMG Aquifer is characterised by low concentrations of Na^+ (<84 mg/L) and Cl^- (<160 mg/L). The Malmesbury Aquifer is associated with elevated HCO_3^- concentrations as high as 260 mg/L. The alluvial aquifers are often challenging to identify as they often have variable chemistry ranging from very good quality, which is similar to that of the TMG, to poorer quality with elevated HCO_3^- and SO_4^{2-} concentrations. Groundwater samples from the Bokkeveld Aquifer possessed the highest SO_4^{2-} concentrations (281 mg/L), but it is uncertain whether or not this is solely due to the host rock. The Witteberg Aquifer is associated with higher Ca^{2+}, Mg^{2+} and HCO_3^- concentrations compared to any other aquifer systems sampled. The CGS, however, did not seem to possess any distinctive trends with regards to its basic geochemistry. The most distinctive parameter appears to be the total ionic concentration (TDS). The TMG Aquifer is typically characterised by concentrations less than 100 mg/L which clearly sets it apart from the other aquifers (Turner, 2018).

As the sample set overlaps with that of Agyare-Dwomoh (2020) and Costaras (2019), samples were classified using the above parameters. Due to the dataset size and areal extent thereof, samples were classified into aquifer systems rather than subaquifers in order to make further interpretations. On the basis of the above, the sample sites were thus classified into the six aquifers as follows: the alluvial, Witteberg, Bokkeveld, TMG, Cape Granite Suite and Malmesbury Aquifers. Results are presented per aquifer in the subsequent sections. Although 28 noble gas, 59 tritium and 64 radiocarbon samples were collected (Sect. 3.1), a number of samples could not be analysed due to analytical limitations, and were subsequently categorised as lost. The final sample distribution is tabulated below (Table 4) and overlap between samples are presented in Table 5.

Table 4 – The final distribution of samples collected from the six aquifer systems in the study site.

Aquifer	^{3}H	^{3}He	^{14}C	$\delta^{13}C$
Alluvial	6	5	6	8
Witteberg	1	1	1	1
Bokkeveld	6	2	5	6
TMG	26	14	13	34
CGS	9	2	8	10
Malmesbury	4	4	6	8
	52	28	39	67

Table 5 – Isotope tracers collected from the sample sites classified into their respective aquifers.

Sample Name	Aquifer	^{3}H	^{3}He	$\delta^{13}C$	^{14}C
ZH18-SU001	Alluvial	x	x	x	x
ZH18-SU002	Alluvial	x	x		
ZH18-SU003	Alluvial	x	x		
ZH18-SW001	Alluvial	x	x	x	x
ZH18-SW002	Alluvial	x	x	x	x
ZH19-CPT001	Alluvial			x	
ZH19-CPT004	Alluvial			x	
ZH19-KR001	Alluvial			x	x
ZH19-STB001	Alluvial	x		x	x
ZH19-STB002	Alluvial			x	x
ZH18-ROB001	Witteberg	x	x	x	x
ZH18-BD001	Bokkeveld	x	x	x	x
ZH18-C001	Bokkeveld	x	x	x	x
ZH18-MON001	Bokkeveld	x		x	x
ZH19-CAL001	Bokkeveld	x		x	x
ZH19-CAL002	Bokkeveld	x		x	x
ZH19-VD005	Bokkeveld	x		x	
ZH18-BD002	TMG	x	x	x	x
ZH18-C002	TMG	x	x	x	x
ZH18-DB002	TMG	x	x	x	
ZH18-DB003	TMG	x	x	x	
ZH18-DB004	TMG	x	x	x	
ZH18-DD001	TMG	x	x	x	x
ZH18-DD002	TMG	x	x	x	x
ZH18-FH001	TMG	x	x	x	x
ZH19-FH004	TMG	x		x	
ZH19-FH009	TMG			x	
ZH18-GRB001	TMG	x	x	x	
ZH18-PE001	TMG	x	x		
ZH18-VD001	TMG	x		x	x
ZH18-VD002	TMG	x	x	x	x
ZH18-VD003	TMG	x	x	x	x
ZH19-VD004	TMG	x	x	x	
ZH19-VD006	TMG	x		x	
ZH19-BK002	TMG	x		x	

Table 5 Continued.

Sample Name	Aquifer	^{3}H activity	^{3}He	δ^{13}C VPDB	^{14}C activity
ZH19-CD001	TMG			x	x
ZH19-CD002	TMG	x		x	
ZH19-CD003	TMG	x		x	
ZH19-CD004	TMG	x		x	
ZH19-CPT002	TMG			x	
ZH19-CPT003	TMG			x	x
ZH19-CPT005	TMG			x	
ZH19-CPT006	TMG			x	
ZH19-KM001	TMG			x	
ZH19-KM002	TMG			x	
ZH19-KM003	TMG			x	
ZH19-NY001	TMG	x		x	x
ZH19-PV002	TMG	x		x	
ZH19-RV001	TMG	x		x	
ZH19-SW003	TMG	x		x	x
ZH19-TM001	TMG			x	
ZH18-KB001	TMG	x	x	x	x
ZH18-FH003	Granite	x		x	x
ZH19-BK001	Granite	x		x	x
ZH19-FH005	Granite	x		x	x
ZH19-FH006	Granite			x	
ZH19-FH007	Granite	x		x	x
ZH19-FH008	Granite	x		x	x
ZH19-MAL001	Granite	x		x	x
ZH19-W001	Granite	x		x	
ZH18-KB002	Granite	x	x	x	x
ZH18-R001	Granite	x	x	x	x
ZH18-DB001	Malmesbury		x	x	
ZH18-DK001	Malmesbury	x	x	x	x
ZH18-FH002	Malmesbury	x	x	x	x
ZH18-PV001	Malmesbury	x	x	x	x
ZH19-MB001	Malmesbury	x		x	x
ZH19-PAA001	Malmesbury			x	x
ZH19-RBK001	Malmesbury			x	
ZH18-SV001	Malmesbury			x	x

4 RESULTS

As discussed in section 3.5, the samples have been divided into the six aquifers. The alluvial samples are represented by yellow circles, the Witteberg by grey circles, the Bokkeveld by green triangles, the TMG by blue diamonds, the CGS by red triangles and the Malmesbury by orange squares. All results are presented per aquifer in the section below following this symbol classification.

4.1 Field Chemistry

4.1.1 Electrical Conductivity (EC)

The TMG Aquifer has an average EC of 210.3 µS/cm, but ranges from 12.6 – 2570.0 µS/cm (n = 35). A few coastal samples have elevated EC values that are not generally associated with the aquifer, particularly samples from Kleinmond (KM001 – KM003) and Cape Town (CPT003, CPT005 and CPT006). Generally, groundwater EC values for the TMG Aquifer are lower and less variable than the other aquifers (Table 6). Groundwater from the alluvial aquifers range from 195.5 – 951.0 µS/cm ($\bar{x}$ = 531.4; n = 10). The Stellenbosch samples (SU001 – SU003 and STB001 – STB003) have lower EC values compared to samples from Kuils River (KR001) and the coastal towns of Somerset West (SW001 and SW002) and Cape Town (CPT001 and CPT004). The CGS Aquifer has EC values between 40.9 – 1 074.0 µS/cm ($\bar{x}$ = 365.9; n = 10). EC values from the Franschhoek (FH003, FH005 – FH008) and Bainskloof area (BK001) are 150 µS/cm or below whereas other granitic samples are higher. EC ranges from 63.7 – 1 753.0 µS/cm ($\bar{x}$ = 603.3; n = 8) in groundwater from the Malmesbury Aquifer. The Bokkeveld Aquifer has the highest EC values, ranging between 135.2 – 2 970.0 µS/cm ($\bar{x}$ = 1 272.3; n = 6). Conductivity for the Witteberg Aquifer was measured at 2 500 µS/cm.

4.1.2 Alkalinity

Groundwater samples from the TMG are characterised by significantly lower alkalinity values than the other aquifers. A number of samples had no measurable alkalinity and are recorded as 0 mg/L in Table 6 below. The maximum recorded alkalinity for the TMG Aquifer was 42.2 mg/L ($\bar{x}$ = 6.1). Samples from the alluvial and CGS Aquifers have similar alkalinity values to the TMG Aquifer, ranging from 4.6 – 50.3 ($\bar{x}$ = 25.1) and 2.6 – 47.9 mg/L ($\bar{x}$ = 17.5), respectively. Samples from the Malmesbury, Bokkeveld and Witteberg Aquifers have higher measured alkalinities. The Malmesbury Aquifer has alkalinity values ranging from 18.4 – 213.1 mg/L ($\bar{x}$ = 365.9) whereas groundwater from the Bokkeveld Aquifer has alkalinity values ranging from 41.7 – 282.9 mg/L ($\bar{x}$ = 365.9). The highest recorded alkalinity is from the Witteberg Aquifer at 426.3 mg/L.

4.1.3 pH

pH values for the entire dataset range from 3.8 – 8.0. Groundwater from the TMG Aquifer tends to be quite acidic, and has the largest range from 3.8 – 6.7 ($\bar{x}$ = 5.2). Groundwater from the other aquifers tend to be slightly more basic. pH values for the Malmesbury aquifer range from a minimum of 6.0 to a maximum of 8.0 ($\bar{x}$ = 7.0). pH values from groundwater in the Bokkeveld Aquifer range from 6.3 – 7.6 ($\bar{x}$ = 6.8). The CGS Aquifer ranges from 4.5 – 6.6 ($\bar{x}$ = 6.1). The single Witteberg sample returned a pH of 6.8. The alluvial aquifers had groundwater ranging from 5.2 – 7.1 ($\bar{x}$ = 6.0).

Table 6 – Summary of borehole parameters classified per aquifer with their associated field chemistries.

Sample Name	Area	Aquifer	Groundwater Type	Elevation	Distance from sea	Groundwater Depth	pH	Conductivity	Alkalinity
				mamsl	*km*	*m*		*µS/cm*	*mg/L*
ZH18-SU001	Stellenbosch	Alluvial	Borehole	132	18.9	47.3	5.7	196	30.9
ZH18-SU002	Stellenbosch	Alluvial	Borehole	123	18.1	51.6	5.9	385	38.9
ZH18-SU003	Stellenbosch	Alluvial	Borehole	115	18.5	59.9	6.8	304	50.3
ZH19-STB001	Stellenbosch	Alluvial	Borehole	125	19.0	48	6.1	228	8.5
ZH19-STB002	Stellenbosch	Alluvial	Borehole	127	19.6	55.6	6.1	559	30.8
ZH18-SW001	Somerset West	Alluvial	Borehole	137	4.3	50	5.3	518	14.4
ZH18-SW002	Somerset West	Alluvial	Borehole	124	5.0		5.7	734	35.0
ZH19-CPT001	Cape Town	Alluvial	Borehole	21	5.5		5.2	734	4.6
ZH19-CPT004	Cape Town	Alluvial	Borehole	14	6.5		5.7	705	8.6
ZH19-KR001	Kuils River	Alluvial	Borehole	52	17.5	30	7.1	951	28.5
ZH18-ROB001	Robertson	Witteberg	Borehole	306	82.8		6.8	2500	426.3
ZH18-BD001	Barrydale	Bokkeveld	Borehole	401	150.4	100	6.5	2970	132.7
ZH18-C001	Ceres	Bokkeveld	Borehole	1086	106.6	120	6.5	389	65.3
ZH18-MON001	Montagu	Bokkeveld	Hot Spring	262	104.7	2000	6.5	135	41.7
ZH19-CAL001	Riviersonderend	Bokkeveld	Borehole	161	63.1	90	6.3	174	43.5
ZH19-CAL002	Caledon	Bokkeveld	Borehole	246	24.9	70	7.2	2810	249.3
ZH19-VD005	Villiersdorp	Bokkeveld	Borehole	263	55.9	125	7.6	1155	282.9
ZH18-BD002	Barrydale	TMG	Borehole	568	140.7	120	5.1	101	4.0
ZH18-C002	Ceres	TMG	Borehole	1037	100.2	36	5.1	29	4.9
ZH18-DB002	Paarl	TMG	Cold Spring	252	39.3	0	5.3	57	3.5
ZH18-DB003	Paarl	TMG	Cold Spring	250	39.1	0	4.9	53	3.2
ZH18-DB004	Paarl	TMG	Cold Spring	249	39.1	0	4.9	55	3.6
ZH18-DD001	De Doorns	TMG	Borehole	541	107.3	258	5.4	25	5.4

Table 6 Continued.

Sample Name	Area	Aquifer	Groundwater Type	Elevation	Distance from sea	Groundwater Depth	pH	Conductivity	Alkalinity
				mamsl	*km*	*m*		*µS/cm*	*mg/L*
ZH18-DD002	De Doorns	TMG	Borehole	533	107.9	180	5.8	47	10.8
ZH18-GRB001	Grabouw	TMG	Borehole	301	11.2		4.6	90	3.2
ZH18-VD001	Villiersdorp	TMG	Borehole	411	43.2		5.1	91	3.7
ZH18-VD002	Villiersdorp	TMG	Borehole	668	47.3	100	5.1	100	4.4
ZH18-VD003	Villiersdorp	TMG	Borehole	377	44.5	120	5.2	80	6.0
ZH19-VD004	Villiersdorp	TMG	Borehole	1208	57.0	80	5.3	91	5.3
ZH19-VD006	Villiersdorp	TMG	Borehole	304	56.9	207	4.6	34	2.0
ZH19-BK002	Bainskloof	TMG	Borehole	287	69.1	110	5.0	47	3.7
ZH19-CD001	Citrusdal	TMG	Borehole	190	65.1	183	3.9	181	0.0
ZH19-CD002	Citrusdal	TMG	Borehole	525	59.6	180	4.5	13	1.8
ZH19-CD003	Citrusdal	TMG	Borehole	559	59.8	100	4.5	33	1.8
ZH19-CD004	Citrusdal	TMG	Hot Spring	294	70.9		5.8	20	11.8
ZH19-CPT002	Cape Town	TMG	Cold Spring	25	8.2	0	5.5	130	4.6
ZH19-CPT003	Cape Town	TMG	Borehole	20	1.9		5.7	1046	7.8
ZH19-CPT005	Cape Town	TMG	Borehole	97	0.3		5.0	489	2.1
ZH19-CPT006	Cape Town	TMG	Borehole	98	0.3		3.8	2570	0.0
ZH19-TM001	Cape Town	TMG	Cold Spring	828	2.3	0	4.3	136	0.0
ZH18-FH001	Franschhoek	TMG	Borehole	190	33.3	325	6.0	81	24.9
ZH19-FH004	Franschhoek	TMG	Borehole	340	35.5	235	6.0	61	2.2
ZH19-FH009	Franschhoek	TMG	Cold Spring	721	38.7	0	4.6	62	1.0
ZH19-KM001	Kleinmond	TMG	Borehole	36	1.0	15.5	4.9	188	1.8
ZH19-KM002	Kleinmond	TMG	Borehole	36	0.9	14	5.2	273	2.0
ZH19-KM003	Kleinmond	TMG	Borehole	33	1.1	10	5.8	380	6.4

Table 6 Continued.

Sample Name	Area	Aquifer	Groundwater Type	Elevation	Distance from sea	Groundwater Depth	pH	Conductivity	Alkalinity
				mamsl	*km*	*m*		*µS/cm*	*mg/L*
ZH18-PE001	Oudtshoorn	TMG	Borehole	628	21.3				
ZH19-NY001	Nuy	TMG	Borehole	362	94.4		6.7	122	42.2
ZH19-PV002	Porterville	TMG	Borehole	470	96.2		4.7	30	2.7
ZH19-RV001	Rawsonville	TMG	Borehole	247	64.4	12	5.8	64	7.4
ZH19-SW003	Somerset West	TMG	Borehole	42	4.2	30.8	6.3	240	8.4
ZH18-KB001	Kirstenbosch	TMG	Borehole	182	6.0	70	5.8	134	16.3
ZH19-BK001	Bainskloof	Granite	Borehole	307	58.8	28	5.8	48	11.1
ZH18-FH003	Franschhoek	Granite	Borehole	277	35.0	100	6.4	150	27.9
ZH19-FH005	Franschhoek	Granite	Borehole	182	30.9		6.5	267	12.5
ZH19-FH006	Franschhoek	Granite	Borehole	214	29.5		6.3	41	3.8
ZH19-FH007	Franschhoek	Granite	Borehole	429	21.9	51.3	6.2	109	6.8
ZH19-FH008	Franschhoek	Granite	Borehole	417	22.1	142	6.4	105	7.0
ZH19-MAL001	Malmesbury	Granite	Borehole	212	37.4	50	6.6	838	47.9
ZH19-W001	Wellington	Granite	Borehole	203	43.7	75	5.6	1074	9.4
ZH18-KB002	Kirstenbosch	Granite	Borehole	202	6.1	65	6.3	199	46.4
ZH18-R001	Paarl	Granite	Borehole	106	49.7	70	4.5	828	2.6
ZH18-DB001	Paarl	Malmesbury	Borehole	203	39.3	120	6.0	107	18.4
ZH18-SV001	Paarl	Malmesbury	Borehole	144	35.5	100	6.6	159	23.6
ZH19-PAA001	Paarl	Malmesbury	Borehole	126	35.6		8.0	1158	92.7
ZH18-DK001	Robertson	Malmesbury	Borehole	500	90.2		7.0	1180	213.1
ZH18-FH002	Franschhoek	Malmesbury	Borehole	167	32.2		6.8	210	76.5
ZH18-PV001	Porterville	Malmesbury	Borehole	102	72.2	55	6.9	1753	90.2
ZH19-MB001	Moorreesburg	Malmesbury	Borehole	133	67.4		7.5	197	198.4
ZH19-RBK001	R. Kasteel	Malmesbury	Borehole	152	53.4		6.9	64	84.8

4.2 Isotopes

4.2.1 δ^{13}C-DIC

Groundwater from the TMG Aquifer has δ^{13}C values ranging from -20.66 to -11.51 ‰ ($\bar{x}$ = -15.47). The Malmesbury Aquifer samples possess a similar range of -25.37 to -11.13 ‰ ($\bar{x}$ = -15.80). The alluvial aquifers have a range of -15.87 to -9.52 ‰ ($\bar{x}$ = -12.17) whereas the δ^{13}C values from the granitic aquifer range from -18.32 to 12.11 ‰ ($\bar{x}$ = -15.26). Groundwater from the Witteberg and Bokkeveld Aquifers have the most positive δ^{13}C values in the dataset. δ^{13}C for the Witteberg Aquifer was measured at -5.11 ‰ whereas a range of -18.28 to -1.47 ‰ ($\bar{x}$ = -10.45) is measured for the Bokkeveld. The three relatively enriched samples from the Bokkeveld and Witteberg are uncommon in the dataset and have had an addition of carbon along the flow path. In contrast, the more negative values from the alluvial, TMG, CGS and Malmesbury aquifer suggest an interaction with inorganic sediments. δ^{13}C values are presented as a function of δ^{18}O for the respective aquifers in Fig. 26 below.

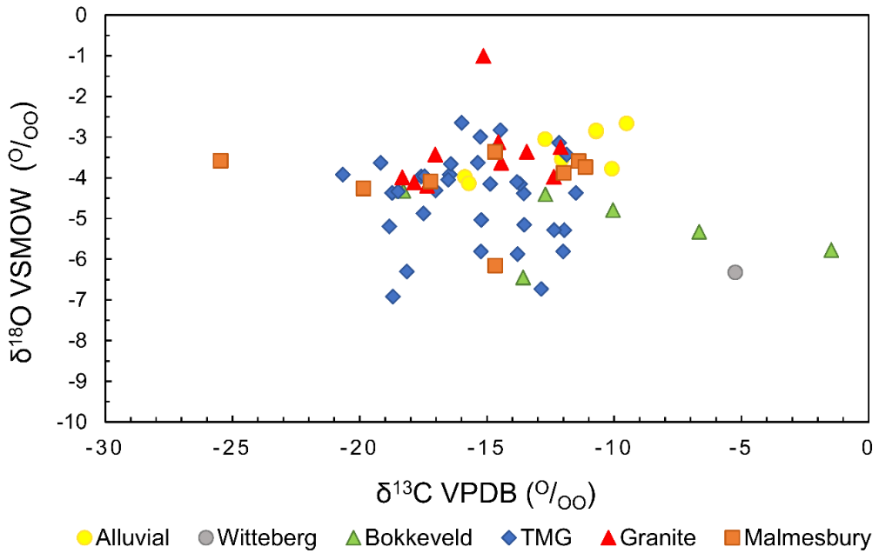

Figure 26 – Range of groundwater DIC δ^{13}C values compared to δ^{18}O values from Agyare-Dwomoh (2020).

4.2.2 Radiocarbon Activity

Measured activities for the entire dataset range from 11.39 – 102.62 pMC (Fig. 27). From the statistical data, the TMG and alluvial aquifers have the highest radiocarbon activities. Radiocarbon activity in the TMG Aquifer ranges from 72.80 – 99.55 pMC. ^{14}C activity in the alluvial aquifer ranges from 80.46 to 110.96 pMC. The Cape Granite Aquifer has a large range in radiocarbon activities (33.94 – 101.57 pMC), however the bulk of these samples tend to have higher activities. Radiocarbon activities exceeding 100 pMC from both the CGS and alluvial aquifers suggests the groundwater was recharged after 1950. The Malmesbury (26.65 – 59.55 pMC) and Bokkeveld Aquifers (23.10 – 77.75 pMC) are the aquifers that exhibit the lowest radiocarbon activities, indicating generally older water. Only a single sample was collected from the Witteberg Aquifer which had a measured ^{14}C activity of 11.39 pMC.

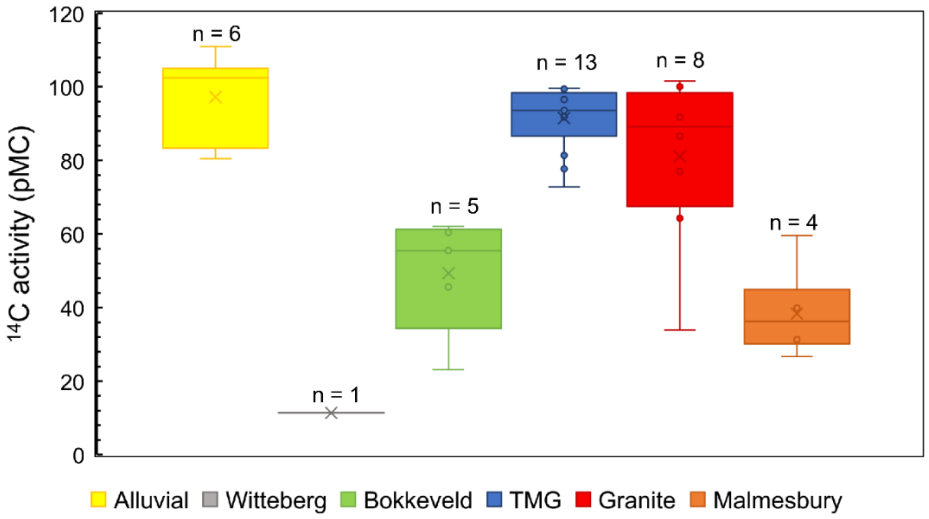

Figure 27 – Statistical data of measured radiocarbon activities per aquifer presented in a box and whisker plot.

Despite having collected 64 samples to be measured for radiocarbon activity, only 37 yielded results. This is due to the fact that many of the samples did not contain enough dissolved inorganic carbon on which to conduct analyses. The bulk of these samples have been classified as having come from the TMG Aquifer which is characterised as having low alkalinity (Sect. 4.1.2).

4.2.3 Tritium Activity

Tritium activities in the dataset range from 0.10 – 3.22 TU. Both samples collected from Ceres, C001 (Bokkeveld) and C002 (TMG), have elevated tritium values (2.8 – 3.2 TU) in comparison to samples collected from other regions (0.0 – 1.4 TU). Otherwise, a general trend exists where higher tritium activities (+/- 1.4 TU) are associated with high radiocarbon activities (Fig. 28). As radiocarbon activities exponentially decrease, so do tritium activities. High tritium activities are generally associated with the alluvial, TMG and CGS Aquifers whereas low tritium activities are associated with the Witteberg and Malmesbury Aquifers. All measurements are presented in Table 7 at the end of this section.

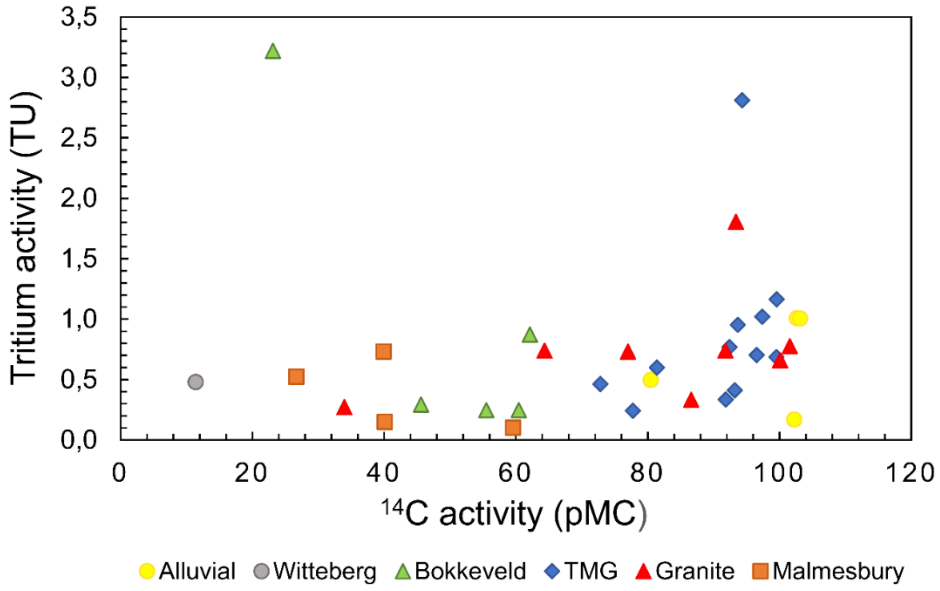

Figure 28 – An exponential decrease in radiocarbon activities is evident as tritium activities of groundwater decrease.

Table 7 – Summary of $\delta^{13}C$, ^{14}C activities, ^{3}H activities and their associated errors presented per aquifer.

Sample Name	Aquifer	$\delta^{13}C$ VPDB	±1σ	^{14}C activity	±1σ	^{3}H activity	±1σ
		‰		*pMC*		*TU*	
ZH18-SU001	Alluvial	-12.7	*0.04*	103.13	*0.35*	1.005	*0.12*
ZH18-SU002	Alluvial					1.113	*0.11*
ZH18-SU003	Alluvial					0.270	*0.09*
ZH18-SW001	Alluvial	-15.7	*0.05*	102.25	*0.24*	0.169	*0.05*
ZH18-SW002	Alluvial	-10.1	*0.06*	102.62	*0.25*	1.008	*0.11*
ZH19-CPT001	Alluvial	-9.5	*0.08*				
ZH19-CPT004	Alluvial	-10.7	*0.09*				
ZH19-KR001	Alluvial	-10.7	*0.03*	84.24	*0.50*		
ZH19-STB001	Alluvial	-15.9	*0.04*	80.46	*0.29*	0.497	*0.11*
ZH19-STB002	Alluvial	-12.1	*0.04*	110.96	*0.35*		
ZH18-ROB001	Witteberg	-5.2	*0.08*	11.39	*0.09*	0.480	*0.09*
ZH18-BD001	Bokkeveld	-6.7	*0.07*	62.12	*0.19*	0.873	*0.13*
ZH18-C001	Bokkeveld	-1.5	*0.06*	23.10	*0.11*	3.222	*0.09*
ZH18-MON001	Bokkeveld	-13.6	*0.05*	55.49	*0.18*	0.247	*0.06*
ZH19-CAL001	Bokkeveld	-18.3	*0.02*	60.43	*0.25*	0.248	*0.04*
ZH19-CAL002	Bokkeveld	-12.7	*0.03*	45.60	*0.21*	0.294	*0.04*
ZH19-VD005	Bokkeveld	-10.0	*0.08*			0.116	*0.04*
ZH18-BD002	TMG	-12.9	*0.11*	91.84	*0.21*	0.335	*0.05*
ZH18-C002	TMG	-15.2	*0.09*	94.31	*0.22*	2.812	*0.13*
ZH18-DB002	TMG	-13.8	*0.10*			0.821	*0.10*
ZH18-DB003	TMG	-13.7	*0.10*			0.955	*0.09*
ZH18-DB004	TMG	-14.9	*0.10*			0.537	*0.11*
ZH18-DD001	TMG	-13.8	*0.07*	99.55	*0.23*	1.163	*0.10*

Table 7 Continued.

Sample Name	Aquifer	$\delta^{13}C$ VPDB	±1σ	^{14}C activity	±1σ	^{3}H activity	±1σ
		‰		*pMC*		*TU*	
ZH18-DD002	TMG	-12.0	*0.05*	99.52	*0.24*	0.687	*0.10*
ZH18-FH001	TMG	-11.5	*0.05*	96.56	*0.23*	0.704	*0.09*
ZH19-FH004	TMG	-16.0	*0.18*			1.032	*0.23*
ZH19-FH009	TMG	-15.2	*0.09*				
ZH18-GRB001	TMG	-17.5	*0.05*			1.528	*0.08*
ZH18-PE001	TMG					0.409	*0.12*
ZH18-VD001	TMG	-13.5	*0.10*	97.40	*0.22*	1.022	*0.07*
ZH18-VD002	TMG	-12.4	*0.15*	93.19	*0.22*	0.412	*0.06*
ZH18-VD003	TMG	-12.0	*0.07*	81.41	*0.29*	0.599	*0.08*
ZH19-VD004	TMG	-18.7	*0.02*			0.500	*0.09*
ZH19-VD006	TMG	-18.8	*0.04*			0.410	*0.06*
ZH19-BK002	TMG	-20.7	*0.03*			0.243	*0.11*
ZH19-CD001	TMG	-13.6	*0.08*	77.75	*0.29*		
ZH19-CD002	TMG	-18.5	*0.04*			0.404	*0.06*
ZH19-CD003	TMG	-18.7	*0.03*			0.427	*0.05*
ZH19-CD004	TMG	-17.5	*0.02*			0.286	*0.03*
ZH19-CPT002	TMG	-15.3	*0.08*				
ZH19-CPT003	TMG	-12.2	*0.10*	99.43	*0.49*		
ZH19-CPT005	TMG	-16.5	*0.19*				
ZH19-CPT006	TMG	-14.5	*10.77*				
ZH19-KM001	TMG	-16.4	*0.07*				
ZH19-KM002	TMG	-16.5	*0.16*				
ZH19-KM003	TMG	-11.9	*0.04*				

Table 7 Continued.

Sample Name	Aquifer	$\delta^{13}C$ VPDB	±1σ	^{14}C activity	±1σ	^{3}H activity	±1σ
		‰		*pMC*		*TU*	
ZH19-NY001	TMG	-18.2	*0.03*	72.80	*0.33*	0.462	*0.04*
ZH19-PV002	TMG	-17.6	*0.03*			0.870	*0.06*
ZH19-RV001	TMG	-17.0	*0.05*			1.021	*0.07*
ZH19-SW003	TMG	-15.4	*0.03*	92.41	*0.30*	0.769	*0.28*
ZH19-TM001	TMG	-19.2	*0.11*				
ZH18-KB001	TMG	-14.7	*0.05*	93.64	*0.35*	0.952	*0.08*
ZH18-FH003	Granite	-12.4	*0.05*	86.60	*0.21*	0.332	*0.08*
ZH19-BK001	Granite	-18.3	*0.01*	93.38	*0.35*	1.807	*0.27*
ZH19-FH005	Granite	-17.0	*0.04*	77.00	*0.28*	0.733	*0.19*
ZH19-FH006	Granite	-15.1	*0.08*				
ZH19-FH007	Granite	-17.4	*0.03*	100.08	*0.32*	0.660	*0.11*
ZH19-FH008	Granite	-17.9	*0.05*	91.79	*0.31*	0.740	*0.12*
ZH19-MAL001	Granite	-14.4	*0.05*	33.94	*0.18*	0.272	*0.03*
ZH19-W001	Granite	-12.1	*0.03*			0.362	*0.05*
ZH18-KB002	Granite	-13.4	*0.04*	64.32	*0.25*	0.740	*0.07*
ZH18-R001	Granite	-14.6	*0.06*	101.57	*0.36*	0.775	*0.08*
ZH18-DB001	Malmesbury	-12.0	*0.07*				
ZH18-DK001	Malmesbury	-14.7	*0.06*	39.89	*0.17*	0.731	*0.09*
ZH18-FH002	Malmesbury	-17.2	*0.05*	26.65	*0.11*	0.523	*0.11*
ZH18-PV001	Malmesbury	-14.7	*0.05*	59.55	*0.18*	0.102	*0.05*
ZH19-MB001	Malmesbury	-11.1	*0.05*	40.09	*0.21*	0.150	*0.03*
ZH19-PAA001	Malmesbury	-19.9	*0.04*	31.33	*0.17*		
ZH19-RBK001	Malmesbury	-11.4	*0.05*				
ZH18-SV001	Malmesbury	-25.5	*0.05*	32.62	*0.22*		

4.2.4 Noble Gas Data

R/R_a values are presented as a function of ^{14}C activity (Fig. 29). TMG and alluvial aquifer samples tend to have R/R_a ratios close to 1 whereas samples from the Witteberg, Bokkeveld and Malmesbury have lower ratios. Most samples display an exponential decrease in R/R_a values as the ^{14}C activity decreases, implying that samples with high ^{14}C activities have been in contact with the atmosphere more recently than the samples with lower R/R_a values. The ^{14}C activity of an anomalous Malmesbury sample (FH002) with 26.65 pMC suggests it is old, however the R/R_a value indicates it may have had recent atmospheric interaction.

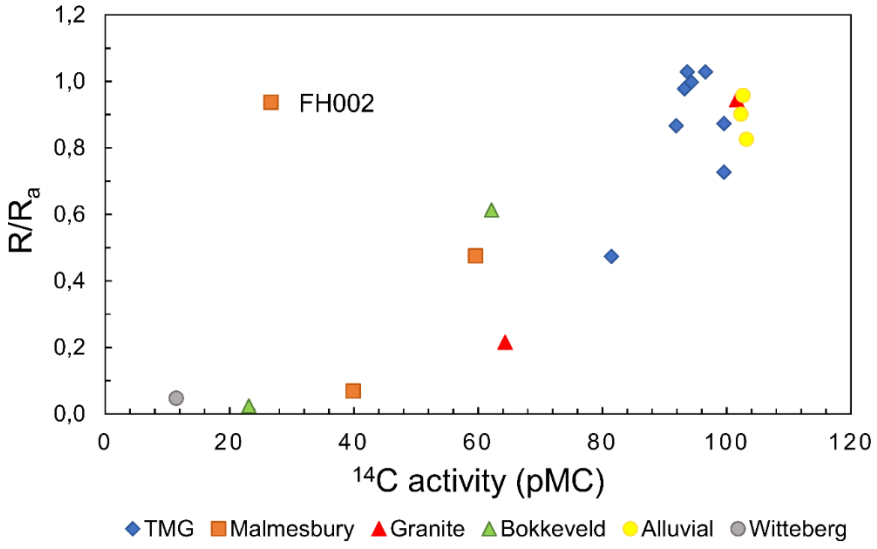

Figure 29 – $^{3}He/^{4}He$ ratios of measured samples (R) compared to atmospheric concentrations (R_a) as a function of measured radiocarbon activity.

Samples collected for helium were additionally analysed for Ne, Ar, Kr and Xe and are reported in Table 8 in the section below.

5 GROUNDWATER RESIDENCE TIME

The calculation of groundwater residence times from measured isotopic tracer activities, particularly those of radiocarbon, often involve a number of assumptions. The approach and calculations used to determine apparent ages are discussed below. The suitability of the resultant residence times and the factors which impact them, will also be evaluated in the following section.

5.1 Calculation Methodology

5.1.1 Noble Gas Residence Times

In order to calculate the apparent ages through the tritogenic helium system, the following equation is used:

$$\tau = \ln\left(\frac{^3He + {}^3H}{^3H}\right) * \frac{12.32}{\ln 2} \qquad \text{(Eq. 8)}$$

where τ is the apparent age;

^3He is the helium concentration produced by tritium decay;

^3H is the tritium activity; and

12.32 is the half-life of ^{3}H.

Using the calculation above, apparent ages were calculated for 27 samples which are reported with their associated errors in Table 8. An age could not be calculated for sample DB001 as the tritium sample was lost. Calculated ages range from 0.00 to 84.71 years. Of the 27 samples, 7 samples returned an apparent age of zero years. Zero aged samples which are associated with reasonably large errors (>25.0 years) are assumed to have not been recently

recharged, but rather that an age could not be obtained as the water is older than what the $^{3}H/^{3}He$ system is able to date. Zero aged samples with lower uncertainty (<25 years), however, could possibly be very recently recharged and the true residence time may be within error.

Excluding zero ages, apparent ages for the alluvial aquifers range from 2.8 ± 15.5 to 62.5 ± 6.1 years. Samples collected from the TMG Aquifer range from 0.3 ± 7.4 – 44.6 ± 4.9 years. The two Bokkeveld samples returned ages of 58.5 ± 0.9 and 84.7 ± 3.4 years. Groundwater from the CGS Aquifer has apparent ages between 3.7 ± 19.2 – 10.0 ± 13.0 years. Of the four noble gas samples collected from the Malmesbury Aquifer, only a single age of 45.50 ± 3.0 years could be calculated. An age could not be calculated for the noble gas sample collected from the Witteberg Aquifer.

Table 8 – Apparent ages and noble gas temperatures (NGT) calculated from noble gas and tritium concentrations.

Sample Name	Aquifer	He	Ne	Ar	Kr	Xe	R/Ra	^{3}He	±1σ	Age	± 1σ	^{3}H+^{3}He
				x 10^{-6} ccSTP/g				*TU*		*years*		*TU*
ZH18-SU001	Alluvial	0.079	0.261	365.034	0.079	0.011	0.83	0.17	1.02	**2.8**	*15.5*	1.18
ZH18-SU002	Alluvial	0.105	0.236	347.712	0.075	0.011	0.53	0.00	0.88	**0.0**	*14.1*	1.11
ZH18-SU003	Alluvial	0.722	0.249	357.080	0.074	0.010	0.11	8.82	1.15	**62.5**	*6.1*	9.09
ZH18-SW001	Alluvial	0.064	0.229	960.594	0.127	0.013	0.90	0.73	0.91	**29.8**	*18.4*	0.9
ZH18-SW002	Alluvial	0.056	0.212	332.116	0.071	0.010	0.96	1.73	0.83	**17.7**	*5.5*	2.73
ZH18-ROB001	Witteberg	1.879	0.252	1145.869	0.145	0.013	0.05	0.00	7.90	**0.0**	*292.5*	0.48
ZH18-BD001	Bokkeveld	1.198	2.038	1493.083	0.212	0.021	0.61	101.60	12.46	**84.7**	*3.4*	102.47
ZH18-C001	Bokkeveld	10.787	0.459	506.106	0.093	0.010	0.02	83.50	3.90	**58.5**	*0.9*	86.72
ZH18-BD002	TMG	0.073	0.235	355.300	0.076	0.010	0.87	3.78	0.97	**44.6**	*4.9*	4.12
ZH18-C002	TMG	0.075	0.305	413.628	0.086	0.012	1.00	0.05	1.20	**0.3**	*7.4*	2.86
ZH18-DB002	TMG	0.066	0.224	362.147	0.077	0.010	0.93	4.43	0.93	**33.0**	*3.6*	5.26
ZH18-DB003	TMG	0.051	0.202	337.432	0.075	0.011	0.96	0.63	0.76	**9.0**	*8.5*	1.59
ZH18-DB004	TMG	0.048	0.199	329.258	0.073	0.010	0.96	0.00	0.73	**0.0**	*24.0*	0.54
ZH18-DD001	TMG	0.079	0.266	372.717	0.082	0.011	0.87	2.40	1.08	**19.9**	*5.5*	3.56
ZH18-DD002	TMG	0.117	0.326	400.377	0.082	0.011	0.73	2.07	1.39	**24.7**	*9.2*	2.75
ZH18-FH001	TMG	0.097	0.349	435.736	0.088	0.011	1.03	7.28	1.58	**43.2**	*4.1*	7.99
ZH18-GRB001	TMG	0.015	0.164	2175.812	0.230	0.021	1.14	0.00	0.38	**0.0**	*4.5*	1.53
ZH18-PE001	TMG	0.081	0.306	394.132	0.084	0.011	0.99	2.53	1.28	**35.1**	*9.0*	2.94
ZH18-VD002	TMG	0.141	0.494	1037.552	0.137	0.015	0.98	0.00	6.35	**0.0**	*273.9*	0.41
ZH18-VD003	TMG	0.175	0.32	401.140	0.082	0.011	0.47	1.64	1.34	**23.4**	*10.8*	2.24
ZH19-VD004	TMG	0.082	0.227	321.846	0.069	0.010	0.69	0.04	0.89	**1.4**	*29.2*	0.54
ZH18-KB001	TMG	0.067	0.26	407.520	0.087	0.012	1.03	4.14	1.05	**29.8**	*3.9*	5.1
ZH18-KB002	Granite	0.289	0.234	287.742	0.051	0.004	0.22	0.17	0.99	**3.7**	*19.2*	0.91
ZH18-R001	Granite	0.067	0.254	354.714	0.076	0.010	0.95	0.59	1.00	**10.0**	*13.0*	1.36
ZH18-DB001	Malmesbury	0.087	0.31	392.271	0.080	0.011	0.86	0.00	1.22			
ZH18-DK001	Malmesbury	1.113	0.256	378.847	0.080	0.011	0.07	8.73	1.16	**45.5**	*3.0*	9.46
ZH18-FH002	Malmesbury	0.047	0.197	385.768	0.083	0.011	0.94	0.00	0.88	**0.0**	*29.9*	0.52
ZH18-PV001	Malmesbury	0.204	0.392	429.774	0.082	0.010	0.48	0.00	1.64	**0.0**	*283.7*	0.1

5.1.2 Radiocarbon Model Ages

To calculate the apparent age of groundwater using radiocarbon activity, the following equation is used:

$$\tau = \frac{5\,568}{\ln 2} * \ln(\frac{A_0}{A}) \quad \text{(Eq. 9)}$$

where τ is the apparent residence time;

5 568 is the Libby half-life of radiocarbon (Libby, 1955);

A_0 is the initial radiocarbon activity; and

A_0 is the measured radiocarbon activity.

Residence time calculations are often more complicated than this as Equation 8 does not take into account the loss or addition of carbon along the flow path. Mixing of groundwater with inorganic sediments may lower the $\delta^{13}C_{DIC}$ whereas mixing with carbonatic rocks will increase the $\delta^{13}C_{DIC}$. Elevated ^{14}C in precipitation also poses a problem as radiocarbon activities exceeding 100 pMC suggest modern waters that have been recharged after 1950 when atmospheric carbon concentrations were artificially elevated due to nuclear weapons testing. As a result, recharge radiocarbon (A_0) is difficult to constrain.

After considering the available data, the suitability of a number of correction models was evaluated and a bulk correction using the Ingerson-Pearson model (1964) was used. This model assumes simple mixing between soil CO_2 and carbon produced by the dissolution of carbonate minerals in the host rock or its matrix. The model assumes that any changes in ^{14}C will be reflected in ^{13}C and does not account for any other additions or losses of carbon (Ingerson & Pearson 1964). The dilution of carbon along the flow path is represented by Equation 9:

$$q = \frac{(\delta^{13}C_{DIC} - \delta^{13}C_{carbonate})}{(\delta^{13}C_{soil} - \delta^{13}C_{Carbonate})} \quad \text{(Eq. 9)}$$

where q is the dilution factor

$\delta^{13}C_{DIC}$ is the $\delta^{13}C$ of the groundwater sample;

$\delta^{13}C_{soil}$ is the $\delta^{13}C$ of soil gas; and

$\delta^{13}C_{carbonate}$ is the $\delta^{13}C$ of the rock.

$\delta^{13}C$ is affected by the vegetation cover and the photosynthetic pathways it uses. The $\delta^{13}C$ values of C_3 and C_4 plants are supposedly very distinct, with C_4 species ranging in value from -19 to -9‰ whereas C_3 species possess values of -35 to -22‰ (O'Leary, 1988). Values between -14 and -26‰ suggest a mix of C_3 and C_4 plants in the vegetation cover (Stock et al. 1993). The dominant plant species in the Western Cape, Renosterveld and Fynbos, have been estimated as equal parts C_3 and C_4 plants. Despite the fact that the indigenous plant cover has been extensively mapped, no literature was available detailing the $\delta^{13}C$ values thereof. In addition, sample sites were often either built-up (urban) or replaced by production crops, further complicating calibration. As no soil samples were taken for DIC analysis, $\delta^{13}C$ of the soil is estimated in the correction model.

Due to the fact that the samples were collected across an extensive area, samples are grouped according to aquifer/region and assumptions regarding soil $\delta^{13}C$ are made. Sample $\delta^{13}C$ and ^{14}C activities are plotted per aquifer type and a 'mixing' line from 100 pMC to 0 pMC is drawn through the samples to represent the addition of dead carbon along the flow path. The y-axis value, corresponding to the input radiocarbon (100 pMC), is the assumed initial $\delta^{13}C$ value of the soil. Vertical lines assume that the soil $\delta^{13}C$ at groundwater infiltration does not acquire dead carbon along its flow path and remains more or less similar as the water ages.

Due to the fact that samples were taken from a large area across the province and are from multiple aquifers, soil and vegetation types, this 'mixing' line is not applicable to all samples within an aquifer and multiple possible mixing lines have been constructed. Multiple $\delta^{13}C$ soil values are assumed using this method and sampled values that are grouped are often found to be in same region. This is the case with samples in the Franschhoek Valley that are located close to one another (likely the same bulk vegetation and soil) and from the same aquifer. In these cases, with multiple possible soil $\delta^{13}C$ values, a $\delta^{13}C$ value is selected on which best fits the data.

This approach works well for samples in the alluvial, Bokkeveld, TMG and CGS Aquifers. The approach, however does not work for the Witteberg and Malmesbury Aquifers. The Witteberg sample does not allow for the construction of a mixing line as two or more samples are needed. It is, however, suspected that there has been some dissolution of carbonate-bearing minerals as this aquifer boasts the highest concentrations of Ca^{2+}, Mg^{2+} and HCO_3^- (Agyare-Dwomoh, 2020). The Malmesbury Aquifer has ample sample sites but a mixing line through three of the samples assumes a soil $\delta^{13}C$ value of -60 ‰, which seems unlikely. For these three samples, a $\delta^{13}C$ value of -19.5 ‰ is assumed instead.

All aquifer rock types except the Bokkeveld are assumed to have $\delta^{13}C$ values of 0 ‰. A $\delta^{13}C$ value of 2 ‰ is assumed for the Bokkeveld as 0 ‰ results in a clearly false over correction of ^{14}C activity as one sample had increased by 130 pMC during correction. All possible mixing lines are constructed per aquifer (Fig. 30). Assumptions regarding $\delta^{13}C$, the resultant dilution factors and apparent ages are presented in Table 9 below.

Ages calculated from samples with corrected radiocarbon activities exceeding 100 pMC are reported as being younger than 70 years as the input radiocarbon post-1950 is unconstrained. Calculated ages from the alluvial aquifer indicate that the alluvial aquifer has been recharged within the last 70 years except for sample STB001 which has an apparent age of 1 903 years BP (before present). The Witteberg sample has an apparent age of 6 699 years. The Bokkeveld Aquifer ranges from 1 200 – 6 038 years BP. A large proportion of TMG samples are younger than 70 years, however there are a few older samples which range from 46 – 1 626 years BP (before 1950). Ages for the CGS Aquifer range from <70 – 8 648 years. The Malmesbury Aquifer has the oldest groundwater as apparent ages range from 3 994 – 11 146 years.

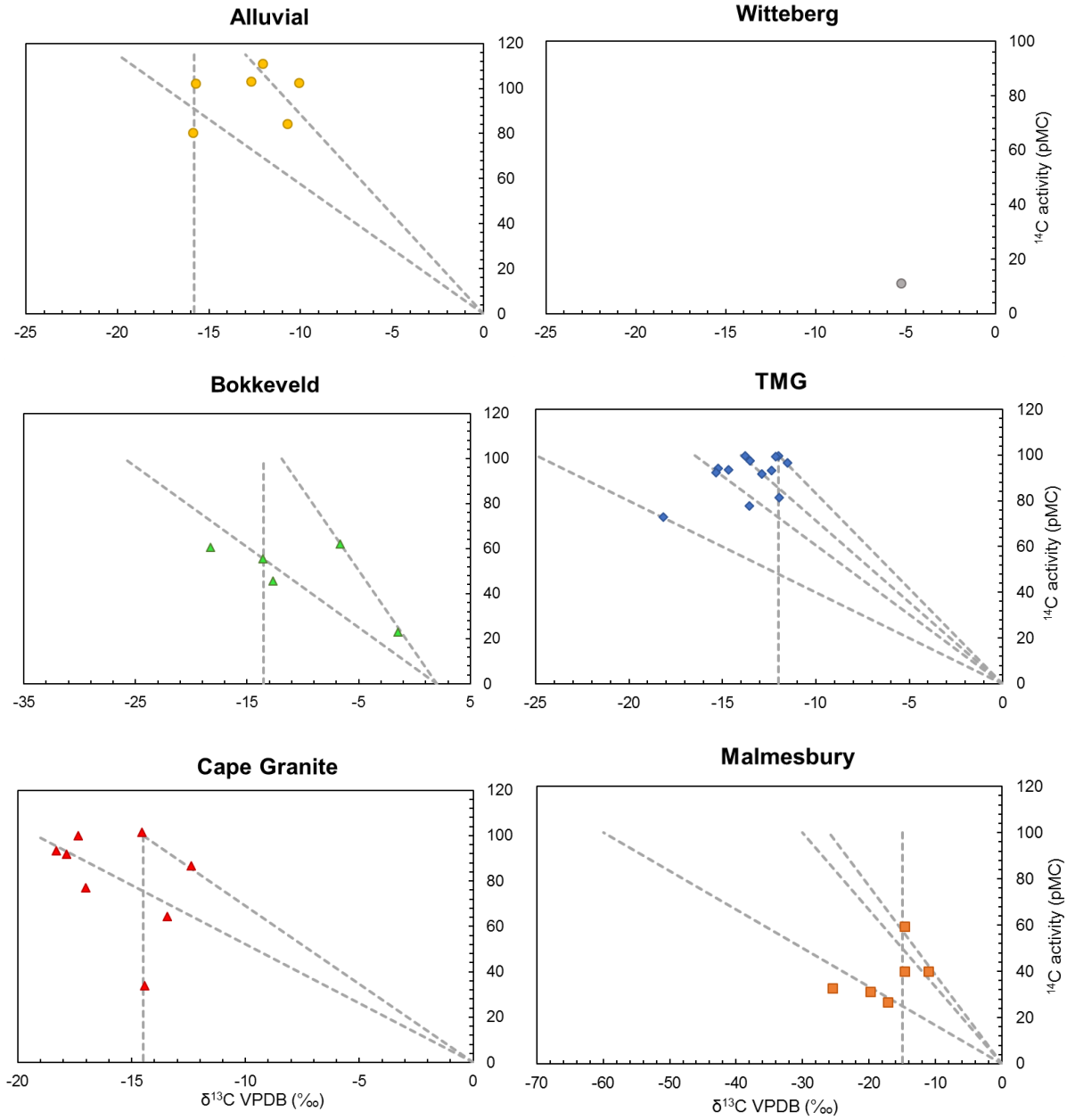

Figure 30 – Possible mixing lines of $\delta^{13}C$ VPDB (‰) along the groundwater flow path per aquifer type.

Table 9 – Carbon data used to correct radiocarbon activity and produce model ^{14}C ages.

Sample	Aquifer	$\delta^{13}C$ VPDB	Measured ^{14}C	±1σ	$\delta^{13}C$ rock	$\delta^{13}C$ soil	q	Corrected ^{14}C	^{14}C Age
		‰	*pMC*		*‰*	*‰*		*pMC*	*years BP*
ZH19-KR001	Alluvial	-10.72	84.2	*0.50*	0.0	-13.0	*0.8*	102.2	<70
ZH18-SW001	Alluvial	-15.71	102.3	*0.24*	0.0	-15.8	*1.0*	102.8	<70
ZH18-SW002	Alluvial	-10.09	102.6	*0.25*	0.0	-10.0	*1.0*	101.7	<70
ZH18-STB001	Alluvial	-15.87	80.5	*0.29*	0.0	-15.8	*1.0*	80.1	1783
ZH18-STB002	Alluvial	-12.06	111.0	*0.35*	0.0	-13.0	*0.9*	119.6	<70
ZH18-STB003	Alluvial	-12.71	103.1	*0.35*	0.0	-13.0	*1.0*	105.5	<70
ZH18-ROB001	Witteberg	-5.24	11.4	*0.09*	0.0	-20.0	*0.3*	43.4	6699
ZH18-C001	Bokkeveld	-1.47	23.1	*0.11*	2.0	-10.0	*0.3*	80.0	1794
ZH19-CAL001	Bokkeveld	-18.28	60.4	*0.25*	2.0	-26.0	*0.7*	83.4	1454
ZH19-CAL002	Bokkeveld	-12.70	45.6	*0.21*	2.0	-13.2	*1.0*	47.2	6038
ZH18-MON001	Bokkeveld	-13.58	55.5	*0.18*	2.0	-13.2	*1.0*	54.1	4929
ZH18-BD001	Bokkeveld	-6.66	62.1	*0.19*	2.0	-10.0	*0.7*	86.1	1200
ZH18-BD002	TMG	-12.87	91.8	*0.21*	0.0	-14.1	*0.9*	100.6	<70
ZH18-FH001	TMG	-11.51	96.56	*0.23*	0.0	-12.0	*1.0*	100.7	<70
ZH19-CPT003	TMG	-12.16	99.4	*0.49*	0.0	-14.1	*0.9*	114.5	<70
ZH18-VD001	TMG	-13.54	97.4	*0.22*	0.0	-14.1	*1.0*	100.7	<70
ZH18-VD002	TMG	-12.36	93.2	*0.22*	0.0	-14.1	*0.9*	106.3	<70
ZH18-VD003	TMG	-11.96	81.4	*0.29*	0.0	-12.0	*1.0*	81.7	1626
ZH18-DD001	TMG	-13.80	99.6	*0.23*	0.0	-14.1	*1.0*	101.0	<70

Table 9 Continued.

Sample	Aquifer	$\delta^{13}C$ VPDB	Measured ^{14}C	±1σ	$\delta^{13}C$ rock	$\delta^{13}C$ soil	q	Corrected ^{14}C	^{14}C Age
		‰	*pMC*		*‰*	*‰*		*pMC*	*years BP*
ZH18-DD002	TMG	-12.01	99.5	*0.24*	0.0	-12.5	*1.0*	103.6	46
ZH18-C002	TMG	-15.24	94.3	*0.22*	0.0	-16.5	*0.9*	102.1	<70
ZH19-SW003	TMG	-15.36	92.4	*0.30*	0.0	-16.5	*0.9*	99.3	58
ZH19-NY001	TMG	-18.15	72.8	*0.33*	0.0	-25.0	*0.7*	100.3	<70
ZH19-CD001	TMG	-13.56	77.8	*0.29*	0.0	-16.5	*0.8*	94.6	445
ZH18-KB001	TMG	-14.69	93.6	*0.35*	0.0	-16.5	*0.9*	105.2	<70
ZH18-KB002	Granite	-13.43	64.3	*0.25*	0.0	-15.0	*0.9*	71.8	2,660
ZH19-MAL001	Granite	-14.44	33.9	*0.18*	0.0	-14.5	*1.0*	34.1	8,648
ZH18-R001	Granite	-14.55	101.6	*0.36*	0.0	-14.5	*1.0*	101.2	<70
ZH18-FH003	Granite	-12.37	86.6	*0.21*	0.0	-14.5	*0.9*	101.5	<70
ZH19-FH005	Granite	-17.03	77.0	*0.28*	0.0	-18.0	*0.9*	81.4	1,655
ZH19-FH007	Granite	-17.36	100.1	*0.32*	0.0	-18.0	*1.0*	103.8	<70
ZH19-FH008	Granite	-17.86	91.8	*0.31*	0.0	-18.0	*1.0*	92.5	625
ZH19-BK001	Granite	-18.32	93.4	*0.35*	0.0	-18.0	*1.0*	91.7	693
ZH19-MB001	Malmesbury	-11.13	40.1	*0.21*	0.0	-15.0	*0.7*	54.0	4,944
ZH18-DK001	Malmesbury	-14.67	39.9	*0.17*	0.0	-15.0	*1.0*	40.8	7,204
ZH18-PV001	Malmesbury	-14.69	59.6	*0.18*	0.0	-15.0	*1.0*	60.8	3,994
ZH18-FH002	Malmesbury	-17.22	26.7	*0.11*	0.0	-19.5	*0.9*	30.2	9,624
ZH19-PAA001	Malmesbury	-19.85	31.3	*0.17*	0.0	-19.5	*1.0*	30.8	9,468
ZH18-SV001	Malmesbury	-25.47	32.6	*0.22*	0.0	-19.5	*1.3*	25.0	11,146

5.2 Evaluation of Residence Times

The calculation of noble gas and radiocarbon ages involves propagation in measurement error, therefore it is important to evaluate the validity of the resultant ages. In particular, radiocarbon calibration relies on many assumptions and as a result, there is often considerable variability in the results depending on what assumptions were made. Although the $^{3}H/^{3}He$ system is more accurate than ^{14}C in dating groundwater, sampling and measurement errors may also result in variable ages. Before any conclusions can be drawn on residence times, the validity of apparent ages needs to be evaluated.

5.2.1 $^{3}H/^{3}He$ Apparent Ages

5.2.1.1 Analytical Error

In Fig. 31, apparent $^{3}H/^{3}He$ ages have been plotted against atmospheric tritium concentrations for Cape Town from the Global Network of Isotopes in Precipitation (GNIP) (IAEA/WMO, 2016). The graph indicates elevated ^{3}H in precipitation around 1960, which reaches peak concentrations of approximately 45 TU around 1968 before decreasing back to background levels. Despite the fact that precipitation data is erratic after 1988, the tritium curve still provides insight into modern tritium in precipitation. The reliability of calculated ages was assessed by their helium concentrations and reliable samples should intersect the tritium curve.

Samples with green markers are considered reliable as they usually lie on the tritium curve and have small margins of error associated with them (Fig. 31). Samples with red markers, however, are regarded as unreliable as they have large associated errors, and are often not located on the tritium curve. These errors are propagated during calculations from the initial error in measurement. Unreliable ages belong to samples ROB001, BD001, VD002 and GRB001. ROB001 and BD001 contain excess helium whereas sample VD002 contains too much excess air that cannot be corrected for. Sample GRB001 shows evidence of degassing as its noble gas concentrations are less than that of solubility equilibrium. These four samples with unreliable ages are some of the youngest in the dataset.

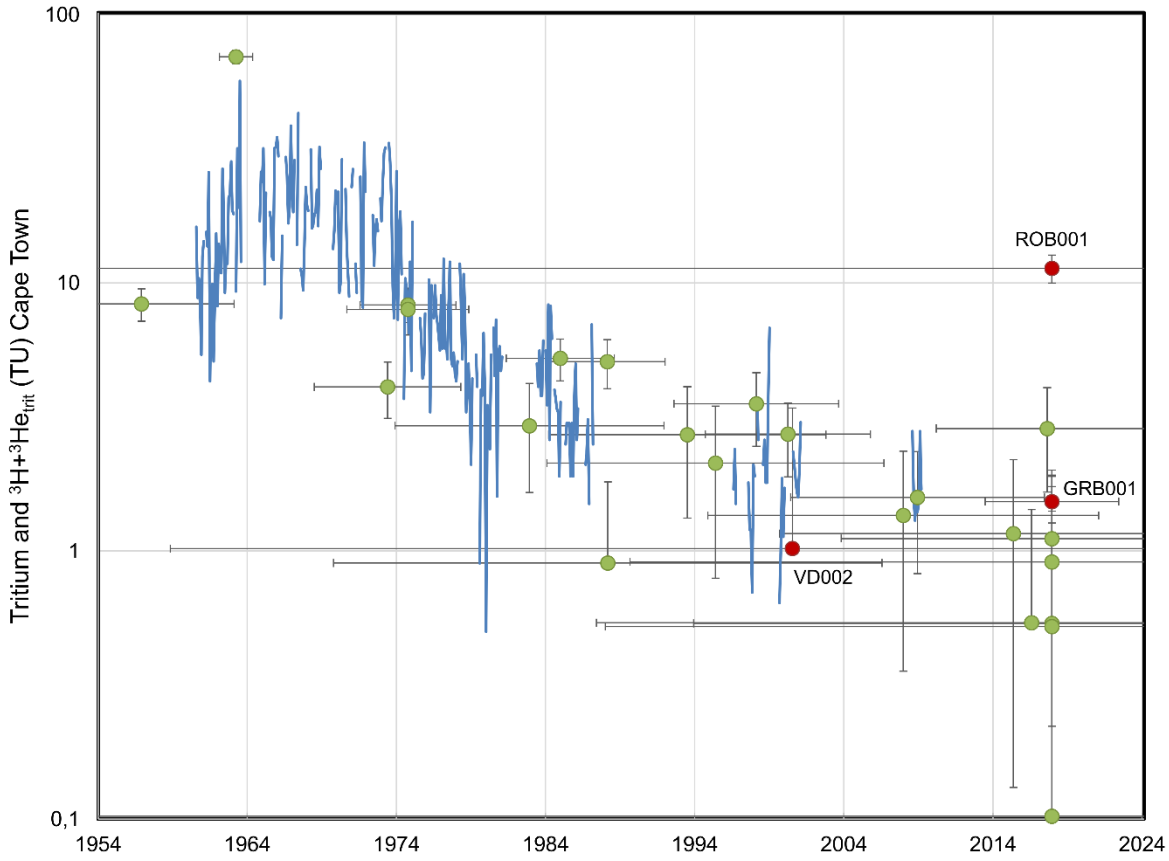

Figure 31 – Tritium curve for Cape Town precipitation (blue line) from the GNIP database (IAEA/WMO, 2019) with residence ages and ^3H + $^3He_{trit}$ values for samples; samples GRB001, VD002 and ROB001 are considered unreliable, sample BD001 plots off the graph.

From both Fig. 31 and 32, it is evident that there is higher uncertainty in younger samples as there are larger errors in their ^3H and ^3He measurements. Comparing the calculated noble gas ages for the 20 samples with ages above zero with their uncertainty shows that there is an exponential decrease in the error of the calculated age the older the apparent age. The large error in dating young waters can be attributed to the fact that as tritium concentrations have returned to background levels, the input tritium becomes quite low. When tritium activities are low, analytical precision of subsequent measurements are lower which introduces error.

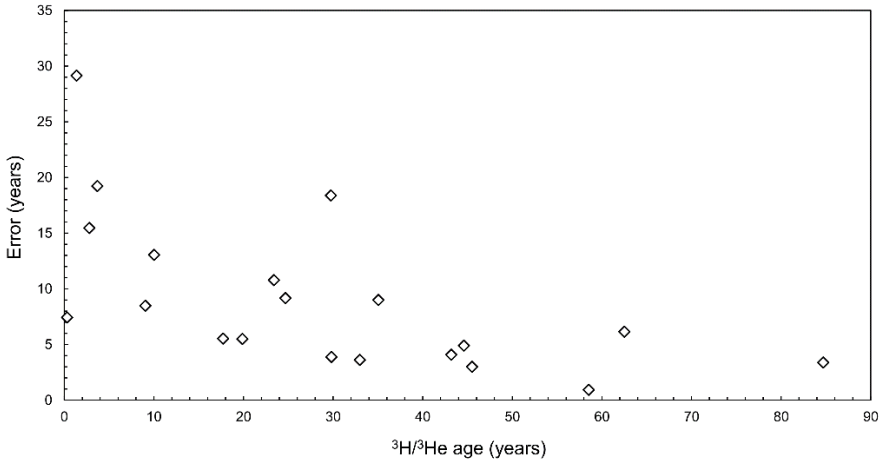

Figure 32 – Calculated ages of young samples tend to have higher associated errors than compared to older samples.

5.2.1.2 Input Tritium Activity

Some difficulty arises in tritium data analysis as modern input tritium for the Western Cape is not definitively constrained. Isotope data is available from the GNIP database but is incomplete for modern precipitation as sample collection became sparse around 1980. Concentrations in precipitation are highly variable and are dependent on a number of factors that include but are not limited to: rainfall intensity, duration and proximity to the coast.

In Paarl, tritium activities in rainwater ranged from as low as 0.2 TU to as high as 4 TU for different rainfall events measured over the course of a year (van Rooyen, unpublished data). From this data, the mean annual tritium input is calculated to be approximately 1.58 TU. For rainfall events greater than 5 mm, which is thought to contribute to the bulk of groundwater recharge, an annual average tritium concentration of 1.33 TU has been calculated. In contrast, rainfall events less than 5 mm have an average annual concentration of 1.97 TU. Considering winter rainfall only, the average input is approximately 1.26 TU (Van Rooyen, unpublished data). The type of rainfall events that actively recharge the aquifers in this study are also unconstrained but it is assumed that the main recharge occurs in winter through rainfall events greater than 5 mm. Due to the fact that input tritium is highly variable, the resultant concentrations in newly infiltrated groundwater will be highly variable as well, creating difficulty in distinguishing between young and older waters through tritium alone. Despite having reached levels up to 30 times as high as pre-bomb values (levels (GNIP data, Fig. 31), bomb peak concentrations are also no longer identifiable as they would have decayed to background levels by now.

Another factor which impacts analytical accuracy is distance from the ocean. In Fig. 33 below, it is evident that analytical error on tritium measurements increases with increasing proximity of the sample site to the coast. The ocean is a vast water body which is relatively depleted in tritium (compared to ^{2}H), effectively diluting the tritium concentrations of the water vapour which forms above it. As a result, coastal precipitation contains low concentrations of tritium (Schell et al., 1970). As a weather system migrates from the coast further inland, recorded tritium concentrations in precipitation tend to increase. This is due to the injection of stratospheric air with high tritium concentrations into the troposphere and the exchange of atmospheric water vapor with continental surface waters that generally have higher tritium concentrations than those found in ocean water. (Michel et al., 2018). This would suggest that the source of tritium in precipitation in continental regions is mostly the tritium produced in the upper atmosphere with little contribution from ocean evaporate (Cauquoin et al., 2015).

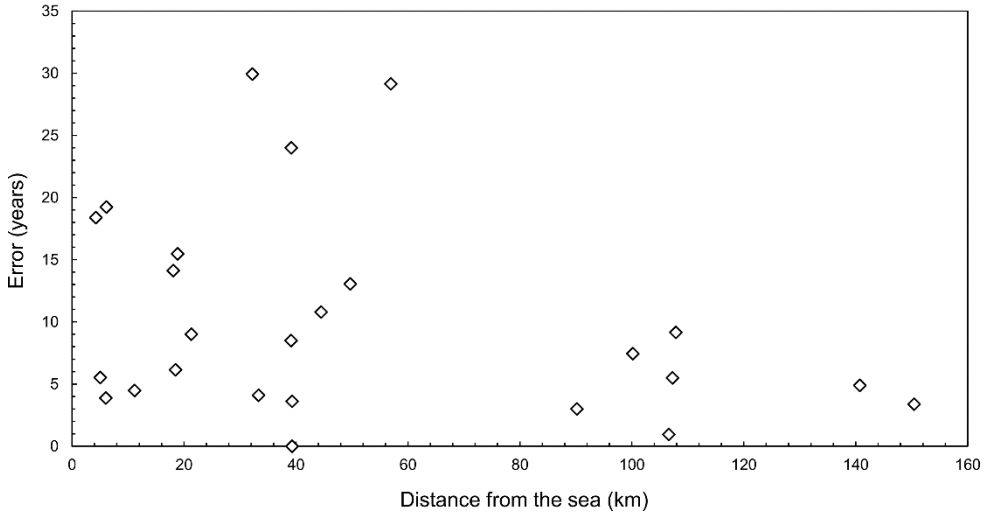

Figure 33 – Increasing distance from the coast is associated with smaller measurement errors in samples.

5.2.1.3 Comparison to Previous Work

Several springs in the Drakenstein Mountains (Paarl) that emanate from the Peninsula Formation of the TMG and flow throughout the year have been dated using the tritogenic helium method (Fig. 34) (Miller et al., 2017) Residence times for these springs from the Miller et al. (2017) study were constrained to be between 17.6 ± 14.0 and 33.8 ± 7.1 years. This study dated the same springs after the drought in 2018 and found the residence times to be similar at 0.0 ± 24.0 years to 33.0 ± 3.6 years (Table 10).

Table 10 – Comparison of residence times for springs in the Drakenstein Mountains using the $^{3}H/^{3}He$ dating system in 2017 and 2018.

			2017 (Miller et al.)		**2018 (This study)**	
Spring Nr	Latitude	Longitude	Residence Time	^{3}H	Residence Time	^{3}H
	°S	*°E*	*yr*	*TU*	*yr*	*TU*
3 / DB002	-33.785273	19.00311	33.8 ± 7.1	0.5	33.0 ± 3.6	0.82
4 / DB003	-33.78544	19.002665	17.6 ± 14.0	0.4	9.0 ± 8.5	0.96
5 / DB004	-33.785524	19.002441	27.4 ± 6.4	0.6	0.0 ± 24	0.54

The calculated ages for both studies lie within the same range, indicating reliable ages. Data for springs 3 and 4 have better constraints on residence times in 2018 as the uncertainty in age is smaller. Calculated ages for the two springs (3 and 4) are slightly younger in 2018 than in 2017, which can be further substantiated by the increase in tritium in 2018. The apparent age for spring 5, however, had lower uncertainty in 2018. After evaluating the 2017 data for spring 5 (upper limit: 33.8 years; lower limit: 21.0 years), it can be assumed that the residence time for the spring is between 21 – 24 years in 2018.

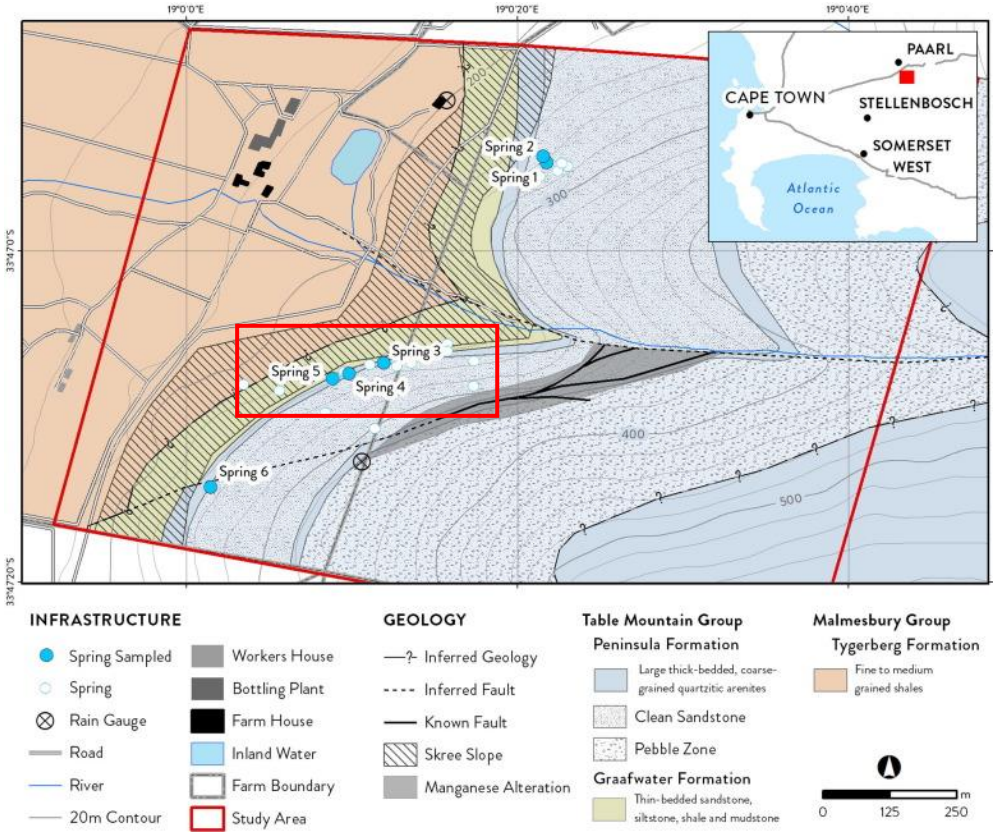

Figure 34 – Location of the three Peninsula springs (enclosed in red box) in the Drakenstein Mountains, Paarl (Miller et al., 2017).

These three springs are located less than 100 metres apart, so it is assumed that they are recharged at the same source. Stable isotope studies of both spring water and precipitation at the study site suggest the springs are recharged by local precipitation that falls in the area hinterland to the springs (~820 mamsl) and not derived from higher elevations (mamsl) (Miller et al., 2017). Miller et al. (2017) further concluded that the springs are recharged by all rainfall events and not just orographic rainfall. A decrease in tritium concentrations due to the radioactive decay of existing tritium and no addition of new tritium, is an indication of very little (no considerable mixing to affect the existing concentrations) to no recharge of the groundwater. The increase in tritium activity in springs 3 and 4 between 2017 and 2018, however, indicates that tritium has entered the system between the two sampling dates further confirming that these springs are quickly recharged by the precipitation that falls in the Drakenstein Mountains. Spring 5, however, does not appear to have shown a response to recharge a year after the drought broke and it is assumed that there is a delay in recharge compared to the other two springs.

Groundwater of the TMG Aquifer in the Verlorenvlei Catchment (near Elands Bay) has also been age dated by Turner (2018). Three ages were obtained for the aquifer and range between 57.41 ± 3.1 to 34.83 ± 6.4 years. Although there is no overlap in study area between these two studies, the young apparent ages determined by Turner (2018) suggest that the TMG Aquifer may have short residence times throughout the entire extent of the aquifer. As noble gas dating is still relatively novel in South Africa, the residence times determined in this project cannot be compared to any sources other than Miller (2017) and Turner (2018) as there has been no further investigation of the five aquifers that have been studied in this project.

5.2.2 ^{14}C Model Ages

5.2.2.1 Analytical Error

The main complication concerning radiocarbon dating in this study was in obtaining samples with sufficient carbon content. Consequently, a number of samples were unable to be analysed, particularly from the alluvial and TMG Aquifers. ^{14}C occurs in trace amounts and has concentrations that are relatively low in comparison to its stable counterparts – ^{12}C and ^{13}C – all of which are measured using the total carbon content dissolved in the groundwater. Samples with the highest ^{14}C activities tend to have the lowest carbon contents. This can be

attributed to the fact that modern water, which is associated with high ^{14}C activities, is sourced from precipitation that has low amounts of dissolved carbon. These modern waters have often not yet had time to pick up additional carbon from inorganic or organic sources (aquifer host or sediments and vegetation). Consequently, samples that have been recently recharged, have little dissolved carbon. This is particularly true in the case of the TMG Aquifer as the geology does not have a high concentration of carbon/carbonate-bearing minerals and recharge often occurs in regions where the bare rock is exposed with little soil and vegetation cover. As a result, the lower the carbon content of the groundwater on which to perform analyses, the greater the error in measurement due to analytical sensitivity (Fig. 35).

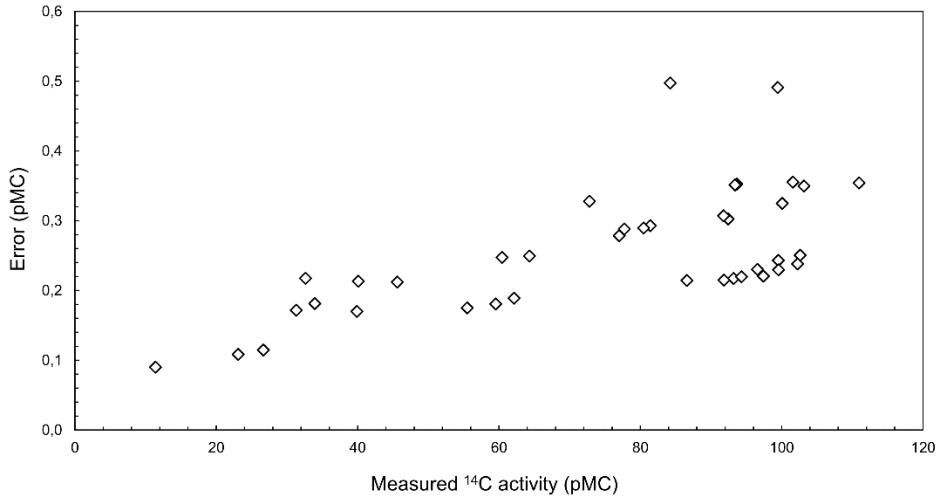

Figure 35 – An increase in measured radiocarbon activity of samples (white diamonds) is associated with increased analytical error.

5.2.2.2 Input Carbon Content

Although ^{14}C activities could not be determined for several samples, this in itself may be an indication of young waters as a relationship exists between total carbon (TC) and ^{14}C activity. There is an increase in total carbon as ^{14}C activity decreases (Fig. 36). The bulk of the TMG, alluvial and CGS samples have high ^{14}C activities but low carbon content. Samples from these aquifers are the samples that were often lost due to insufficient carbon. After evaluation of the carbon data in Appendix II and apparent trends within each of the aquifers, it is assumed that samples which could not be analysed for ^{14}C, likely have activities between 80 – 110 pMC. They are assumed to be younger as they have not yet had time to pick up significant quantities of carbon along their flow paths. Based on this assumption, samples PE001 and GRB001 are

assumed to have radiocarbon residence times of less than 70 years, which is corroborated by their noble gas ages (Table 8, sect. 5.1.1).

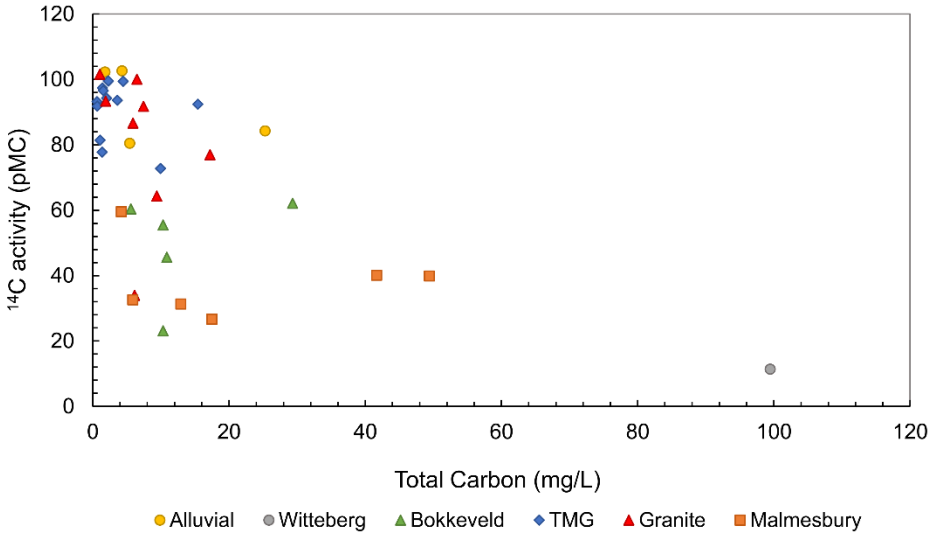

Figure 36 – ^{14}C activity as a function of total carbon concentrations per aquifer.

5.2.2.3 Comparison to Previous Work

Radiocarbon ages for the TMG Aquifer correspond reasonably well with previous work conducted by Weaver et al. (1999), Miller et al. (2017) and Turner (2018). Attempts to date the TMG Aquifer in the Agter-Witzenberg Valley (near Ceres), produced ^{14}C contents exceeding 100 pMC (Weaver et al., 1999). To corroborate the noble gas dating of the springs in the Drakenstein Mountains (section 5.2.1.3), radiocarbon samples were collected at the same sites and yielded activities between 99.9 ± 0.4 and 102.8 ± 0.3 pMC (Miller et al., 2017). Finally, radiocarbon dating in the Verlorenvlei catchment (near Elands Bay) produced carbon contents of 95.2 and 98.7 pMC and calibrated ages of 235 and 597 years before present (BP) (Turner, 2018). Although ^{14}C activities have often not been calibrated to residence times, measured radiocarbon activities in the aforementioned studies often exceed 100 pMC which is an indication of modern recharge. This correlates well with the dataset of this study as the correction model produced several samples that are less than 70 years old. Despite only two calibrated ages, the residence times calculated by Turner (2018) also indicate that calibration of radiocarbon ages for this study are realistic as ages range between <70 – 1 742 years.

Additionally, Weaver et al. (1999) dated boreholes drilled into the Bokkeveld Aquifer, which produced radiocarbon activities between 30 and 73 pMC, corresponding to residence times of

8.1 – 1.2 ky. Residence times determined by Weaver et al., (1999) correlate well with data captured for the Bokkeveld in this study as ^{14}C contents range between 23.1 – 62.1 pMC, producing residence times of 6.0 – 1.2 ky. It is possible that these samples may have been over-corrected as evaluation of their $\delta^{13}C$ values indicates addition of dead carbon along the flow path. Residence times for groundwater of the Malmesbury Aquifer in the Verlorenvlei catchment have been constrained to 9.4 – 2.5 ky (Turner, 2018). This indicates good correspondence of calculated residence times of 11.1 – 4.0 ky for the same aquifer in this study. Turner (2018) constrained residence times for the alluvial aquifer to be between 1597 – 268 years. This is in slight disagreement with data captured in this study which constrain residence times as younger than 70 years although one sample returned an age of 1 783 years. Turner's noble gas ages for this aquifer, however, were in the range of 34.6 – 47.6 years. Turner hypothesized that the discrepancy between ^{14}C and noble gas ages is due to additional packages of water continuously contributing to recharge along the flow path.

There have been extensive studies on the thermal springs which emanate from the TMG Aquifer. Through the use of ^{14}C in conjunction with $\delta^{2}H$ and $\delta^{18}O$, Mazor and Verhagen (1983) and Diamond and Harris (2000) have confirmed that thermal springs along the CFB have meteoric origins and have been recharged during the Holocene (Olivier and Jonker, 2013). Of the numerous springs in the Western Cape, two were sampled in this study, namely the Montagu and Citrusdal (The Baths) springs. The Citrusdal spring emanates from the Nardouw (TMG) Aquifer whilst the origin of the Montagu spring has been reported as the fault between the Bokkeveld and TMG lithologies (Diamond and Harris, 2000). Due to its chemistry, the Montagu spring has been classified as a Bokkeveld sample in this study.

Although the Citrusdal spring was sampled for radiocarbon in this study, unfortunately no measurement could be obtained. Mazor and Verhagen (1983), however, estimate the residence time of The Baths (Citrusdal) to be on the order of approximately 3 ky (71 pMC). The Montagu Baths sampled in the same study had a measured ^{14}C activity of 49.1 pMC (Mazor and Verhagen, 1983). This is in fair agreement with the Montagu sample collected in 2018 which provided a ^{14}C activity of 55.5 pMC which corresponds to a residence time of approximately 5 ky.

5.3 Comparison between $^{3}H/^{3}He$ and ^{14}C ages

The radiocarbon correction model is evaluated by plotting tritium activity (TU) against that of radiocarbon activity (pMC). Due to unconstrained modern input tritium and radiocarbon, the model assumes pre-bomb peak concentrations. Tritium has a short half-life ($t_{1/2}$ – 12.32 years) in comparison to radiocarbon ($t_{1/2}$ – 5 730 years), and hence it is expected that any measurable tritium would have decayed out of the water system by the time the radiocarbon activity decreases to approximately 99 pMC. This would be an ideal piston flow system where there is no mixing along the flow path, resulting in the decay curve seen in Fig. 37. The average input tritium in the Western Cape around 1950 is assumed to be similar to modern input and a value of 1.6 TU is assumed (Van Rooyen, unpublished data; section 5.2.1.2). Multiple mixing lines are constructed from input/recharge concentrations (100 pMC, 1.6 TU) to every ten pMC. These lines assume that recharge (precipitation) mixes with an older water body effectively altering the concentrations in the resultant water body, moving it along the mixing line. Increased mixing ratios will push concentrations closer to recharge concentrations.

Samples that plot on the decay line are suspected to not have undergone significant mixing with any other water bodies as both tritium and radiocarbon are decaying in appropriate proportions. Samples that deviate to the right of the decay line are assumed to have been recharged during the ‘bomb-peak’ era as they have increased input radiocarbon which exceeds 100 pMC. A number of TMG samples plot on the decay line so it can be assumed that these samples have been recharged before the onset of nuclear weapons testing but have not undergone significant mixing with other water bodies. However, the bulk of the TMG and alluvial samples plot to the right of the decay line as well, suggesting that they have been recharged post-1950.

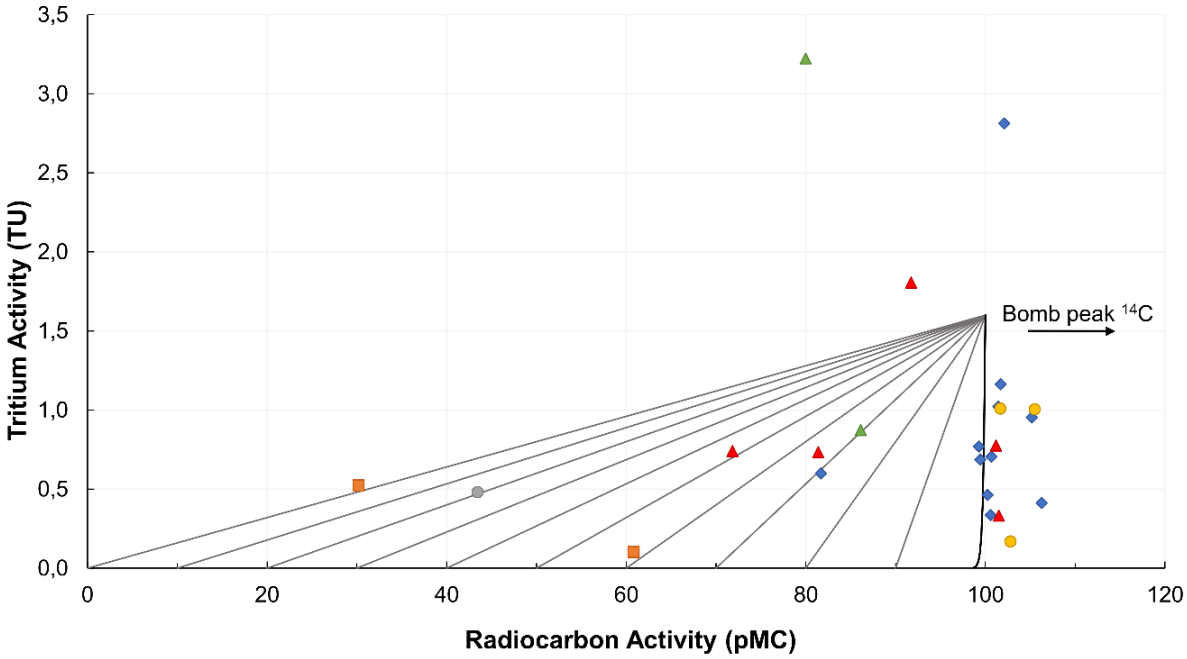

Figure 37 – Corrected radiocarbon activities plotted against tritium concentrations in groundwater.

Samples that deviate to the left of the decay line are suspected to have undergone mixing with one or more water bodies of a significantly different age. One TMG sample, VD003 indicates mixing with an older body of water. This is substantiated by a radiocarbon residence time of 1.7 ky and a noble gas age of 23.4 years. Two CGS samples, KB002 and FH005, indicate mixing with a water body or water bodies with an average pMC of 50 and 65 pMC, respectively. These samples appear to have high mixing ratios of close to 50% with recent recharge. Malmesbury sample PV001 indicates significant mixing (~30%) between recharge and a very old water body from which ^{14}C has completely decayed out of. The position of another Malmesbury sample, FH002, indicates low mixing ratios of modern water and old water with 55 – 60 pMC. Significant mixing (~30%) is also evident between ROB001 (Witteberg Aquifer) and modern water. Sample BD001 (Bokkeveld) indicates approximately 50% mixing of modern water with groundwater with an average ^{14}C activity of ~70 pMC, which is evidenced by a younger noble gas age of 84.7 years.

The mixing lines (Fig. 37) would look very different depending on the input tritium values, which can vary substantially. For this dataset they appear to fit the data reasonably well, however, the two samples from Ceres, C001 (Bokkeveld) and C002 (TMG) have higher tritium values than the other samples and plot above the mixing curves. It is uncertain whether this is attributed to the fact that the Ceres samples have been recharged post-1950 or that if the

region receives rainfall with higher tritium concentrations. From the positions of these samples, it can be assumed that the TMG sample has not undergone significant mixing whereas the Bokkeveld has high tritium and 80 pMC, indicating mixing of water along its flow path.

Locations where residence times were calculated using both noble gas and ^{14}C are compared in Table 11. Where ^{14}C ages could not be determined due to the lack of DIC, this is indicated as 'not determined' (nd). Overall, there is good correlation between the two dating systems as many of the samples that could be dated with noble gas have returned radiocarbon ages younger than 70 years old. Samples ROB001, BD001, PV001 and FH002 which returned zero noble gas ages and relatively old radiocarbon ages provide further evidence of mixing. Samples SU001, GRB001 and VD002 have returned zero ages in noble gas calculations, and either have radiocarbon ages younger than 70 years or activity could not be determined.

There is, however, concern that there may be larger errors in the calculated ^{14}C model ages for the older Bokkeveld, Witteberg and Malmesbury Aquifers than there are for ages in the TMG, CGS and alluvial aquifers. The approach used to estimate soil $\delta^{13}C$ for these aquifers which have clearly had an addition of dead carbon along their flow path, may have over or under-corrected the ^{14}C activities which could result in errors of hundreds to possibly thousands of years. Radiometric dating of groundwater is often associated with larger errors and propagation thereof due to the number of assumptions which are made. This is evident in this study, but evaluation of model ages against previous ages and activities determined for the respective aquifers indicate that the apparent ages calculated in this study are reasonable.

Table 11 - Comparison between apparent ages calculated from the $^{3}H/^{3}He$ and ^{14}C dating systems.

Sample Name	Aquifer	$^{3}H/^{3}He$ age (yr)	±1σ (yr)	^{14}C age (yr)
ZH18-SW001	Alluvial	29.76	*18.4*	*<70*
ZH18-SW002	Alluvial	17.73	*5.5*	*<70*
ZH18-SU001	Alluvial	2.80	*15.5*	*nd*
ZH18-SU002	Alluvial	0.00	*14.1*	*nd*
ZH18-SU003	Alluvial	62.51	*6.1*	*nd*
ZH18-ROB001	Witteberg	0.00	*292.5*	*6699*
ZH18-BD001	Bokkeveld	84.71	*3.4*	*1200*
ZH18-C001	Bokkeveld	58.53	*0.9*	*1794*
ZH18-C002	TMG	0.32	*7.4*	*<70*
ZH18-BD002	TMG	44.59	*4.9*	*<70*
ZH18-GRB001	TMG	0.00	*4.5*	*nd*
ZH18-VD002	TMG	0.00	*273.9*	*<70*
ZH18-VD003	TMG	23.40	*10.8*	*1626*
ZH19-VD004	TMG	1.36	*29.2*	*<70*
ZH18-FH001	TMG	43.18	*4.1*	*<70*
ZH18-DD001	TMG	19.88	*5.5*	*<70*
ZH18-DD002	TMG	24.69	*9.2*	*46*
ZH18-PE001	TMG	35.05	*9.0*	*nd*
ZH18-DB002	TMG	32.99	*3.6*	*nd*
ZH18-DB003	TMG	9.04	*8.5*	*nd*
ZH18-DB004	TMG	0.00	*24.0*	*nd*
ZH18-KB001	TMG	29.81	*3.9*	*<70*
ZH18-KB002	Granite	3.70	*19.2*	*2660*
ZH18-R001	Granite	10.02	*13.0*	*<70*
ZH18-PV001	Malmesbury	0.00	*283.7*	*3994*
ZH18-FH002	Malmesbury	0.00	*29.9*	*9624*
ZH18-DK001	Malmesbury	45.50	*3.0*	*7204*

5.4 Potential Proxies for Groundwater Residence Time

With increasing groundwater residence time, the chemistry of the water is subject to change along the flow path. Dissolution of minerals, ion exchange and mixing of distinctly different water bodies may alter the groundwater chemistry. Physical characteristics of aquifers and boreholes also a play a role in recharge volumes, effectively impacting groundwater residence times. As a result, chemical and physical parameters may be an indication of relative residence times. Stable isotopes of hydrogen ($\delta^{2}H$) and oxygen ($\delta^{18}O$) as well as basic cations (Ca^{2+}, Mg^{2+}, Na^{+}, K^{+}) and anions (Cl^{-}, HCO_3^{-}, PO_4^{2}-, SO_4^{2-}) were collected at the same sample sites by Agyare-Dwomoh (2020) and have been compared to the findings of this study to

ascertain whether it might be feasible to develop a proxy for residence time without doing the labour intensive work on determining actual residence time.

5.4.1.1 Borehole Depth

Boreholes of varying depths were sampled in this dataset, but some boreholes have unknown depths due to the fact that this information was provided by the water users. Borehole and wellpoint depths for the sample set range from 10 – 325 metres (Table 6). Additionally, a number of springs were sampled, both cold and hot. Depths of cold springs were recorded at 0 m and depths of thermal springs were obtained from literature as extensive research has been conducted (Mazor and Verhagen; 1983; Diamond, 1997; Diamond and Harris, 2000). The Citrusdal and Montagu springs sampled in this study, circulate at great depths which as indicated by their groundwater temperatures (43 – 45 °C). Boreholes and well points drilled into the alluvial aquifer tend to be relatively shallow, not exceeding 60 metres below ground level. The Cape Granite and Malmesbury boreholes had intermediate depths, reaching maximum depths of 142 and 235 metres, respectively. The deepest recorded boreholes are into the TMG and Bokkeveld Aquifers, which are 325 and 207 metres respectively. It is generally predicted that the residence time of groundwater will increase the further one moves away from the recharge zone as well as with increasing depth (Ma et al., 2019). As expected, there appears to be a general trend where the deeper the borehole from which the sample was collected, the longer the residence time of the sample. This holds true for all the aquifers sampled but the TMG Aquifer. Groundwater from the TMG Aquifer has proven to be young irrespective of borehole depth (Fig. 38). This is likely due to the fact that the extensive TMG Aquifer has a good fracture network allowing for relatively fast infiltration as well as uninhibited flow paths.

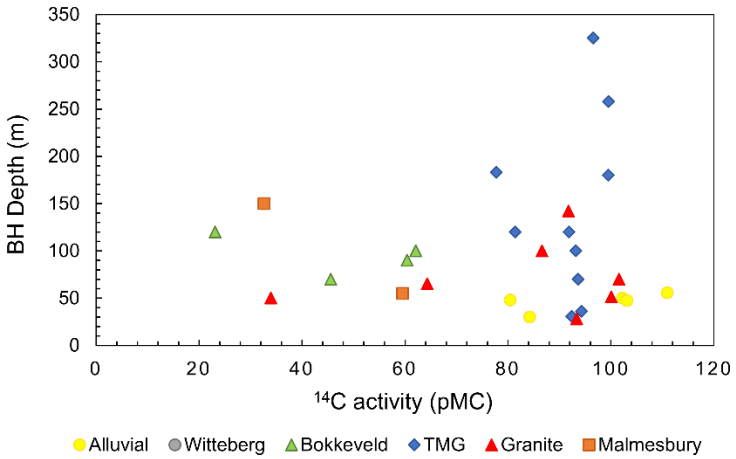

Figure 38 – Radiocarbon activity plotted against borehole depth per geological group.

There appears to be a rough correlation between borehole depth and $\delta^{2}H$ and $\delta^{18}O$ values (Agyare-Dwomoh, 2020). For samples collected from the Malmesbury, Cape Granite, Bokkeveld and alluvial aquifers, the isotopic signatures for both $\delta^{2}H$ and $\delta^{18}O$ become increasingly depleted in the heavier isotopes as borehole depth increases (Fig. 39-A and B). This is likely due to the fact that shallow, subsurface water is more likely to be influenced by rainfall and is younger whereas the deeper boreholes are not. Increasingly negative isotope signatures at depths may be an indication of older water that has been recharged in a colder climate by precipitation that is relatively depleted compared to modern day precipitation (Koehler et al., 2000). This, however, does not hold true for TMG groundwater. TMG samples are scattered and seem to have a more random distribution regardless of depth. As the areal extent of the TMG Aquifer is quite vast and the aquifer outcrops at various elevations and geomorphological structures, the scattered distribution of isotope values for TMG groundwater is subject to a number of isotopic effects which include the continental, altitude and rain-out effects (Dansgaard, 1963; Diamond, 1997; Diamond, 2000).

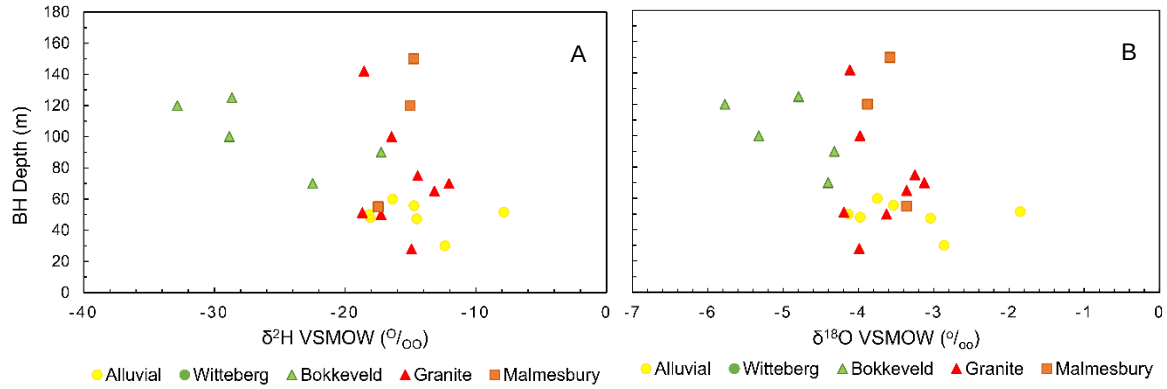

Figure 39 – Borehole depths compared to isotopic compositions of A) δ²H and B) δ¹⁸O (Agyare-Dwomoh, 2020).

5.4.1.2 Groundwater Chemistry

Groundwater chemistry data is also able to provide rough indications of groundwater residence time. pH values of rainwater typically fall within the range of 5.0 – 5.5 (Smith et al., 1984). It is therefore expected that samples with shorter residence times will have pH values similar to that of rainwater whereas samples with longer residence times have higher pH values as the groundwater has interacted with the host rock allowing for the dissolution of OH^- ions. Rocks from the TMG, however, are dominated by silicate minerals. Dissolution of silica will decrease pH through the formation of silicic acid (H_4SiO_4) and H^+/H_3O^+ ions (Appendix III). The groundwater in the TMG Aquifer system, however, is often young, not having spent enough time in the system to significantly alter its chemistry. Porous quaternary sands which host the alluvial aquifers also contain a great deal of silica. The water in these aquifers also tend to be more recently recharged (Hay et al., 2015). Modern water initially possessing low pH values, coupled with the chemistry of the aquifer host, result in pH values that tend to be more acidic.

Silicate weathering, however, is slower than the weathering of carbonate-bearing minerals (Lacroix et al., 2017) which are more abundant in the Malmesbury, Bokkeveld and Witteberg Groups. Ca^{2+} and Mg^{2+}, which are most often associated with CO_3^{2-}, both increase in groundwater as time increases. Ca^{2+}, however, increases at much higher rates than Mg^{2+} (likely a higher proportion of $CaCO_3$ than $MgCO_3$), resulting in an exponential increase in Ca/Mg ratios in the groundwater as measured radiocarbon increases. Carbonate dissolution also causes an exponential increase in HCO_3^- (a function of alkalinity), which in turn linearly increases pH (Fig. 40). The addition of Ca^{2+} and Mg^{2+}, however, may not be solely from the

host rock. It may be derived from the soil, naturally or artificially, as carbonates are often used in agricultural practices to reduce soil acidity. Although the granites possess a considerable amount of silica in both quartz and feldspar, they more readily produce HCO_3^- through the hydrolysis of feldspar, resulting in a larger range of pH values. As mineral dissolution and the subsequent change in pH occurs progressively over time, Ca/Mg ratios, HCO_3^- concentrations and pH can serve as proxies to groundwater residence time.

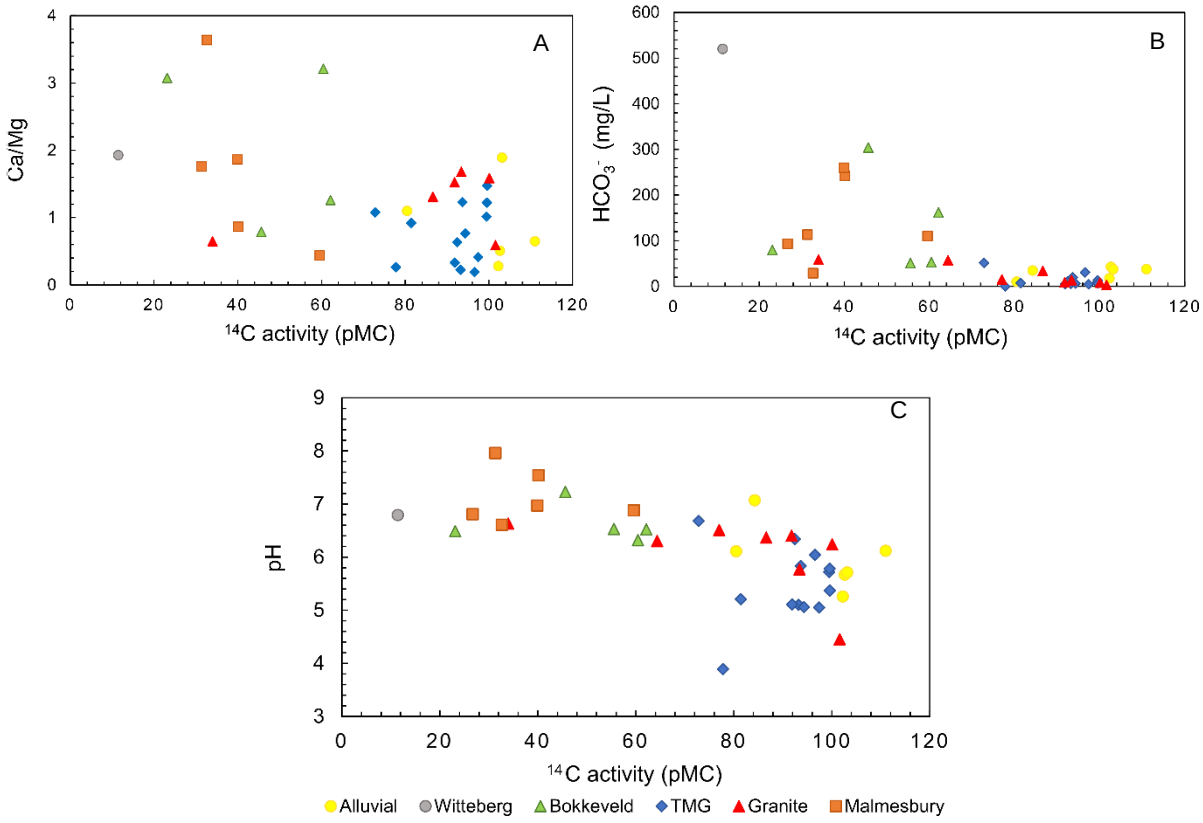

Figure 40 – Measured radiocarbon activity plotted as a function of A) Ca/Mg ratios; B) HCO_3^- concentrations and C) pH.

It is important to note that an increase in 'dead' carbon (carbon that does not contain any measurable ^{14}C; from HCO_3^- and CO_3^{2-}) dilutes the measured radiocarbon. As a result, the measured ^{14}C may not necessarily reflect the true residence time and requires some correction (sect. 5.1.2). When pH is compared to the corrected radiocarbon activity (Fig. 41), a linear increase can still be observed in many instances, but instead a wider range of 'input' pH values exist. This may be attributed to factors such as soil chemistry that may affect the water chemistry as it enters the saturated zone before eventually entering the groundwater system. Soil, particularly on irrigated land, is subject to acidification through the use of

fertilizers, which is then countered through the use lime/limestone to neutralise the soil. The resulting trends in both measured and corrected radiocarbon activities, lead pH to be used as a qualitative indicator of both residence time and radiocarbon activity, although it would be better suited to the latter.

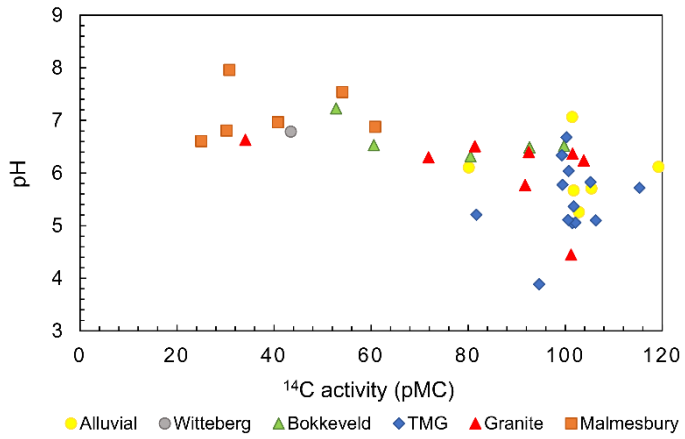

Figure 41 – Corrected radiocarbon activities compared to groundwater pH.

5.4.1.3 Distance from the Coast

When measured radiocarbon activity is compared to δ^2H and $\delta^{18}O$, two distinct groupings can be identified (more prominent in Fig. 42-A). The first group consists of samples that plot below -25 ‰ δ^2H and between -4.5 and -7 ‰ $\delta^{18}O$ and are referred to as isotopically “light” or depleted in the heavier isotope. The second group is comprised of samples that plot above -25 ‰ δ^2H and -5 ‰ $\delta^{18}O$ and are referred to as isotopically “heavy” or enriched in the heavier isotope. These two groupings can be attributed to the partitioning effect of the Cape Fold Belt (Fig. 43).

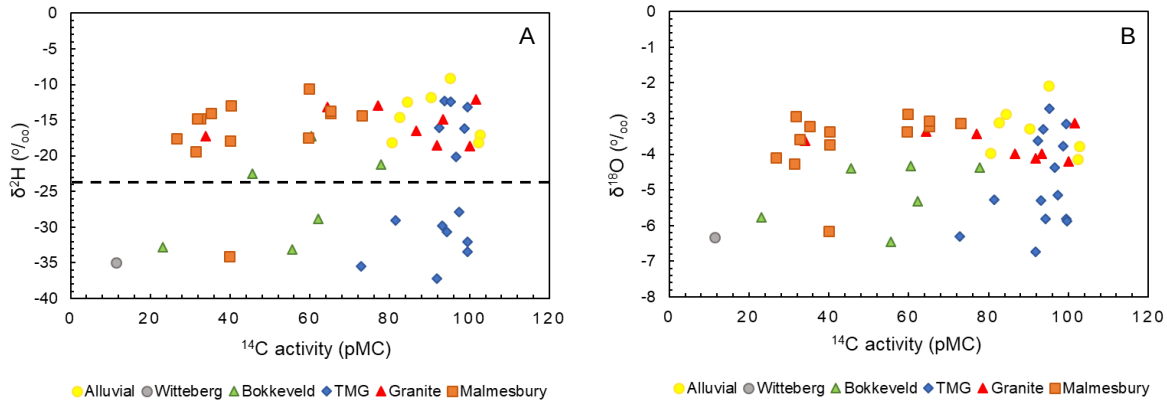

Figure 42 – Radiocarbon activity per aquifer plotted against A) δ^2H and B) $\delta^{18}O$ can be divided into two groups (separated by dashed black line).

Cold front systems originating in the South Atlantic Ocean to the south west of the country, bring rain to the west coast during the winter months (Du Plessis and Schloms, 2017). As a cold front system moves from the coast towards the interior, the heavy isotopes preferentially rain out first. Through the process of Rayleigh fractionation, the evolving water vapour system becomes increasingly depleted of heavy isotopes as it moves from the coast further inland. The heavier isotopes favour the liquid phase and are removed from the system in the form of the precipitation. The resultant weather system as well as the falling precipitation become isotopically lighter each time a packet of water, i.e. rain is removed. Samples that are relatively enriched in the heavy isotope are located to the west of the North-South trending limb of the Cape Fold Belt (CFB). This region is much closer to the sea, from areas like Cape Town, Strand, Stellenbosch and Franschhoek. The isotopically light samples are from sites to the east of the CFB, and include Robertson, De Doorns, Barrydale, Villiersdorp and Ceres amongst others. In part, two distinct groupings may be due to the fact that no samples were taken on the peaks of the CFB. The mountainous regions receive high amounts of rainfall and the need for groundwater is minimal, so boreholes are exceedingly rare.

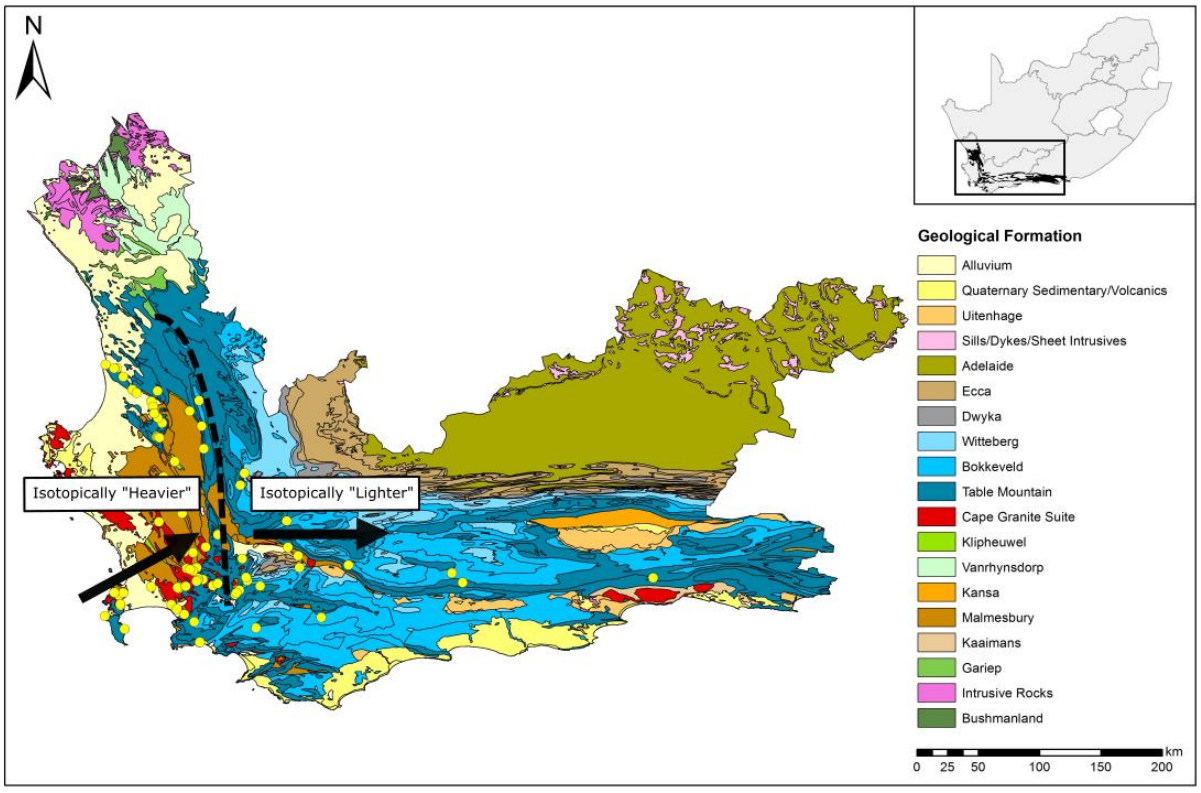

Figure 43 – Map illustrating how the Cape Fold Belt (CFB) (dashed black line) divides samples into two regions of generally isotopically 'heavier' (left) and isotopically 'lighter' (right). The black arrows indicate the general migration of a cold front system.

This is a well-documented process termed the 'continental effect' (Dansgaard, 1964). This trend is further substantiated by the graphs in Fig. 44-A and B below. These graphs illustrate how the isotopic signatures of both $\delta^{2}H$ and $\delta^{18}O$ become increasingly more depleted with increasing distance from the sea (Table 6) (Diamond, 1997; Diamond, 2014).

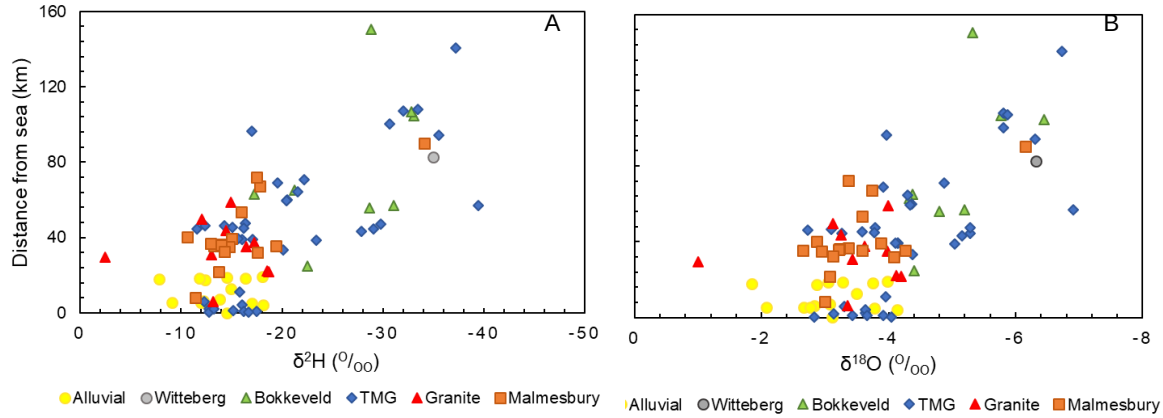

Figure 44 – Stable hydrogen (A) and oxygen (B) isotopes becoming increasingly depleted with increasing distance from the sea.

It was initially thought that the residence times would increase from the mountainous regions towards the coast as it is assumed that recharge occurs at high elevations and subsequently flows to low-lying near-shore areas. However, there appears to be no relationship between distance from the coast and groundwater residence time as the measured radiocarbon activity ranges from 11 to 110 pMC regardless of coastal distance or the isotopic composition. This is likely due to the fact that samples were taken from multiple aquifers in multiple catchments across an extensive area. Sampling along a suspected flow path within a single aquifer and catchment may yield an increase in residence time from mountain zones to discharge zones and further targeted sampling and analysis of radioisotopes is necessary to test this theory.

6 RELATIONSHIP BETWEEN RESIDENCE TIME AND GROUNDWATER RECHARGE

The noble gas data and groundwater residence times (sect. 5, Table 8) can provide insight into more than just turnover time of groundwater in an aquifer system. Noble gas concentrations provide insight into recharge temperatures and as a result, locations. Additionally, the helium data can also provide indication of mixing between groundwater and crustal or mantle components. Discrepancies between apparent $^{3}H/^{3}He$ and ^{14}C ages, which have been established in section 5.2, provide an indication of groundwater mixing as the water ages and moves along a flow path. These groundwater interactions are discussed in the section below.

6.1 Groundwater Recharge Temperatures

Solubility curves for noble gases He, Ne, Ar, Kr and Xe have long been established using Henry's Law (Potter and Clynne, 1978). Noble gas solubilities are temperature dependent with solubility generally decreasing as temperature increases (Appendix IV). Through the use of groundwater noble gas concentrations and estimated recharge elevations, it is possible to determine the temperature of groundwater recharge as well as entrapped air per litre of water being recharged (1 litre = 1 kg).

Recharge elevations are assumed to be the high-lying mountainous regions for each catchment as this is where the bulk of groundwater infiltration occurs (Scanlon, 2002; Watson et al., 2018). Calculated values for entrapped air (A) and recharge temperatures (NGT) were evaluated according to Aeschbach-Hertig's model (1999, 2000). Fit to the model is represented by a chi^2 value (Table 12). Samples with chi^2 values tending to zero are ideally suited whereas values exceeding 3.0 are not suited to the Aeschbach-Hertig model. Chi^2 values exceeding 3.0 are not necessarily indicative of unreliable data but rather that it is not suited to the model.

The recharge elevation model sometimes produces unrealistic solutions when fitting noble gas concentrations to recharge temperatures for groundwater. Problematic solutions are commonly associated with high A values (>100 cm^3/kg), high temperatures as well as high errors obtained from the algorithm. Issues are related to and caused by a deviation in noble gas concentrations, particularly elevated Ar combined with decreased Xe (Jung et al., 2013). Deviations in noble gas concentrations (caused by degassing or excess air) less than typical measurement uncertainties are already sufficient to create problematic solutions to the model (Aeschbach-Hertig et al., 2008; Jung et al., 2013). Groundwater samples from warmer regions or areas where infiltrating groundwater contains a high amount of entrapped air, tend to be particularly sensitive to deviations (Jung et al., 2013).

Samples ROB001, GRB001 and KB002 are considered to have impossible recharge temperatures as their NGT's exceed 56°C. ROB001 and GRB001 are associated with elevated Ar whereas KB002 has the lowest recorded Xe concentration in the sample set. It is possible that these samples may have issues regarding measurement errors as Ar solubility should decrease with increasing temperature. Two of these samples have already been marked as unreliable through the evaluation of their helium concentrations (ROB001, GRB001). It is possible that the inaccurate recharge temperature for KB002 is due to an incorrect assumption of where recharge occurs and hence its recharge elevation. The model is quite sensitive to changes in parameters.

Excluding impossible recharge temperatures for samples ROB001, GRB001 and KB002 (temp > 56°C), recharge temperatures have been calculated to range from 9.4 – 28.6 °C and chi^2 values range from 0.0 – 3.1 (Table 8). To evaluate the realistic noble gas temperatures, historic mean daily temperature and rainfall volumes were compared for four weather stations on the SASSCAL network (Muche et al., 2018). Automated weather stations (AWS) at Porterville (122 mamsl), Elgin (311 mamsl), Cape Town (46 mamsl) and Dwarsberg (Stellenbosch, 1 214 mamsl) were chosen. Temperatures for Porterville and Dwarsberg have the highest and lowest recorded temperatures, respectively and range from 5.4 – 34.1°C ($\bar{x}$ = 17.7) and -1.1 – 26°C ($\bar{x}$ = 11.4). Temperatures for Elgin and Cape Town are more moderate, ranging between 2.6 – 29.9°C ($\bar{x}$ = 17.7) and 5.0 – 29.8°C ($\bar{x}$ = 11.4), respectively. As the groundwater samples in this study are collected from a large area (Fig 16), stations were chosen on the basis of the time range of available temperature and rainfall data as well as locations that would best represent the dataset as a whole.

The station located in Porterville would be more or less representative of continental regions which are semi-arid, experience temperature extremes and receive less rainfall. This station can be compared to sites in Ceres, Barrydale and De Doorns. The weather station in Elgin is located closer to the coast at an intermediate elevation, likely receiving more rainfall. The Cape Town station is located at a low elevation, proximal to the coast and experiences a more temperate climate. This station would be particularly useful in comparing samples from the Peninsula and will have comparable weather to areas like Somerset West. The last station in Dwarsberg, is located at a high elevation which typically receives higher rainfall volumes. Due to the variety in locality of the weather stations, the temperature and rainfall data may not be completely accurate for each sample but will be representative of most.

The interception volume – the volume of precipitation that effectively contributes to groundwater recharge – varies for each aquifer as it is dependent on a number of factors which include porosity and permeability/fracturing of the rock body, soil type, vegetation cover, elevation, topography, etc. The interception value for exposed bare rock of the TMG in high-lying areas is likely to be low (~5 mm or possibly less) whereas recharge in valleys where dense vegetation covers geology of the Malmesbury, may require more than 5 mm of rainfall. An average rainfall volume of 10 mm is assumed to contribute to recharge across all six aquifers to some extent. The temperature recorded during rainfall events exceeding 10 mm (further referred to as recharge events) is recorded for each month over the entire time series. The number of rainfall events and the percentage they constitute of all 10 mm+ events are recorded as well (Table 13). Additionally, these 10 mm rainfall event temperatures (dark blue circles) are compared to daily mean temperatures (light blue lines) (Fig. 45).

Daily mean temperatures possess a much larger range in values than the range for temperatures during which recharge events occur. For all for stations, the majority of recharge events occur during May – August whereas the least number of events generally occur during December – February. This indicates that recharge occurs mainly during winter (May – Aug; 58 – 65%) although there is some contribution during summer (Jan – Dec; 9 – 14%). Although a percentage of recharge does occur during summer months, the temperature is raised and precipitation is subject to evaporation, so it is not sure how much recharge these events actually contribute to groundwater.

Despite similar time ranges for the Porterville and Elgin stations, it is evident that there are less recharge events recorded in the arid Porterville region. The Porterville station, which is located at the base of the Groot Winterhoek Mountains, experiences the greatest range in temperatures during recharge events across the four weather stations as temperatures range between 8.7 – 22.0°C. The highest elevation station, Dwarsberg, is associated with the coldest temperatures during rainfall, which range between 4.3 – 10.4°C. Despite having the shortest time range data of the four stations, the number of recharge events during this period indicate that the Dwarsberg station receives the highest volumes of rainfall. The Dwarsberg station also receives the highest percentage of rainfall events during summer (~14%). The Cape Town airport station has the longest running weather station and has moderate recharge event temperatures between 10.3 – 17.1°C. A large percentage of the rain that falls in this region is likely to quickly infiltrate into the alluvial aquifer. Similar to Cape Town, a mean temperature range of 8.0 – 18.6°C is recorded for the intermediate elevation Elgin station.

After evaluation of the climate data, the noble gas temperatures determined for the samples are both possible and reasonable. Elevated regions are associated with lowered temperatures and high volumes of rainfall, whereas the opposite is true for low-lying areas. As a result, it can be assumed that lowered noble gas temperatures (~9 - 15°C) indicate recharge sourced from mountainous regions during winter. As the highest recorded temperature during recharge events does not exceed 18°C at Dwarsberg, it is unlikely that the recharge source for groundwater samples with warmer temperatures (15°C – 30°C) are these mountainous regions. As temperatures at the valley (low elevation) stations have larger ranges as well as a considerable number of recharge events, it is likely that these groundwater samples have been recharged by precipitation that falls in the valley. This introduces the idea that while the bulk of recharge occurs in the mountains, recharge also occurs much further along the groundwater flow path in valleys of intermediate to low elevations.

Table 12 – Noble gas temperatures (NGT), entrapped air (A) and chi^2 values of noble gas samples.

Sample Name	Aquifer	He	Ne	Ar	Kr	Xe	Recharge Elevation	NGT	A	chi^2
				x 10^{-6} ccSTP/g			m	°C	cm^3/kg	
ZH18-SU001	Alluvial	0.079	0.261	365.034	0.079	0.011	1470	12.3	4.78	0.83
ZH18-SU002	Alluvial	0.105	0.236	347.712	0.075	0.011	1470	13.7	4.04	0.56
ZH18-SU003	Alluvial	0.722	0.249	357.080	0.074	0.010	1470	18.0	22.13	0.25
ZH18-SW001	Alluvial	0.064	0.229	960.594	0.127	0.013	1410	28.6	76.81	13.59
ZH18-SW002	Alluvial	0.056	0.212	332.116	0.071	0.010	1410	15.0	14.97	0.45
ZH18-ROB001	Witteberg	1.879	0.252	1145.869	0.145	0.013	1000	56.7	107.01	10.36
ZH18-BD001	Bokkeveld	1.198	2.038	1493.083	0.212	0.021	1440	16.9	143.24	2.59
ZH18-C001	Bokkeveld	10.787	0.459	506.106	0.093	0.010	1620	28.3	70.81	3.13
ZH18-BD002	TMG	0.073	0.235	355.300	0.076	0.010	1440	14.6	12.73	0.41
ZH18-C002	TMG	0.075	0.305	413.628	0.086	0.012	1620	10.6	18.17	0.21
ZH18-DB002	TMG	0.066	0.224	362.147	0.077	0.010	1935	15.4	50.84	0.06
ZH18-DB003	TMG	0.051	0.202	337.432	0.075	0.011	1935	12.4	15.23	0.13
ZH18-DB004	TMG	0.048	0.199	329.258	0.073	0.010	1935	12.4	2.36	2.64
ZH18-DD001	TMG	0.079	0.266	372.717	0.082	0.011	2180	9.4	13.34	1.58
ZH18-DD002	TMG	0.117	0.326	400.377	0.082	0.011	2180	10.8	15.88	0.00
ZH18-FH001	TMG	0.097	0.349	435.736	0.088	0.011	1680	11.9	22.59	0.00
ZH18-GRB001	TMG	0.015	0.164	2175.812	0.230	0.021	1410	126.4	1212.92	181611.00
ZH18-PE001	TMG	0.081	0.306	394.132	0.084	0.011	1840	11.6	16.06	1.74
ZH18-VD002	TMG	0.141	0.494	1037.552	0.137	0.015	1720	24.5	82.92	18.28
ZH18-VD003	TMG	0.175	0.32	401.140	0.082	0.011	1720	12.4	13.84	0.14
ZH19-VD004	TMG	0.082	0.227	321.846	0.069	0.010	1720	15.0	3.65	0.33
ZH18-KB001	TMG	0.067	0.26	407.520	0.087	0.012	1060	12.0	30.43	0.04
ZH18-KB002	Granite	0.289	0.234	287.742	0.051	0.004	1060	74.2	113.28	151.69
ZH18-R001	Granite	0.067	0.254	354.714	0.076	0.010	1815	13.2	8.56	0.16
ZH18-DB001	Malmesbury	0.087	0.31	392.271	0.080	0.011	1935	13.7	14.90	0.18
ZH18-DK001	Malmesbury	1.113	0.256	378.847	0.080	0.011	1805	12.9	20.61	0.03
ZH18-FH002	Malmesbury	0.047	0.197	385.768	0.083	0.011	1680	9.8	7.47	0.02
ZH18-PV001	Malmesbury	0.204	0.392	429.774	0.082	0.010	1010	19.1	21.98	0.05

Table 13 – Mean monthly temperatures recorded when rainfall events exceed 10mm as well as the number of <10mm rainfall events that occur across the timescale for A) Porterville, B) Elgin, C) Cape Town and D) Dwarsberg.

A	**Porterville**			B	**Elgin**		
	1999 - 2019 *Elevation: 122 m*				*1999 - 2019* *Elevation: 311 m*		
Month	Mean temp for rainfall events >10 mm	Number of rainfall events >10 mm	Percentage	Month	Mean temp for rainfall events >10 mm	Number of rainfall events >10 mm	Percentage
Jan	19.3	1	0.57	Jan	18.2	13	2.90
Feb	22.0	9	5.11	Feb	16.5	8	1.78
Mar	18.1	10	5.68	Mar	16.5	11	2.45
Apr	14.3	10	5.68	Apr	13.2	34	7.57
May	14.3	18	10.23	May	13.7	39	8.69
Jun	12.4	38	21.59	Jun	9.7	85	18.93
Jul	10.0	34	19.32	Jul	8.0	77	17.15
Aug	8.9	20	11.36	Aug	8.4	74	16.48
Sep	8.7	13	7.39	Sep	8.7	42	9.35
Oct	16.0	3	1.70	Oct	12.0	28	6.24
Nov	16.1	10	5.68	Nov	13.3	24	5.35
Dec	20.2	10	5.68	Dec	18.6	14	3.12
	13.1	176	100.00		10.9	449	100.00

C	**Dwarsberg**			D	**Cape Town International**		
	2013 - 2019 *Elevation: 1 214 m*				*1973 - 2019* *Elevation: 46 m*		
Month	Mean temp for rainfall events >10 mm	Number of rainfall events >10 mm	Percentage	Month	Mean temp for rainfall events >10 mm	Number of rainfall events >10 mm	Percentage
Jan	9.7	18	4.40	Jan	12.9	13	2.06
Feb	10.4	7	1.71	Feb	15.7	18	2.86
Mar	8.5	22	5.38	Mar	17.1	23	3.65
Apr	7.5	26	6.36	Apr	15.3	49	7.78
May	7.4	39	9.54	May	14.0	91	14.44
Jun	5.6	71	17.36	Jun	12.1	112	17.78
Jul	4.9	58	14.18	Jul	10.3	112	17.78
Aug	4.3	68	16.63	Aug	10.5	96	15.24
Sep	5.2	35	8.56	Sep	12.6	38	6.03
Oct	6.3	24	5.87	Oct	14.1	33	5.24
Nov	7.5	28	6.85	Nov	16.4	29	4.60
Dec	6.2	13	3.18	Dec	16.3	16	2.54
	6.2	409	100.00		12.8	630	100.00

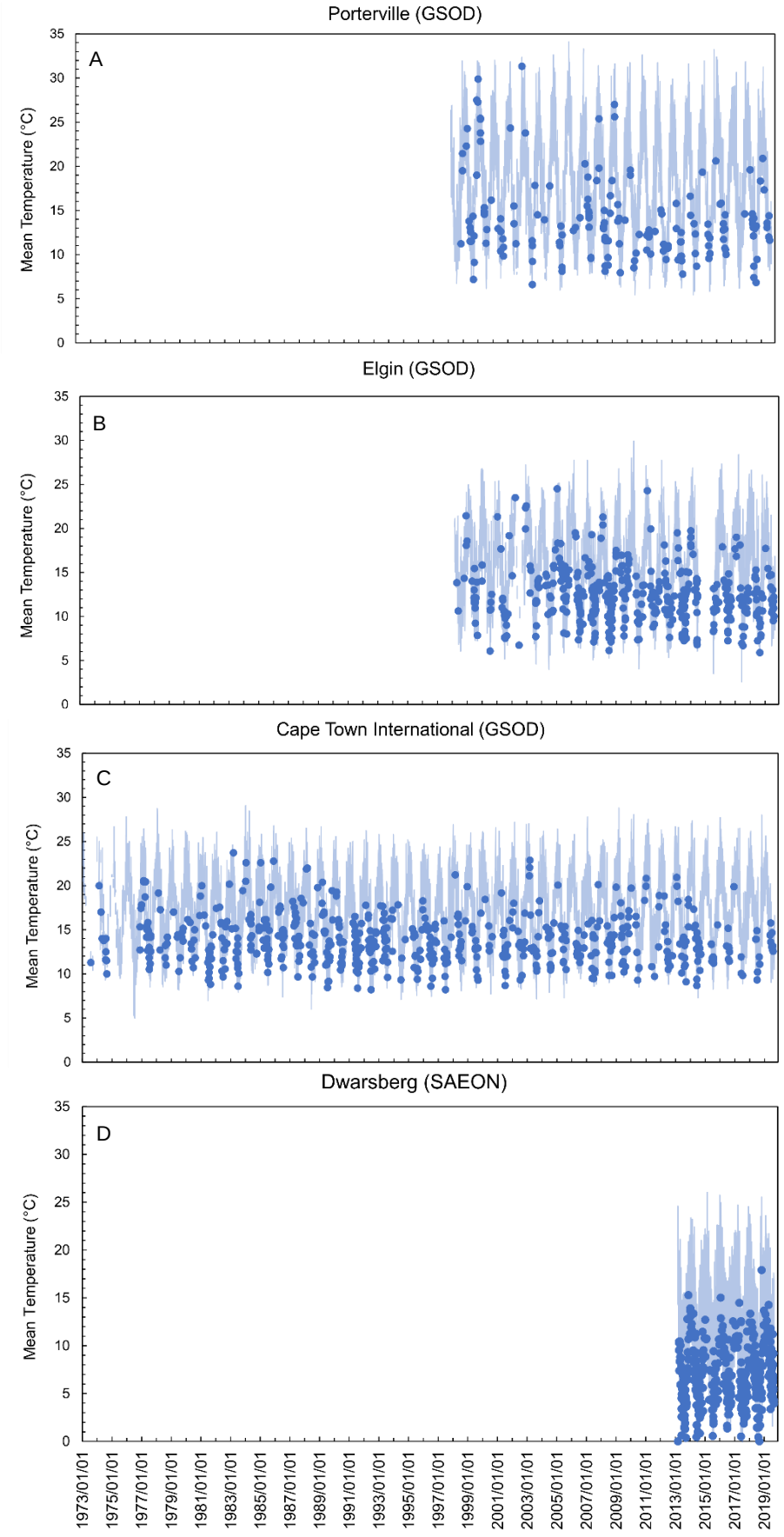

Figure 45 – Mean temperatures (light blue lines) and temperatures for precipitation events greater than 10 mm (dark blue dots) for A) Porterville, B) Elgin, C) Cape Town and D) Dwarsberg.

6.2 Groundwater Mixing

Based on the isotopic measurements and resultant residence times, a simplified model for groundwater flow in the TMG Aquifer is presented in Fig. 46. Measurements in this study confirm a spatial component to isotopic ratios in the respective aquifers, particularly based on their elevations. Assumptions are made on a large scale due to the areal extent of the study, based on tritium and radiocarbon activities as well as noble gas recharge temperatures. On a micro-scale within a catchment, there may be greater refinements that allow for the identification of mixing between individual samples. However, this is not possible in this model. This model builds on possible mixing within the TMG suggested by Turner (2018).

The model assumes that bulk recharge to the TMG is primarily through direct recharge of infiltrating precipitation in mountainous regions. The precipitation then infiltrates into either the soil, where it is subject to evaporation, or fractures in bare rock which is often exposed. Groundwater moves along the fracture network of joints and faults, progressively aging with increasing depth. Groundwater may discharge shortly after recharge in the form of cold springs (A), as is the case for the Drakenstein springs (sect. 5.2.1.3, Fig. 34). Boreholes proximal to the recharge zone (B) will have high ^{14}C and ^{3}H activities, showing good correlation between calculated residence times for the two dating systems, as is the case with the majority of TMG samples. The bulk of precipitation that falls in the recharge zone becomes run off that joins stream flow and is subject to evaporation. Base flow may also contribute indirect recharge to the aquifer. This, coupled with additional smaller packets of water from valley rainfall contribute additional recharge to the aquifer. Although these additional packages of water are relatively small, there is evidence indicating that they indeed contribute to groundwater recharge (Watson et al., 2018; Turner, 2018). This younger water may mix with the initial recharge water which is much farther along its flow path and consequently, much older. A borehole sampled at this point (C), further from the recharge source, will have a discrepancy in apparent ages between the noble gas and ^{14}C dating methods as is evident in samples VD003 and KB002. Mixing between water bodies of significantly different ages is suspected for the Witteberg, Bokkeveld, CGS and Malmesbury aquifers.

Additionally, groundwater that has infiltrated to great depths will increase in temperature because of the thermal mass of the rock body through which is passes. Once this water hits a large fault, contact, or unconformity, it flows upward and discharges at the surface in the

form of a thermal/hot spring (not pictured). This is the case with the Montagu and Citrusdal thermal springs (Diamond and Harris, 2000; Lambrakis and Kallergis, 2005). Inter-aquifer mixing is also suspected in some parts of the TMG as the aquifer is thought to contribute indirect recharge to the Malmesbury Aquifer (Watson et al., 2018).

Mixing scenarios for groundwater in other aquifers are expected to be similar where the oldest groundwater component is derived from precipitation in the mountainous regions, subsequently picking up smaller packages of younger groundwater as it moves along its flow path. This is substantiated by noble gas temperatures which indicate that recharge does not solely occur at high elevations. Recharge in the alluvial aquifer (particularly the Cape Flats aquifer), however, is sourced from the recharge that falls in the region. The porous material which is covered by little vegetation, allows for large amounts of infiltration into the shallow aquifer. Consequently, high hydraulic conductivities and short flow paths result in groundwater containing high ^{3}H and ^{14}C contents in the area (D).

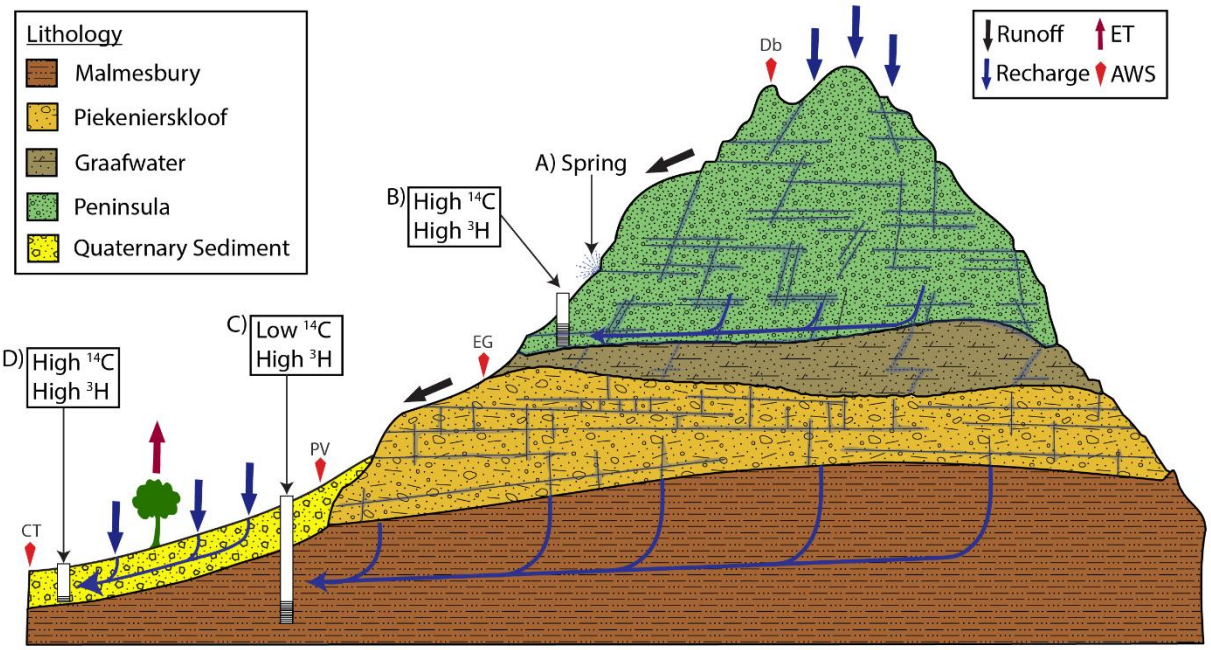

Figure 46 – Assumed mixing model within the TMG Aquifer indicates that bulk recharge occurs at high elevations and colder temperatures with additional recharge at lower elevations and higher temperatures; automated weather stations (ASW, red diamonds) of Dwarsberg (Db), Elgin (EG), Porterville (PV) and Cape Town (CT) are included in the conceptual diagram as a visual reference as their elevations and regional geology are comparable.

6.3 Crustal Assimilation (^{4}He Contribution)

He and Ne concentrations in the groundwater also provide insight into the evolution of groundwater along its flow path. It is particularly useful in distinguishing whether there has been addition of ^{4}He from the crust or the mantle. Before introduction into the groundwater system, water becomes equilibrated with air and has He and Ne concentrations similar to that of air. After it gets incorporated into the groundwater system, there is no longer atmospheric contribution and He is only altered through ^{3}H decay and interaction with either the crust or mantle.

Interaction with the mantle will increase both the ^{3}He/^{4}He and ^{4}He/^{20}Ne ratios as the mantle has ^{3}He/^{4}He concentrations close to 7 times higher than the atmosphere (Bayon et al., 2008). Interaction with the crust, however, will lower the ^{3}He/^{4}He ratio while increasing the ^{4}He/^{20}Ne ratio as ^{4}He is added from the crust. Although ^{3}He is formed through the decay of ^{3}H as the groundwater ages, this is miniscule in relation to the ^{4}He concentrations. No mantle contribution is expected in this dataset as the average crustal thickness in the Western Cape is 42 km (Qiu et al., 1996), too thick to result in mantle interaction.

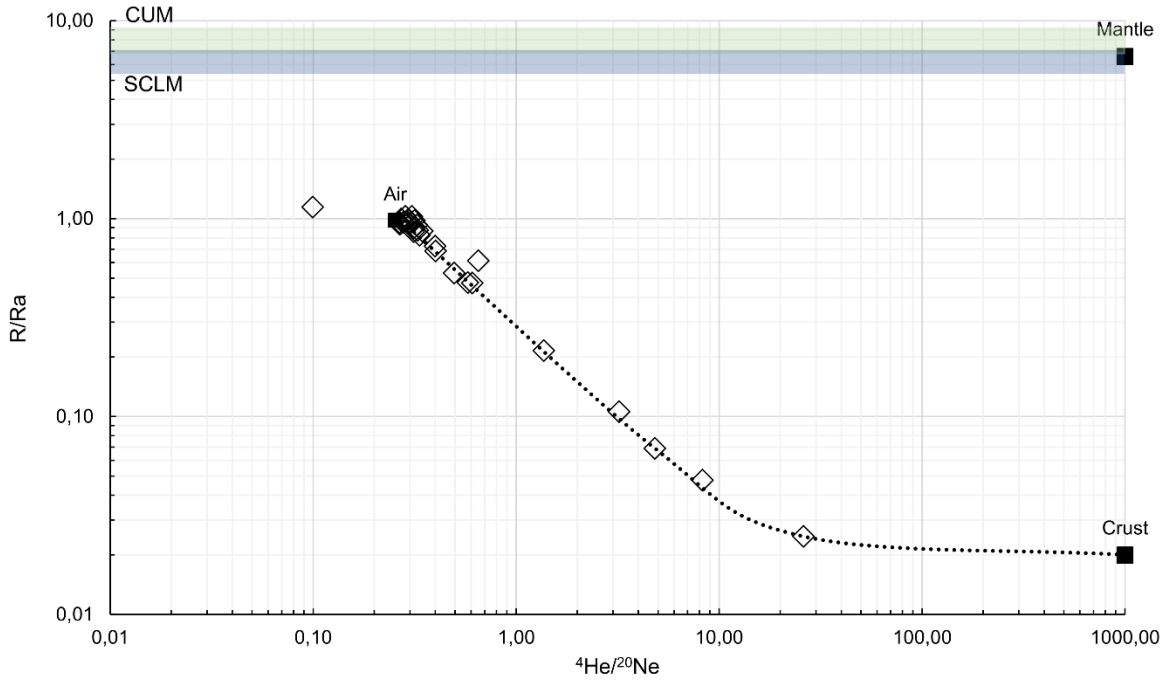

Figure 47 – ^{4}He/^{20}Ne concentrations as a function of ^{3}He/^{4}He ratios (R/R_a); three end members of air, crust and mantle are compared to the groundwater samples (white diamonds).

The $^{4}He/^{20}Ne$ graph (Fig. 47) indicates three end members: air/air saturated water (R/R_a = 0.983; $^{4}He/^{20}Ne$ = 0.253) (Bellani et al., 2015), the crust (R/R_a = 0.02; $^{4}He/^{20}Ne$ = 1 000) (Bayon et al., 2008) and the mantle (R/R_a = 6.62; $^{4}He/^{20}Ne$ = 1 000) (Mikhail et al., 2019). Bands of ranges for the convecting upper mantle (CUM) and the subcontinental lithospheric mantle (SCLM) are provided (Mikhail et al., 2019). All samples plot closely along the mixing line (black dotted line) between air/air saturated water and the crust. If there was sole mixing with the mantle, there would be a mixing curve between air and the mantle end members similar to the curve between air and crustal values. If both crustal and mantle interactions occur, the samples would plot between all three end members. The well constrained array of data between air/air saturated water and the crust indicates there is no mantle He contribution in any samples.

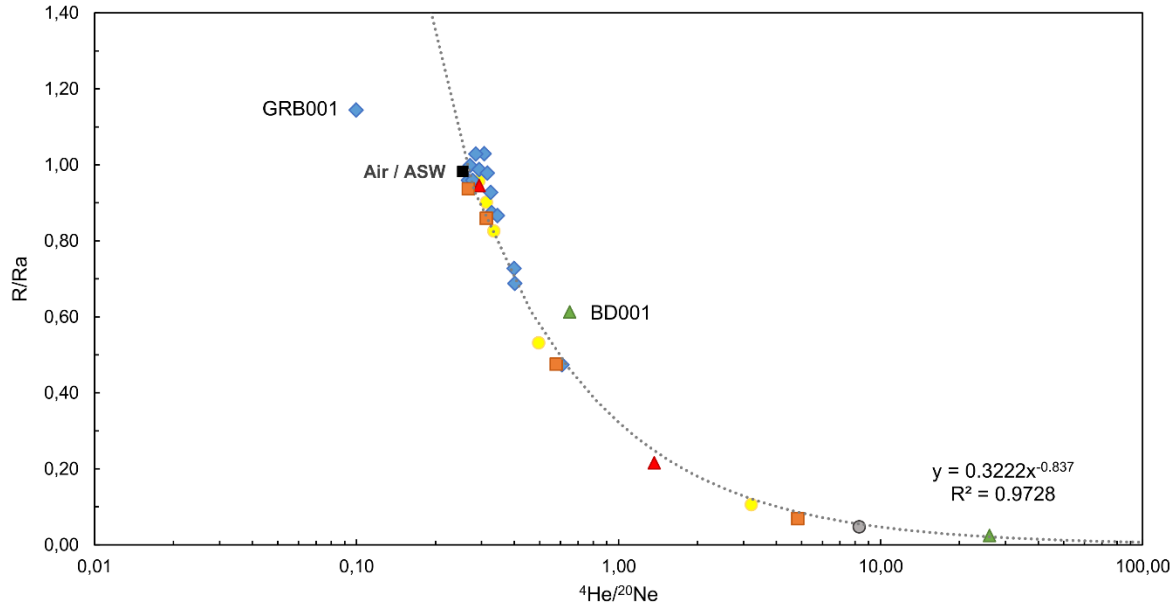

Figure 48 – Mixing of aquifer samples between air/air saturated water and the crust is represented by $y = 0.3222x^{-0.837}$ ($R^2 = 0.9728$).

Bokkeveld sample BD001 plots slightly to the right of the mixing line indicating excess helium in the sample (Fig. 48). Small percentages of excess air in the sample can be corrected as atmospheric noble gas concentrations are known whereas degassing of samples is hard to correct for as it is uncertain how much dissolved gas has been lost. As a result, excess air in BD001 has been corrected for and the calculated age is reliable.

Samples from the TMG Aquifer have R/R_a values closer to air/air saturated water indicating that there was little time for the samples to incorporate crustal helium into their chemistry (Fig.

48). Of the TMG samples, however, it is apparent that sample GRB001 does not plot along the mixing line. It is suspected there has been degassing from this sample as it has lower concentrations than solubility equilibrium causing it to deviate to the left of the mixing line. Degassing may occur when biogenic gases exsolve or when there is a decrease in pressure (Aeschbach-Hertig et al., 2008). Hence, degassing may have occurred during sampling as a consequence of not tightening the clamps properly. It may also be an issue during sample preparation as it is admitted to the preparation line before entering the mass spectrometer. The samples are incredibly sensitive to any input from or loss to the atmosphere. As a result, this is not a reliable age.

Samples with the lowest R/R_a values have the highest $^{4}He/^{20}Ne$ ratios indicating that considerable time has elapsed since these groundwater samples have been infiltrated into the aquifer and have since incorporated ^{4}He from the host rock. Samples from the Malmesbury and Bokkeveld aquifers, which have been identified as fairly old, tend to plot further along the mixing line, away from atmospheric concentrations. The TMG and alluvial aquifers, however, tend to have higher R/R_a values indicating less time has elapsed since recharge has occurred. As these low R/Ra values are associated with low $^{4}He/^{20}Ne$ ratios, these younger samples have had smaller contributions of crustal ^{4}He to the groundwater.

6.4 TMG Aquifer as an Exploitable Resource

Despite the heterogeneity in hydraulic properties of the TMG Aquifer, groundwater samples collected from the aquifer in this study have produced reasonably similar chemistries and residence times. While not attempting to constrain flow paths within the TMG, but rather the turnaround times for groundwater in the system, findings are similar to those of previous studies (Weaver et al, 1999; Miller et al., 2017; Turner, 2018), which have all determined the TMG to have relatively short residence times. Of the samples measured for the aquifer, very few indicate mixing of young and old water (VD003, DD002, Table 11). This suggests that the turnover time for the TMG is relatively quick compared to that of other aquifers in the study region. This is evidenced by a large number of cold springs that flow throughout the year. It is possible that anomalous samples which yielded slightly longer residence times, may be sampled from pooling within the aquifer where there is limited interconnectivity of the fracture network.

Groundwater abstraction is already taking place from boreholes in recharge zones that possess very young waters. Such is the case for samples C001 and VD004 which returned apparent ages as young as 0.3 and 1.4 years, respectively. Large scale abstraction in the recharge zones will most likely hinder groundwater flow to areas further along the flow path. The TMG coincidentally also dominantly occurs within farming regions which likely constitute the largest percentage of TMG groundwater users. An increased population would likely result in the expansion of the agricultural sector as well, further straining groundwater supplies.

There are already reports of localised depletion within the aquifer. There has been abstraction for decades in the Kamanassie region through the Klein Karoo Rural Water Supply Scheme. Long records for a production borehole in the Vermaaks wellfield report that groundwater levels have been declining from as early as 1984, reporting a 90 m decline by 2009 (Jolly and Kotze, 2002). In 1993, after a series of step-tests, geohydrologists estimated 24-hour production yields for the wellfield to be on the order of 72 L/s. The quick decline in water levels led to the adjustment of these values several times. In 2000, after the revision of historical data and new step tests, the long-term yield of the wellfield was estimated to be 8.5 L/s (Kotze, 2000). Despite a reduction in abstraction rates from this wellfield, the situation could not be remedied as it is believed that there has been an overestimation of recharge rates to the aquifer and subsequently, its sustainability (Duah, 2010).

Yields of TMG boreholes have often been over-estimated as ‘blow yields’ have been assumed to represent true yields of the boreholes. Blow yields from shallow boreholes into the TMG surely exceed sustainable yields (Jolly, 2002). Storativity of the aquifer may also have been overestimated as previously established storativity values of 5×10^{3} (Rosewarne, 1984), 2×10^{2} to 1×10^{3} (Mulder et al., 1995), were derived from high yielding boreholes which lie directly adjacent to a fracture zone (Jolly, 2002). As a result, this is not representative of the entire aquifer, especially boreholes that are distal to big fractures (Jolly, 2002).

Multiple studies confirm that the Western Cape will become drier in the near future, with an increased prevalence of drought (Midgeley et al., 2005; Hewitson and Crane, 2006; Lumsden, 2009; Abiodun et al., 2017; Pinto et al., 2018). The 2014 – 2017 drought provided a valuable lesson in that the City cannot solely rely on surface water for supplies. However, just as the surface water is dependent on precipitation, so is groundwater from the TMG Aquifer. Increased abstraction, coupled with the very likely decrease in precipitation, will likely diminish

recharge supplies to the TMG. Quick turnaround times established in this study, imply that the TMG is more vulnerable to climate change than initially thought.

7 CONCLUSION

In the section below, the important findings of this study are summarised and presented. To summarise the extensive work provided in the thesis, the research aims are addressed objective by objective. This section further discusses limitations and shortcomings in the project. As the study was conducted over a large areal extent, within multiple catchments and a number of aquifers, there is definitely room for improvement. Based on issues encountered in this study, recommendations for further work are discussed should this study be continued or a similar one, conducted.

7.1 Research Aims

Key Objective 1: *To characterise ^{3}H and ^{14}C activities of groundwater in the TMG Aquifer and its surrounding aquifer systems.*

High $^{3}H/^{3}He$ ratios and ^{14}C activities are indicative of young groundwater and low $^{3}H/^{3}He$ ratios and ^{14}C activities are characteristic of older groundwater whereas discrepancy between the two isotope systems, is an indication of mixing. $^{3}H/^{3}He$ ratios and ^{14}C activities are relatively high for the TMG and alluvial aquifers whereas $^{3}H/^{3}He$ ratios and ^{14}C activities show a high discrepancy for the Witteberg, Bokkeveld, CGS and Malmesbury aquifers which is an indication of mixing within these aquifers. Although mixing of modern and older groundwater can be identified in samples, mixing between individual aquifers cannot. Despite the use of multiple chemical tracers, it was difficult to differentiate between samples collected from different subaquifers within the TMG as there were no distinct groupings. Field chemistry (EC, pH, alkalinity) as well as ionic concentrations were close to uniform across the aquifer system. As a result, the TMG Aquifer was distinguished from the other aquifers relatively easily but aquifer units within the system could not be differentiated from one another.

The spatial distribution of $^{3}H/^{3}He$ and ^{14}C activities suggests that samples with the youngest ages are generally located in the mountainous regions. The exception to this, however, would be the young alluvial samples in the Stellenbosch valley. The porous alluvium allows for the relatively easy infiltration of precipitation, resulting in high $^{3}H/^{3}He$ and ^{14}C activities and consequently, younger waters at lower elevations. Further analysis of noble gas recharge temperatures, which range between 9.4 – 28.6°C, confirm that the bulk of recharge occurs in the mountains at lower temperatures, but there is additional groundwater recharge at higher temperatures along the flow paths toward the valleys.

Key Objective 2: *To calculate residence times of groundwater within the TMG and its surrounding aquifers.*

Groundwater from the TMG Aquifer is generally characterised by high activities of both tritium and radiocarbon, resulting in groundwater residence times of less than 130 years. Only a single sample from the aquifer yielded a radiocarbon age of 1.6 ky, however, its noble gas age revealed a residence time of 23.4 years, indicating mixing of water bodies with different ages. Of the groundwater sampled from the TMG, mixing of modern water with significantly older groundwater, is relatively uncommon within the aquifer, suggesting that the turnaround time for water in the aquifer is reasonably short.

Groundwater from the alluvial aquifers are also quite young with good agreement between noble gas and radiocarbon ages. Both dating systems place the bulk of residence times calculated for the alluvial aquifer to be less than 70 years old whereas a single sample produced a radiocarbon age of 1.8 ky. The other aquifers (Witteberg, Bokkeveld, CGS and Malmesbury), however, indicate significant mixing of modern and older waters as there is less agreement between radiocarbon and noble gas ages. All groundwater samples from the Witteberg (6.7 ky), Bokkeveld (1.2 – 6.0 ky) and Malmesbury (4.0 – 11.1 ky) aquifers yielded radiocarbon ages in excess of 1 200 years whereas noble gas ages range between 45.5 – 84.7 years where $^{3}H/^{3}He$ dating was possible.

Although analytical precision of $^{3}H/^{3}He$ dating decreases linearly with distance toward the coast and a decrease in apparent age, the dating system remains more accurate than ^{14}C

dating. With radiocarbon age calibration, the greatest concern in age determination is the accuracy of the radiocarbon correction. Ages of older ground waters are likely to have increased error in calculated residence times due to the assumptions made regarding changes in $\delta^{13}C$ along the flow path. Because the approach in correcting the $\delta^{13}C$ values for the Malmesbury Aquifer did not work, this is the aquifer where the ages are most likely to show variance from true residence times. The approach in assuming initial $\delta^{13}C$ soil values was ineffective as this assumed $\delta^{13}C$ values would be ~ -60‰ whereas $\delta^{13}C$ of soils typically range between -35 to -10‰. Residence times calculated using soil $\delta^{13}C$ values of -19.5‰, however, resulted in calculated residence times ranging between 4.0 – 11.1 ky. This corresponds well to previous studies which place groundwater residence times between 2.5 – 9.4 ky. Due to overall good agreement between the two dating systems and comparison to previous work for both the Malmesbury Aquifer and the other aquifers, it is likely that the corrections are reasonable.

Although two dating systems were used to provide constraints on residence times in the study area, a number of other parameters were identified as potential proxies for groundwater residence time. Groundwater pH serves as the best indicator of ground water residence time as pH values increase linearly as the groundwater ages. Ca/Mg ratios and HCO_3^- concentrations also tend to increase as groundwater ages due to the dissolution of carbonate-bearing minerals. Borehole depth was identified as a potential proxy for all of the sampled aquifers except for the TMG Aquifer which had young apparent residence times, irrespective of their borehole depth.

Key Objective 3: *To evaluate the vulnerability of TMG groundwater to future climate change.*

Through various methods of the assessment, it has been determined that the TMG Aquifer possesses young groundwater (<130 years) over a large extent of the system. This is corroborated by a number of previous studies conducted in localised regions of the aquifer, particularly Cape Town, Paarl, Agter-Witzenberg and Verlorenvlei. As a result, the aquifer is likely quite sensitive to changes in weather patterns, i.e. climate change. Periods of water stress when surface water supplies are diminished, is most likely when water supplementation from the TMG Aquifer will occur. During these periods, recharge to the aquifer system will be

lower. Reductions in groundwater recharge and increased abstraction may cause groundwater depletion in a relatively short time span. These factors need to be taken into consideration before wide-scale use of groundwater in the TMG occurs, as unsustainable abstraction could relatively quickly cause the aquifer to become a non-renewable water resource.

The TMG, however, can be sustainably managed if groundwater abstraction is closely manged against recharge to the aquifer. Due to the aquifer's highly fractured nature, favourable outcrop and vast areal extent, as long as there is regular and sufficient rainfall that is equal to the volume abstracted, the TMG Aquifer can provide a large volume of water to the City of Cape Town. The residence times calculated for the TMG Aquifer indicate that with proper management, resources from the TMG have vast potential for future use. Sustainability of the TMG Aquifer inevitably depends on good governance of the resource.

7.2 Recommendations for Further Work

Due to the fact that tritium in rainfall is highly variable across the country, a uniform ^{3}H input should not be assumed for all catchments. As tritium concentrations in rainfall will be lower in coastal regions of the country than in their interior counterparts, regular sampling of rainfall should take place in multiple areas of the study area. This should be done so that measurements are representative of the sample sites as a whole and can be applied to isotope studies throughout. Insight into the variability of the input tritium concentration will enable better understanding of measured concentrations, quantifications of recharge and if used without its daughter product, ^{3}He, residence time. This will also be particularly helpful as the GNIP data has been sparse over the last few decades, making comparison to available data quite difficult.

As ^{14}C dating involves many assumptions to calibrate activities to model ages, further work should incorporate eliminating the guesswork behind calibration. This, however, would involve working within smaller catchments of the aquifer where flow paths and recharge areas have been constrained. As stricter constraints on soil $\delta^{13}C$ will limit the variability in the dilution factor (q) of radiocarbon activity, $\delta^{13}C$ samples should be taken of soils along the flow path, particularly at recharge sites. Additionally, as bomb peak radiocarbon has declined but not

completely decayed out of the atmosphere, ^{14}C activity should be measured from groundwater proximal to the recharge zone to provide constraints on modern input ^{14}C activity.

Groundwater ages that have been resolved by $^{3}H/^{3}He$ are considered to be young (<100 years) whereas groundwater ages derived from the ^{14}C dating system are considerably older (>500 years). Due to the fact that most samples have significant measured activities for both tracers, it can be assumed that most groundwater bodies are characterised by a mixture of differently aged packages. The issue, however, arises in that radiocarbon dating in this study has proven difficult in instances where the carbon content is low, particularly in the TMG. In instances where radiocarbon content could not be determined, the total carbon content of young samples in this study suggest that the radiocarbon activity is likely to be 80 pMC (<2 000 years) and higher. As a result, groundwater on the younger end of the spectrum cannot be accurately dated with radiocarbon. Due to this, an age gap exists between the two dating systems where groundwater samples cannot be reliably dated (Fig. 49).

39-argon (^{39}Ar) is abundant in the atmosphere and is an excellent hydrological tracer due to its conservative nature (Chen et al., 1999). ^{39}Ar has a half-life of 269 years and can reliably date ground waters with residence times between 70 – 1 000 years (Corcho Alvarado et al., 2007; Welte, 2011). It is possible that using ^{39}Ar dating in conjunction with $^{3}H/^{3}He$ and ^{14}C, would yield a different age than the other two tracers, further substantiating the idea of mixing along the flow path. Although Ar is abundant in the atmosphere, its solubility leads to low dissolved content in groundwater. Therefore, the complication in sampling ^{39}Ar is that it requires large volumes of groundwater from which to extract dissolved gas for analysis as sample volumes are often in excess of 2 m^3 (Corcho Alvarado et al., 2007). This, consequently, leads to longer sampling times (Welte, 2011). As argon is a noble gas, the same limitations to sampling apply as with the $^{3}H/^{3}He$ dating system. During sampling, groundwater needs to be isolated from the atmosphere.

It is recommended that ^{4}He be used as a secondary tracer to ^{14}C. The calibration of ^{14}C activities to model ages requires a number of assumptions which can often result in the over- or under-correction of ages by centuries to millennia. As ^{4}He has a dating range which overlaps that of ^{14}C (Fig. 49), the isotope can be used to support the correction of activities to ages as well as provide intermediate ages for which radiocarbon does not provide adequate resolution. Additionally, working with multiple tracers in a small but important catchment where

the TMG occurs (possibly the Franschhoek or Villiersdorp area), could provide a better quantification of recharge along the flow paths as well as mixing between different aquifer systems.

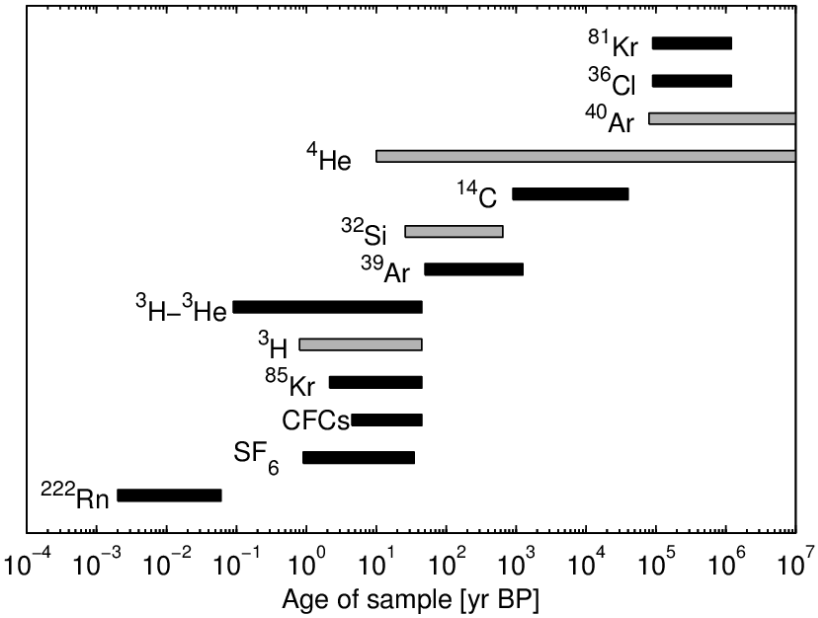

Figure 49 – Dating ranges of various isotopes used in hydrological studies, black bars indicate reliable dating systems where grey bars indicate less reliable systems (Welte, 2011).

8 REFERENCES

Abiodun, B.J., Adegoke, J., Abatan, A.A., Ibe, C.A., Egbebiyi, T.S., Engelbrecht, F. & Pinto, I. (2017). Potential impacts of climate change on extreme precipitation over four African coastal cities. *Climatic Change*, *143*(3-4),399-413.

Adelana, S. M. A., & Xu, Y. (2006). Contamination and protection of the Cape Flats Aquifer, South Africa. *Groundwater Pollution in Africa*, 265.

Adelana, S. M. A., Xu, Y., & Adams, S. (2006). Identifying sources and mechanism of groundwater recharge in the Cape Flats, South Africa: Implications for sustainable resource management.1-12.

Adelana, S. M. A., Xu, Y., & Vrbka, P. (2010). A conceptual model for the development and management of the Cape Flats aquifer, South Africa. *Water SA*, *36*(4), 461-474.

Aeschbach-Hertig, W., Peeters, F., Beyerle, U., & Kipfer, R. (1999). Interpretation of dissolved atmospheric noble gases in natural waters. *Water Resources Research*, *35*(9), 2779-2792.

Aeschbach-Hertig, W., Peeters, F., Beyerle, U., & Kipfer, R. (2000). Palaeotemperature reconstruction from noble gases in ground water taking into account equilibration with entrapped air. *Nature*, *405*(6790), 1040.

Aeschbach-Hertig, W., El-Gamal, H., Wieser, M., & Palcsu, L. (2008). Modeling excess air and degassing in groundwater by equilibrium partitioning with a gas phase. *Water Resources Research*, *44*(8).

Agyare-Dwomoh, Y. (2020). *The application of Radon-222 in constraining groundwater recharge in the City of Cape Town and its surrounds*. (MSc Dissertation, Stellenbosch University).

Loucks, D. P., & Gladwell, J. S. (1999). *Sustainability criteria for water resource systems*. Cambridge University Press.

Anderson, M. E., Almond, J. E., Evans, F. J., & Long, J. A. (1999). Devonian (Emsian-Eifelian) fish from the Lower Bokkeveld Group (Ceres Subgroup), South Africa. *Journal of African Earth Sciences*, *29*(1), 179-193.

Aris, A. Z., Abdullah, M. H., Ahmed, A., & Woong, K. K. (2007). Controlling factors of groundwater hydrochemistry in a small island's aquifer. *International Journal of Environmental Science & Technology*, *4*(4), 441-450.

Aza-Gnandji, C. D. R., Xu, Y., Raitt, L., & Levy, J. (2013). Salinity of irrigation water in the Philippi farming area of the Cape Flats, Cape Town, South Africa. *Water SA*, *39*(2), 199-210.

Balek, J. (1988). Groundwater recharge concepts. In *Estimation of natural groundwater recharge*. *Ed: J. Simmers.* Springer, Dordrecht. 3-9.

Ballentine, C.J. & Hall, C.M. (1999). Determining paleotemperature and other variables by using an error-weighted, nonlinear inversion of noble gas concentrations in water. Geochim. Cosmochim. Acta 63 (16), 2315–2336.

Battersby, J. (2016). *The State of Urban Food Insecurity in Cape Town* (No. 11). Southern African Migration Programme. ISBN 978-1-920409-71-5.

Baxter, J. M., & Walton, A. (1971). Fluctuations of atmospheric carbon-14 concentrations during the past century. *Proceedings of the Royal Society of London. A. Mathematical and Physical Sciences*, *321*(1544), 105-127.

Bayon, F. E. B., See, F. S., Magro, G., & Pennisi, M. (2008). Noble gas and boron isotopic signatures of the Bacon-Manito geothermal fluid, Philippines. *Geofluids*, *8*(4), 230-238.

Belcher, R. W., & Kisters, A. F. (2003). Lithostratigraphic correlations in the western branch of the Pan-African Saldania belt, South Africa: the Malmesbury Group revisited. *South African Journal of Geology*, *106*(4), 327-342.

Bellani, S., Magro, G., & Gherardi, F. (2015). Heat Flow and Helium Isotopes in the Geothermal Areas of Tuscany (Italy). *Transactions - Geothermal Resources Council*. 39. 339-405.

Benhin, J. (2006). Climate Change and South African Agriculture: Impacts and Adaptation Options. ISBN 1-920160-21-3.

Beyerle, U., Aeschbach-Hertig, W., Hofer, M., Imboden, D. M., Baur, H., & Kipfer, R. (1999). Infiltration of river water to a shallow aquifer investigated with 3H/3He, noble gases and CFCs. *Journal of Hydrology*, *220*(3-4), 169-185.

Blake, D., Mlisa, A., & Hartnady, C. (2010). Large scale quantification of aquifer storage and volumes from the Peninsula and Skurweberg Formations in the southwestern Cape. *Water SA*, *36*(2), 177-184.

Bleam, W. F. (2016). *Soil and environmental chemistry*. Academic Press.

Boucher, C. (1983). Floristic and structural features of the coastal foreland vegetation south of the Berg River, western Cape Province, South Africa. *Bothalia*, *14*(3/4), 669-674.

Boucher. C. & Moll, E. J. (1981). South African Mediterranean shrublands. In F. di Castri, D. W. Goodall & R. L. Specht, Mediterranean-type shrublands. Amsterdam: Elsevier.

Brown, C., Colvin, C., Hartnady, C., Hay, R., Le Maitre, D. & Riemann, K. (2003). Ecological and Environmental Impacts of Large-scale Groundwater Development in the Table Mountain Group (TMG) Aquifer System.

Brownlie, S., De Villiers, C., Driver, A., Job, N., Von Hase, A., & Maze, K. (2005). Systematic Conservation Planning in the Cape Floristic Region and Succulent Karoo, South Africa:

enabling sound spatial planning and improved environmental assessment. *Journal of Environmental Assessment Policy and Management*, *7*(02), 201-228.

Brunsdon, G. and Booth, P.W.K. (2009). September. Faulting of the Witteberg Group Rocks, Steytlerville, Eastern Cape. In *11th SAGA Biennial Technical Meeting and Exhibition*.

Buggisch, W., Kleinschmidt, G. & Krumm, S. (2010). Sedimentology, geochemistry and tectonic setting of the Neoproterozoic Malmesbury Group (Tygerberg Terrane) and its relation to neighbouring terranes, Saldania Fold Belt, South Africa. *Neues Jahrbuch für Geologie und Paläontologie-Abhandlungen*, *257*(1), 85-114.

City of Cape Town (CoCT), Cape Town Water Strategy. (2019).

Castagnoli, G. & Lal, D. (1980) 'Solar Modulation Effects in Terrestrial Production of Carbon-14', Radiocarbon, 22(02), 133–158.

Cauquoin, A., Jean-Baptiste, P., Risi, C., Fourré, É., Stenni, B., & Landais, A. (2015). The global distribution of natural tritium in precipitation simulated with an Atmospheric General Circulation Model and comparison with observations. *Earth and Planetary Science Letters*, *427*, 160-170.

Chase, B.M. & Thomas, D.S. (2007). Multiphase late Quaternary aeolian sediment accumulation in western South Africa: timing and relationship to palaeoclimatic changes inferred from the marine record. *Quaternary International*, *166*(1), 29-41.

Chen, C. Y., Li, Y. M., Bailey, K., O'connor, T. P., Young, L., & Lu, Z. T. (1999). Ultrasensitive isotope trace analyses with a magneto-optical trap. *Science*, *286*(5442), 1139-1141.

Chiu, T. C., Fairbanks, R. G., Cao, L., & Mortlock, R. A. (2007). Analysis of the atmospheric 14C record spanning the past 50,000 years derived from high-precision 230Th/234U/238U, 231Pa/235U and 14C dates on fossil corals. *Quaternary Science Reviews*, *26*(1-2), 18-36.

Clark, I. D., & Fritz, P. (1997). Environmental Isotopes in Hydrology Lewis Publishers. *Boca Raton, New York*.

Clarke, W.B., Jenkins, W.J. & Top, Z. (1976). Determination of tritium by mass spectrometric measurement of 3He. The International Journal of Applied Radiation and Isotopes, 27(9), 515-522.

Colvin, C., & Saayman, I. (2007). Challenges to groundwater governance: a case study of groundwater governance in Cape Town, South Africa. *Water Policy*, *9*(S2), 127-148.

Conrad, J., Smit, L., Murray, K., van Gend-Muller, J., & Seyler, H. (2019). The Malmesbury Group-an aquifer of surprising significance. *South African Journal of Geology 2019*, *122*(3), 331-342.

Corcho Alvarado, J. A., Purtschert, R., Barbecot, F., Chabault, C., Rueedi, J., Schneider, V., Aeschbach-Hertig, W., Kipfer, R. & Loosli, H. H. (2007). Constraining the age distribution of highly mixed groundwater using 39Ar: A multiple environmental tracer (3H/3He, 85Kr, 39Ar, and 14C) study in the semiconfined Fontainebleau Sands Aquifer (France). *Water Resources Research*, *43*(3).

Costaras, H. C. (2019). *Characterization of groundwater 87Sr/86Sr ratios and their relationship to bedrock geology in the greater Cape Town region of South Africa.* (Honours Dissertation, Stellenbosch University).

Cotter, E. (2000). Depositional setting and cyclic development of the lower part of the Witteberg Group (Mid-to Upper Devonian), Cape Supergroup, Western Cape, South Africa. *South African Journal of Geology*, *103*(1), 1-14.

Council of Canadian Academies (CCA). 2009. The Sustainable Management of Groundwater in Canada: The Expert Panel on Groundwater.

Craig, H., & Lupton, J. E. (1981). 11. Helium-3 and Mantle Volatiles in the Ocean and the Oceanic Crust. *The Oceanic lithosphere*, 7, 391.

Curtis, O. E. (2013). *Management of critically endangered renosterveld fragments in the Overberg, South Africa* (Doctoral dissertation, University of Cape Town).

Dajun, Q. & Hao, W. (2001). Chlorofluorocarbons and 3H/3He in groundwater - Applications in tracing and dating young groundwater. Science in China (Series E): Technological Sciences, 44, 29–34.

Damon, P. E., Long, A., & Grey, D. C. (1966). Fluctuation of atmospheric C14 during the last six millennia. *Journal of Geophysical Research*, *71*(4), 1055-1063.

Dansgaard, W. (1964). Stable isotopes in precipitation. *Tellus*, *16*(4), 436-468.

De Beer, C. H. (1992). Structural evolution of the Cape Fold Belt syntaxis and its influence on syntectonic sedimentation in the SW Karoo Basin. *Inversion Tectonics of the Cape Fold Belt, Karoo and Cretaceous Basins of Southern Africa*, 197-206.

De Beer, C. H. (2002a). The stratigraphy, lithology and structure of the Table Mountain Group. *A Synthesis of the Hydrogeology of the Table Mountain Group–Formation of a Research Strategy. WRC Report No. TT*, *158*(01), 9-18.

De Beer, C. H. (2002b). Structural investigation of the Koo Valley for the Koo Valley. Water Scheme. Unpublished Council for Geoscience (CGS) Report No. 2002-0067, Bellville.

Department of Water Affairs and Forestry (DWAF). (2002). Utilization and availability of water –Profile of water management in Berg, Breede, Gouritz, Olifants/Doring Water Management Areas, DWAF.

Department of Water Affairs and Forestry (DWAF). (2006). Groundwater Resource Assessment 2: Recharge Literature Review.

Department of Water and Sanitation (DWS). (2016). National Groundwater Strategy. *Cape Town.*

Department of Water and Sanitation (DWS). (2018). Water Outlook 2018 Report. *Cape Town.*

Di Castri, F. (1981). Mediterranean-type shrublands of the world. In. F. di Castri, D. W. Goodall & R. L. Specht, Mediterranean-type shrublands. Amsterdam: Elsevier.

Diamond, R. E. (1997). *Stable isotopes of the thermal springs of the Cape Fold Belt* (Masters dissertation, University of Cape Town).

Diamond, R. E. & Harris, C. (2000). "Oxygen and hydrogen isotope geochemistry of thermal springs of the Western Cape, South Africa: recharge at high altitude?" *Journal of African Earth Sciences,* 31: 467-481.

Diamond, R.E. (2014). Stable Isotope Hydrology of the Table Mountain Group. University of Cape Town, PhD Thesis. 209.

Diamond, R. E., & Harris, C. (2019). Stable isotope constraints on hydrostratigraphy and aquifer connectivity in the Table Mountain Group. *South African Journal of Geology 2019*, *122*(3), 317-330.

Doell, P., Mueller Schmied, H., Schuh, C., Portmann, F. T., & Eicker, A. (2014). Global-scale assessment of groundwater depletion and related groundwater abstractions: Combining hydrological modeling with information from well observations and GRACE satellites. *Water Resources Research*, *50*(7), 5698-5720.

Du Plessis, J. A., & Schloms, B. (2017). An investigation into the evidence of seasonal rainfall pattern shifts in the Western Cape, South Africa. *Journal of the South African Institution of Civil Engineering*, *59*(4), 47-55.

Duah, A. A. (2010). Sustainable utilisation of Table Mountain Group aquifers (Doctoral dissertation, University of the Western Cape).

Ekwurzel, B., Schlosser, P., Smethie Jr, W.M., Plummer, L.N., Busenberg, E., Michel, R.L., Weppernig, R. & Stute, M. (1994). Dating of shallow groundwater: Comparison of the transient tracers 3H/3He, chlorofluorocarbons, and 85Kr. *Water Resources Research*, *30*(6), 1693-1708.

Evolution. (2007). Cold Spring Harbor Laboratory Press.

Enger, E. D., & Smith, B. F. (1995). Environmental science, a study of interrelationships. WCB.

Famiglietti, J. S. (2014). The global groundwater crisis. *Nature Climate Change*, *4*(11), 945.

Ferronskiĭ, V.I. & Poli͡akov, V.A. (1982). Environmental isotopes in the hydrosphere. John Wiley & Sons.

Fourie, P. H., Zimmermann, U., Beukes, N. J., Naidoo, T., Kobayashi, K., Kosler, J., Nakamura, E., Tait, J. & Theron, J.N. (2011). Provenance and reconnaissance study of detrital zircons of the Palaeozoic Cape Supergroup in South Africa: Revealing the interaction of the Kalahari and Río de la Plata Cratons. International Journal of Earth Sciences, 100, 527–541.

Fontes, J. C. (1985). Some considerations on groundwater dating using environmental isotopes. In *Hydrogeology in the Service of Man. Memoires of the 18th Congress of the International Association of Hydrogeologists, Cambridge*. 188-154.

Fontes, J. C., & Garnier, J. M. (1979). Determination of the initial 14C activity of the total dissolved carbon: A review of the existing models and a new approach. *Water resources research*, *15*(2), 399-413.

Freeze, R. A., & Cherry, J. A. (1979). Groundwater: Englewood Cliffs. *New Jersey*.

Gat, J. R., Mook, W. G., & Meijer, H. A. (2001). Environmental isotopes in the hydrological cycle. *Principles and Applications UNESCO/IAEA Series*, *2*, 63-7.

Giljam, R. (2002). *The effect of the Cape Flats Aquifer on the water quality of False Bay* (Doctoral dissertation, University of Cape Town).

Godwin, H. (1962). Half-life of radiocarbon. Nature, 195(4845), 984-984.

Gordon Groundwater Consultancy (Gordon Report). (2011). Sustainable Groundwater Management: Preliminary Approach for Assessing the Sustainability of Groundwater, submitted to CCME Water Management Development Committee. 48.

Graf, W. L. (1999). Dam nation: A geographic census of American dams and their large-scale hydrologic impacts. *Water resources research*, *35*(4), 1305-1311.

Gresse, M.W. & Theron, J.N. (1992). The Geology of the Worcester Area, explanation of sheet 3319. Geological Survey, Department of Mineral and Energy Affairs, Pretoria.

Gupta, S. K., Moravcik, P. S., & Lau, L. S. (1994). Use of injected helium as a hydrological tracer. *Hydrological sciences journal*, *39*(2), 109-119.

Harris, C., Faure, K., Diamond, R.E. & Scheepers, R., (1997). Oxygen and hydrogen isotope geochemistry of S-and I-type granitoids: the Cape Granite suite, South Africa. *Chemical Geology*, *143*(1-2), 95-114.

Harris, C., Oom, B. M., & Diamond, R. E. (1999). A preliminary investigation of the oxygen and hydrogen isotope hydrology of the greater Cape Town area and an assessment of the potential for using stable isotopes as tracers. *Water S. A.*, *25*(1), 15-24.

Harris, C., Burgers, C., Miller, J., & Rawoot, F. (2010). O-and H-isotope record of Cape Town rainfall from 1996 to 2008, and its application to recharge studies of Table Mountain groundwater, South Africa. *South African Journal of Geology*, *113*(1), 33-56.

Hartnady, C. J. H., Newton, A. R., & Theron, J. N. (1974). The stratigraphy and structure of the Malmesbury Group in the southwestern Cape. *Bulletin of the Precambrian Research Unit, University of Cape Town, South Africa*, *15*, 193-214.

Hartnady, C. J., & Hay, E. R. (2000). *Reconnaissance Investigation into the Development and Utilisation of Table Mountain Group Artesian Groundwater, Using the E10 Catchment as a Pilot Study Area*. Umvoto Africa CC.

Hartnady, C.J.H. & Hay, E.R., (2002a). Boschkloof Groundwater Discovery, In: K. Pietersen and R. Parsons (eds.), A synthesis of the hydrogeology of the Table Mountain Group - formation of a research strategy. Water Research Commission (WRC) Report, TT 158/01.

Hartnady, C.J.H., & Hay, E.R., (2002b). Experimental Deep Drilling at Blikhuis, Olifants River Valley, Western Cape: Motivation, Setting and Current Progress, In: K. Pietersen and R. Parsons (eds.), A synthesis of the hydrogeology of the Table Mountain Group - formation of a research strategy. Water Research Commission (WRC) Report, TT 158/01.

Hay, R., McGibbon, D., Botha, F., & Riemann, K. (2015). Cape flats aquifer and false bay–opportunities to change.

Hendey, Q. B., & Dingle, R. V. (1983). Onshore sedimentary phosphate deposits in south-western Africa.

Hewitson, B C & R G Crane (2006). Consensus between GCM climate change projections with empirical downscaling: precipitation downscaling over South Africa, International Journal of Climatology Vol 26, No 10, pages 1315–1337.

Hinkle, S. R. (2009). *Tritium/Helium-3 Apparent Ages of Shallow Ground Water, Portland Basin, Oregon, 1997-98*. U. S. Geological Survey.

International Atomic Energy Agency (IAEA) / World Meteorological Organisation (WMO). (2019). Global Network of Isotopes in Precipitation. The GNIP Database. Accessible at: <http://www.iaea.org/water>, (accessed Sep 2019).

Ingerson, E., & Pearson, F. J. (1964). Estimation of age and rate of motion of groundwater by the 14C-method. *Recent Researches in the Fields of Atmosphere, Hydrosphere and Nuclear Geochemistry*, 263-283.

Jia, H. (2007). *Groundwater resource evaluation in Table Mountain Group aquifer systems* (Doctoral dissertation, University of the Western Cape).

Johnson, M. R. (1976). Stratigraphy and sedimentology of the Cape and Karoo sequences in the Eastern Cape Province.

Jolly, J.L. (2002). Sustainable use of Table Mountain Group aquifers and problems related to scheme failure. In: Pietersen, K., Parsons, R. (Eds). *A synthesis of the hydrogeology of the Table Mountain Group – formation of a research strategy*. WRC Report No. TT 158/01, 108-111.

Jolly, J.L. and Kotze, J.C. (2002). The Klein Karoo rural water supply scheme. In: Pietersen, K., Parsons, R. (Eds). *A synthesis of the hydrogeology of the Table Mountain Group – formation of a research strategy*. WRC Report No. TT 158/01, 198-201.

Joubert, A., Stewart, T. J., & Eberhard, R. (2003). Evaluation of water supply augmentation and water demand management options for the City of Cape Town. *Journal of Multi-Criteria Decision Analysis*, *12*(1), 17-25.

Jung, M., Wieser, M., von Oehsen, A., & Aeschbach-Hertig, W. (2013). Properties of the closed-system equilibration model for dissolved noble gases in groundwater. *Chemical Geology*, 339, 291-300.

Kalin, R. M. (2000). Radiocarbon dating of groundwater systems. In *Environmental tracers in subsurface hydrology.* Springer, Boston, MA. 111-144.

Kamensky, I. L., Tokarev, I. V., & Tolstikhin, I. N. (1991). 3H-3He dating: A case for mixing of young and old groundwaters. *geochimica et Cosmochimica Acta*, *55*(10), 2895-2899.

Koehler, G., Wassenaar, L. I., & Hendry, M. J. (2000). An automated technique for measuring δD and δ18O values of porewater by direct CO2 and H2 equilibration. *Analytical chemistry*, *72*(22), 5659-5664.

Konikow, L. F., & Kendy, E. (2005). Groundwater depletion: A global problem. *Hydrogeology Journal*, *13*(1), 317-320.

Kotze, J. C. (2000). *Hydrogeology of the Table Mountain Group aquifer in the Little Karoo*. Unpublished Ph.D. Thesis, University of Orange Free State.

Kotze, J. C. (2002a) Hydrogeology of the Table Mountain sandstone aquifer – Klein Karoo. University of the Free State, Bloemfontein.

Kotze, J. C. (2002b). Towards a management tool for groundwater exploitation in the Table Mountain sandstone fractured aquifer, Water Research Commission.

Kralik, M. (2015). How to estimate mean residence times of groundwater. *Procedia Earth and Planetary Science*, *13*, 301-306.

Kruger, F. J. (1979). South African heathlands. *Ecosystems of the world*.

Kundzewicz, Z. W., & Doell, P. (2009). Will groundwater ease freshwater stress under climate change? *Hydrological Sciences Journal*, *54*(4), 665-675.

Lacroix, E., Brovelli, A., Barry, D. A., & Holliger, C. (2014). Use of silicate minerals for pH control during reductive dechlorination of chloroethenes in batch cultures of different microbial consortia. *Appl. Environ. Microbiol.*, *80*(13), 3858-3867.

Lambrakis, N., & Kallergis, G. (2005). Contribution to the study of Greek thermal springs: hydrogeological and hydrochemical characteristics and origin of thermal waters. *Hydrogeology Journal*, *13*(3), 506-521.

Le Maitre, D. C., Colvin, C., & Scott, D. F. (2002). Groundwater Dependent Ecosystems in the Fynbos Biome, and their vulnerability to groundwater abstraction. *Paper in WRC Report TT158/01 A Synthesis of the Hydrogeology of the Table Mountain Group–Formation of a Research Strategy*, 112-117.

Le Maitre, D., Colvin, C., & Maherry, A. (2009). Water resources in the Klein Karoo: the challenge of sustainable development in a water-scarce area. *South African Journal of Science*, *105*(1-2), 39-48.

Libby, W. F. (1955). *Radiocarbon Dating.* University of Chicago Press, Chicago, 175.

Lin, L. (2007). *Hydraulic properties of the Table Mountain Group (TMG) aquifers* (Doctoral dissertation, University of Western Cape).

Lohman, S. W., Bennett, R. R., Brown, R. H., Cooper Jr, H. H., Drescher, W. J., Ferris, J. G., Johnson, A. I., McGuinness, C. L., Piper, A. M., Rorabaugh, M. I., & Stallman, R. W. (1972). *Definitions of selected ground-water terms--revisions and conceptual refinements* (p. 21). US Government Printing Office.

Lucas, L. L., & Unterweger, M. P. (2000). Comprehensive review and critical evaluation of the half-life of Tritium. *Journal of research of the National Institute of Standards and Technology*, *105*(4), 541.

Lumsden, T. G. (2009). Evaluation of potential changes in hydrologically relevant statistics of rainfall in Southern Africa under conditions of climate change. *Water SA*, *35*(5).

Ma, B., Jin, M., Liang, X., & Li, J. (2019). Application of environmental tracers for investigation of groundwater mean residence time and aquifer recharge in fault-influenced hydraulic drop alluvium aquifers. *Hydrology & Earth System Sciences*, *23*(1).

Mackay, C., Pandow, M., Polak, P., & Wolfgang, R. (1961). The elementary chemistry of atomic carbon. *Chemical Effects of Nuclear Transformations*, *2*, 17-26.

Mahlalela, P. T., Blamey, R. C., & Reason, C. J. C. (2019). Mechanisms behind early winter rainfall variability in the southwestern Cape, South Africa. *Climate Dynamics*, *53*(1-2), 21-39.

Maimone, M. (2004). Defining and managing sustainable yield. *Groundwater*, *42*(6), 809-814.

Margat, J., Foster, S., & Droubi, A. (2006). Concept and importance of non-renewable resources. *Non-renewable groundwater resources: A guidebook on socially-sustainable management for water-policy makers*, *10*, 13-24.

Mazor, E., & Verhagen, B. T. (1983). Dissolved ions, stable and radioactive isotopes and noble gases in thermal waters of South Africa. *Journal of Hydrology*, *63*(3-4), 315-329.

Maxey, G. B. (1964). Hydrostratigraphic units. *Journal of hydrology*, *2*(2), 124-129.

Maxwell, R. M., Condon, L. E., Kollet, S. J., Maher, K., Haggerty, R., & Forrester, M. M. (2016). The imprint of climate and geology on the residence times of groundwater. *Geophysical Research Letters*, *43*(2), 701-708.

McGuire, K. J., McDonnell, J. J., Weiler, M., Kendall, C., McGlynn, B. L., Welker, J. M., & Seibert, J. (2005). The role of topography on catchment-scale water residence time. *Water Resources Research*, *41*(5).

Meyer, P. S. (2001). *An explanation of the 1: 500 000 general hydrogeological map: Cape Town 3317*. Directorate Geohydrology, Department of Water Affairs and Forestry.

Meyer, P. S. (2002). Springs in the Table Mountain Group, with special reference to fault controlled springs. *A synthesis of the hydrogeology of the Table Mountain Group—Formation of a Research Strategy. Pretoria: Water Research Commission*, 224-5.

Michel, R. L. (1989). Tritium deposition over the continental United States, 1953–1983. *Atmospheric deposition*, *179*, 109-115.

Michel, R. L., Jurgens, B. C., & Young, M. B. (2018). *Tritium deposition in precipitation in the United States, 1953–2012* (No. 2018-5086). US Geological Survey.

Midgley, G.F., Chapman, R.A., Hewitson, B., Johnston, P., De Wit, M., Ziervogel, G., Mukheibir, P., Van Niekerk, L., Tadross, M., Van Wilgen, B.W. & Kgope, B. (2005). A status quo, vulnerability and adaptation assessment of the physical and socio-economic effects of climate change in the Western Cape.

Mikhail, S., Crosby, J., Stuart, F., DiNicola, L., & Abernethy, F. A. (2019). A secretive mechanical exchange between mantle and crustal volatiles revealed by helium isotopes in 13C-depleted diamonds. *Geochemical Perspectives Letters*.

Miller, J. A., Dunford, A. J., Swana, K. A., Palcsu, L., Butler, M., & Clarke, C. E. (2017). Stable isotope and noble gas constraints on the source and residence time of spring water from the Table Mountain Group Aquifer, Paarl, South Africa and implications for large scale abstraction. *Journal of hydrology*, *551*, 100-115.

Miller, W., Armstrong, R. & de Wit, M. (2016). Geology and U/Pb geochronology of the Gamtoos Complex and lower paleozoic Table Mountain Group, Cape Fold Belt, Eastern Cape, South Africa. South African Journal of Geology, 119, 147–170.

Mitchell, D. T., Coley, P. G. F., Webb, S., & Allsopp, N. (1986). Litterfall and decomposition processes in the coastal fynbos vegetation, south-western Cape, South Africa. *The Journal of Ecology*, 977-993.

Molnár, M., Janovics, R., Major, I., Orsovszki, J., Gönczi, R., Veres, M., Leonard, A.G., Castle, S.M., Lange, T.E., Wacker, L. & Hajdas, I. (2013). Status report of the new AMS 14 C sample preparation lab of the Hertelendi laboratory of environmental studies (Debrecen, Hungary). *Radiocarbon*, *55*(2), 665-676

Mook, W., & Rozanski, K. (2000). Environmental isotopes in the hydrological cycle. *IAEA Publish*, *39*.

Moran, J. E., Hudson, G. B., Eaton, G. F., & Leif, R. (2004). *A Contamination Vulnerability Assessment for the Santa Clara and San Mateo County Groundwater Basins* (No. UCRL-TR-201929). Lawrence Livermore National Lab., Livermore, CA (US).

Muche, G., Kruger, S., Hillmann, T., Josenhans, K., Ribeiro, C., Bazibi, M., Seely, M., Nkonde, E., de Clercq, W., Strohbach, B., Kenabatho, K.P., Vogt, R., Kaspar, F., Helmschrot, J. & Jürgens, N. (2018). SASSCAL WeatherNet: present state, challenges, and achievements of the regional climatic observation network and database. In: *Climate change and adaptive land management in southern Africa – assessments, changes, challenges, and solutions* (ed. by Revermann, R., Krewenka, K.M., Schmiedel, U., Olwoch, J.M., Helmschrot, J. & Jürgens, N.), 34–43, *Biodiversity & Ecology*, 6, Klaus Hess Publishers, Göttingen & Windhoek.

Mucina, L. & Rutherford, M. C. (2010). The vegetation of South Africa, Lesotho and Swaziland. *Strelitzia* 19. South African National Biodiversity Institute, Pretoria.

Mulder, P. (1995). Grondwatervoorsiening vir Klein Karoo Landelike Waterskema. Directorate of Geohydrology. Department of Water Affairs and Forestry - Technical Report Gh3854. Pretoria.

Münch, Z., & Conrad, J. (2007). Remote sensing and GIS based determination of groundwater dependent ecosystems in the Western Cape, South Africa. *Hydrogeology Journal*, *15*(1), 19-28.

Netili, K.F. (2007). *A preliminary understanding of deep groundwater flow in the Table Mountain group (TMG) aquifer system* (Doctoral dissertation, University of the Western Cape).

Nordstrom, D., McCleskey, R., Hunt, A. G., & Naus, C. A. (2005). *Questa baseline and pre-mining ground-water quality investigation. 14. Interpretation of ground-water geochemistry in catchments other than the Straight Creek Catchment, Red River Valley, Taos County, New Mexico, 2002-2003*. U. S. Geological Survey.

O'Leary, M. H. (1988). Carbon isotopes in photosynthesis. *BioScience*, 38, 328 – 336

Olivier, J., & Jonker, C. Z. (2013). Optimal utilisation of thermal springs in South Africa. *WRC report no. TT577. Pretoria: Water Research Commission*, 13.

Papp, L., Palcsu, L., Major, Z., Rinyu, L. & Tóth, I. (2012). A mass spectrometric line for tritium analysis of water and noble gas measurements from different water amounts in the range of microlitres and millilitres. *Isotopes in environmental and health studies*, *48*(4), 494-511.

Parsons, R. (2002). Recharge of Table Mountain Group aquifer systems. *A Synthesis of the Hydrogeology of the TMG. WRC Report No TT*, *158*(01).

Phillips, F. M., & Castro, M. C. (2003). Groundwater dating and residence-time measurements. *Treatise on geochemistry*, *5*, 605.

Pietersen, K. & Parsons, R. (2007). A synthesis of the hydrogeology of the Table Mountain Group – formation of a research strategy. Water Research Commission Report No TT 158/01, Pretoria.

Pinto, I., Jack, C. and Hewitson, B., 2018. Process-based model evaluation and projections over southern Africa from coordinated regional climate downscaling experiment and coupled model intercomparison project phase 5 models. *International Journal of Climatology*, *38*(11), 4251-4261.

Plummer, L. N., & Glynn, P. D. (2013). Radiocarbon Dating in groundwater systems. Chapter 4. *Isotope methods for dating old groundwater: Vienna. International Atomic Energy Agency*.

Potter, R. W., & Clynne, M. A. (1978). The solubility of the noble gases He, Ne, Ar, Kr, and Xe in water up to the critical point. *Journal of Solution Chemistry*, *7*(11), 837-844.

Qiu, X., Priestley, K., & McKenzie, D. (1996). Average lithospheric structure of southern Africa. *Geophysical Journal International*, *127*(3), 563-581.

Radloff, F. G. T. (2008). *The ecology of large herbivores native to the coastal lowlands of the Fynbos Biome in the Western Cape, South Africa* (Doctoral dissertation, Stellenbosch: Stellenbosch University).

Reid, M., Bordy, E.M. and Taylor, W. (2015). Taphonomy and sedimentology of an echinoderm obrution bed in the Lower Devonian Voorstehoek formation (Bokkeveld Group, Cape Supergroup) of South Africa. *Journal of African Earth Sciences*, *110*, 135-149.

Robey, K., Tredoux, G., & Chevallier, L. (2014). *Preventing production borehole clogging by in-situ iron removal in South African aquifer systems* (No. 2070/1, 14). WRC Report.

Rodell, M., Velicogna, I., & Famiglietti, J. S. (2009). Satellite-based estimates of groundwater depletion in India. *Nature*, *460*(7258), 999.

Rogers, J. (1982). Lithostratigraphy of Cenozoic sediments between Cape Town and Eland's Bay. *Palaeoecology of Africa*, *15*, 121-137.

Rosewarne, P. N. (1984). *Hydrogeology and Hydrogeochemistry of the Aquifer of the Hex River Valley*. (Unpublished M.Sc. Thesis. Rhodes University).

Rosewarne, P. N. (2002). Hydrogeological Characteristics of the Table Mountain Group Aquifer. In Pietersen and Parson (Ed). A Synthesis of the Hydrogeology of Table Mountain Group-formation of a Research Strategy.

Rosewarne, P., & Weaver, J. M. C. (2002). Identification of Targets for drilling in Table Mountain Group Aquifers. *A synthesis of the hydrogeology of the Table Mountain Group–formation of a research strategy". WRC Report No. TT158/01. Water Research Commission, Pretoria, South Africa*.

Rust, I. C. (1967). On the sedimentation of the Table Mountain Group in the western Cape Province (Doctoral dissertation, Stellenbosch: Stellenbosch University).

Saayman, I. C., & Adams, S. (2002). The use of garden boreholes in Cape Town, South Africa: lessons learnt from Perth, Western Australia. *Physics and Chemistry of the Earth, Parts A/B/C*, *27*(11-22), 961-967.

Scanlon, B. R., Healy, R. W., & Cook, P. G. (2002). Choosing appropriate techniques for quantifying groundwater recharge. *Hydrogeology journal*, *10*(1), 18-39.

Scheepers, R. (1995). Geology, geochemistry and petrogenesis of Late Precambrian S-, I- and A-type granitoids in the Saldania belt, Western Cape Province, South Africa. *Journal of African Earth Sciences*, *21*(1), 35-58.

Scheepers, R. & Schoch, A.E. (2006). The Cape Granite Suite, p421-432 In: M.R. Johnson, C.R. Anhaeusser and R.J. Thomas (Editors), *The Geology of South Africa*, Council for Geoscience, Pretoria.

Schell, W.R., Sauzay, G., and Payne, B.R. (1970). Tritium injection and concentration distribution in the atmosphere: *Journal of Geophysical Research*, 75 (12), 2251– 2266.

Schlosser, P., Stute, M., Dörr, H., Sonntag, C., & Münnich, K. O. (1988). Tritium/3He dating of shallow groundwater. *Earth and Planetary Science Letters*, *89*(3-4), 353-362.

Schlosser, P., Stute, M., Sonntag, C., & Münnich, K. O. (1989). Tritiogenic 3He in shallow groundwater. *Earth and Planetary Science Letters*, *94*(3-4), 245-256.

Schoch, A. E. (1972). *The Darling granite batholith* (Doctoral dissertation, Stellenbosch: Stellenbosch University).

Schoch, A. E., & Burger, A. J. (1976). U-Pb zircon age of the Saldanha quartz porphyry, western Cape Province. *South African Journal of Geology*, *79*(2), 239-241.

Schulze, R. E., Lynch, S. D., & Maharaj, M. (2007). Annual precipitation. *South African Atlas of Climatology and Agrohydrology: Water Research Commission, Pretoria, RSA, WRC Report 1489/1/06, Section 6.2*.

Shanahan, P. (2009). Groundwater in the urban environment. In *The Water Environment of Cities*. Springer, Boston, MA. 29-48.

Shand, N. (2004). TMG Aquifer Feasibility Study and Pilot Project: Draft. Scoping Report. Report Number 400396/3715

Sinclair-Smith, K., & Winter, K. (2019). Water demand management in Cape Town: managing water security in a changing climate. *Mainstreaming Climate Change in Urban Development: Lessons from Cape Town*.

Smith, S. J., Sharpley, A. N. & Menzel, R. G. (1984). The pH of rainfall in the southern plains. In *Proceedings of the Oklahoma Academy of Science*. 64, 40-42.

Solomon, D. K., & Sudicky, E. A. (1991). Tritium and helium 3 isotope ratios for direct estimation of spatial variations in groundwater recharge. *Water Resources Research*, *27*(9), 2309-2319.

Solomon, D.K. and Cook, P.G. (2000). 3 H and 3 He. In Environmental tracers in subsurface hydrology. Springer, Boston, MA. 397-424.

Stock, W. D., Bond, W. J. & Le Roux, D. (1993). *Isotopic evidence from soil carbon to reconstruct vegetation history of the south-western Cape Province*. South African Journal of Science 89: 153- 154.

Stuiver, M. (1965). Carbon-14 content of 18th-and 19th-century wood: variations correlated with sunspot activity. Science, 149(3683), 533-534.

Stuiver, M., & Polach, H. A. (1977). Discussion reporting of 14 C data. *Radiocarbon*, *19*(3), 355-363.

Suess, H.E. (1967). Bristlecone pine calibration of the radiocarbon time scale from 4100 BC to 1500 BC. In Radioactive dating and methods of low-level counting. Proceedings of a symposium.

Tadros, C. V., Hughes, C. E., Crawford, J., Hollins, S. E., & Chisari, R. (2014). Tritium in Australian precipitation: A 50 year record. *Journal of hydrology*, *513*, 262-273.

Takaoka, N., & Mizutani, Y. (1987). Tritiogenic 3He in groundwater in Takaoka. *Earth and Planetary Science Letters*, *85*(1-3), 74-78.

Tamers, M. A., & Scharpenseel, H. W. (1970). Sequential sampling of radiocarbon in groundwater. In *Isotope hydrology 1970. Proceedings of a symposium*.

Tankard, A. J., Jackson, M. P. A., Eriksson, K. A., Hobday, D. K., Hunter, D. R., & Minter, W. E. L. (1982). 3.5 Billion years of Crustal Evolution in Southern Africa. DOI: 10.1007/978-1-4613-8147-1

Taylor, C. B., & Roether, W. (1982). A uniform scale for reporting low-level tritium measurements in water. *The International Journal of Applied Radiation and Isotopes*, *33*(5), 377-382.

Thamm, A.G. & Johnson, M.R. (2006). The Cape Supergroup. In: Johnson MR, Anhaeusser CR, Thomas RJ (Eds), The Geology of South Africa. Geological Society of South Africa and Council of Geoscience, Pretoria, 443–460.

Theron, J. N., & Johnson, M. R. (1991). Bokkeveld Group (including the Ceres, Bidouw and Trafika Subgroups). *Catalogue of South African Lithostratigraphic Units*, (*3)* 3-5.

Theron, J. N., Gresse P. G., Siegfried H. P. & Rogers, J. (1992). The geology of the Cape Town area. Explanation on Sheet 3318, Geological Survey, South Africa. 140.

Todd, D.K. (1959). Groundwater Hydrology. John Wiley & Sons. Inc., New York.

Tolstikhin, I. N., & Kamensky, I. L. (1969). On the possibility of groundwater dating by the tritium–helium 3 method. 1027-1029.

Torgersen, T., Purtschert, R., Phillips, F.M., Plummer, L.N., Sanford, W.E. & Suckow, A. (2013). Defining groundwater age. Chapter 3. *Isotope methods for dating old groundwater. International Atomic Energy Agency, Vienna, Austria*, 21-32.

Tredoux, G., Ross, W. R., & Gerber, A. (1980). The potential of the Cape Flats Aquifer for the storage and abstraction of reclaimed effluents (South Africa). *Deutschen Geologischen Gesellschraft Zeitschrift*, *131*(1), 23-43.

Turner, K. B. (2018). *Characterization of Groundwater Types and Residence Times within the Verlorenvlei Sub-Catchment, west coast, South Africa*. (Honours Dissertation. Stellenbosch University).

Ubelaker, D. H., Thomas, C. & Olson, J. E. (2015) 'The impact of age at death on the lag time of radiocarbon values in human bone', *Forensic Science International*. Elsevier Ireland Ltd, 251, 56–60.

Varni, M., & Carrera, J. (1998). Simulation of groundwater age distributions. *Water Resources Research*, *34*(12), 3271-3281.

Van der Plicht, J. (2002). Calibration of the ^{14}C time scale: towards the complete dating range. *Netherlands Journal of Geosciences*, *81*(1), 85-96.

Van Niekerk, A., & Joubert, S. J. (2011). Input variable selection for interpolating high-resolution climate surfaces for the Western Cape. *Water SA*, *37*(3).

Van Wageningen, A. & Du Plessis, J.A. (2007) Are rainfall intensities changing, could climate change be blamed and what could be the impact for hydrologists? Water SA 33 (4) 571-574.

Visser, H. N., & Schoch, A. E. (1973). *The geology and mineral resources of the Saldanha Bay area*. Government Printer, South Africa. ISBN: 0621010545 9780621010541

Visser, A., Fourré, E., Barbecot, F., Aquilina, L., Labasque, T., Vergnaud, V., & Esser, B. K. (2014). Intercomparison of tritium and noble gases analyses, 3H/3He ages and derived parameters excess air and recharge temperature. *Applied geochemistry*, *50*, 130-141.

Vogel, J. C. (1967). Investigation of groundwater flow with radiocarbon. In *Isotopes in hydrology. Proceedings of a symposium*.

Vogel, J. C. (1970) 'Carbon-14 dating of groundwater', in Isotopes in Hydrology 1970. Vienna: International Atomic Energy Agency, 847–863.

Vogel, J. C. (1978). Isotopic assessment of the dietary habits of ungulates. *South African Journal of Science*, *74*(8), 298.

Vorster, C. (2013). Laser ablation ICP-MS age determination of detrital zircon populations in the Phanerozoic Cape and Lower Karoo Supergroups (South Africa) and correlatives in Argentina. Unpublished PhD. Thesis, University of Johannesburg, South Africa, 648.

Wada, Y., Wisser, D. & Bierkens, M.F. (2014). Global modeling of withdrawal, allocation and consumptive use of surface water and groundwater resources. *Earth System Dynamics Discussions*, *5*(1), 15-40.

Walton, W. C. (1990). *Principles of groundwater engineering* (Vol. 4). CRC press.

Watson, A., Miller, J., Fleischer, M., & de Clercq, W. (2018). Estimation of groundwater recharge via percolation outputs from a rainfall/runoff model for the Verlorenvlei estuarine system, west coast, South Africa. *Journal of hydrology*, *558*, 238-254.

Weaver, J.M.C., Talma, A.S. & Cavé, L.C. (1999). Geochemistry and isotopes for resource evaluation in the fractured rock aquifers of the Table Mountain Group. Water Research Commission.

Welte, J. (2011). *Atom Trap Trace Analysis of Ar-39* (Doctoral dissertation).

Western Cape Government. (2017). City of Cape Town: Socio-Economic Profile.

Wilson, E.M. (1983). *Engineering Hydrology (3rd ed)*. MacMillan Education. Ltd., London, UK.

Winter, K., & Mgese, S. (2011). Stormwater drainage: a convenient conduit for the discharge of urban effluent into the Berg River, South Africa. In *12th International Conference on Urban Drainage, PortoAlegre, Brazil.*
Available: *http://web.sbe.hw.ac.uk/staffprofiles/bdgsa/temp/12th%20ICUD/PDF/PAP005118. pdf*.

Wolski, P., Jack, C., Conradie, S., Hall, A., Hewitson, B., & New, M. (April 2018). Attributing 2015-2017 drought in Western Cape, South Africa. In *EGU General Assembly Conference Abstracts* (20) 13705.

Woodford, A. C. (2000). Interpolation and Applicability of Pumping-tests in Table Mountain Group Aquifers. In: K. Pietersen and R. Parsons (eds.), A synthesis of the hydrogeology of the Table Mountain Group - formation of a research strategy. Water Research Commission (WRC) Report, TT 158/01.

Wright, A., & Conrad, J. (1995). *The Cape Flats aquifer current status*. Groundwater Programme, Watertek, CSIR.

Wu, C. (2008). *Groundwater occurrence of Table Mountain area in Cape Town, South Africa* (Doctoral dissertation, University of the Western Cape).

Wu, Y., & Xu, Y. (2005). Snow impact on groundwater recharge in Table Mountain Group aquifer systems with a case study of the Kommissiekraal River catchment South Africa. *Water SA*, *31*(3), 275-282.

Xu, Y., Lin, L. and Jia, H. (2009). Groundwater flow conceptualisation and storage determination of the Table Mountain Group (TMG) Aquifers. WRC Report No. 1419/1/09, Water Research Commission, Pretoria, South Africa.

Zermeño, P., Kurdyla, D. K., Buchholz, B. A., Heller, S. J., Kashgarian, M., & Frantz, B. R. (2004). Prevention and removal of elevated radiocarbon contamination in the LLNL/CAMS natural radiocarbon sample preparation laboratory. *Nuclear Instruments and Methods in Physics Research Section B: Beam Interactions with Materials and Atoms*, *223*, 293-297.

APPENDIX I

Table 14 – Summary of the cation and anion concentrations in groundwater per sample arranged by aquifer.

		Anions (mg/L)					Cations (mg/L)			
Sample Name	**Formation**	**Chloride**	**Fluoride**	**Nitrate**	**Sulphate**	**Bicarbonate**	**Calcium**	**Magnesium**	**Sodium**	**Potassium**
ZH18-SU001	Alluvial	35.78	0.07	0.03	4.64	37.70	18.91	9.99	38.98	2.48
ZH18-SU002	Alluvial	78.56	0.25	2.62	18.13	47.46	18.90	9.98	38.94	2.48
ZH18-SU003	Alluvial	54.52	0.35	0.01	15.76	61.37	10.27	7.48	38.09	4.36
ZH18-SW001	Alluvial	71.68	0.04	5.73	3.28	17.57	1.47	5.22	41.22	2.41
ZH18-SW002	Alluvial	84.04	0.17	9.83	20.43	42.70	5.11	10.08	49.34	3.05
ZH19-CPT001	Alluvial	105.73	0.02	24.79	36.86	5.61	31.25	15.64	56.76	3.55
ZH19-CPT004	Alluvial	123.04	0.01	11.49	30.59	10.49	17.60	11.25	62.74	3.66
ZH19-KR001	Alluvial	185.23	0.04	0.17	111.13	34.77	60.34	13.29	119.89	10.83
ZH19-STB001	Alluvial	62.54	0.87	0.01	2.45	10.37	5.22	4.74	39.92	3.25
ZH19-STB002	Alluvial	123.307	0.191	3.562	11.596	37.58	7.923	12.193	69.98	3.306
ZH18-ROB001	Witteberg	129.09	0.32	0.03	104.71	520.09	128.56	66.69	84.08	4.82
ZH18-BD001	Bokkeveld	151.35	0.30	0.01	280.98	161.89	105.37	83.48	84.08	4.93
ZH18-C001	Bokkeveld	52.75	0.14	0.05	231.36	79.67	60.22	19.59	53.99	9.23
ZH18-MON001	Bokkeveld	16.50	0.07	0.34	2.55	50.87	11.65	2.70	9.06	4.14
ZH19-CAL001	Bokkeveld	25.66	0.27		2.57	53.07	6.04	1.88	16.91	6.42
ZH19-CAL002	Bokkeveld	186.01	0.11	0.00	46.75	304.15	11.33	14.40	131.95	0.36
ZH19-VD005	Bokkeveld	210.45	0.47	0.06	41.23	345.14	26.00	25.35	154.54	0.77
ZH18-BD002	TMG	27.71	0.01	0.47	1.41	4.88	0.62	1.88	14.46	0.39
ZH18-C002	TMG	6.47	0.01	0.79	1.11	5.98	0.37	0.48	3.77	0.54
ZH18-DB002	TMG	12.58	0.02	0.64	1.07	4.27	0.31	0.92	7.06	0.17
ZH18-DB003	TMG	12.83	0.02	0.62	1.06	3.90	0.33	0.89	7.16	0.08
ZH18-DB004	TMG	12.64	0.02	0.69	1.03	4.39	0.30	0.92	7.17	0.09
ZH18-DD001	TMG	8.47	0.02	0.71	0.63	6.59	0.91	0.62	5.05	2.62
ZH18-DD002	TMG	6.43	0.01	0.56	1.47	13.18	0.34	0.28	3.80	6.25
ZH18-FH001	TMG	20.55	0.01	0.01	1.33	30.38	0.25	1.30	11.13	0.20
ZH18-GRB001	TMG	18.64	0.01	0.24	5.54	3.90	7.02	3.00	25.12	4.12
ZH18-KB001	TMG	27.74	0.07	0.74	4.10	19.89	2.70	2.19	17.96	2.73
ZH18-PE001	TMG									
ZH18-VD001	TMG	17.76	0.01	12.38	1.63	4.51	0.85	2.06	11.68	1.72
ZH18-VD002	TMG	25.83	0.01	0.68	1.63	5.37	0.37	1.64	13.74	0.98
ZH18-VD003	TMG	16.68	0.03	4.93	0.97	7.32	1.73	1.88	8.63	0.98
ZH19-BK002	TMG	11.55	0.02	0.01	1.39	4.51	0.78	0.82	6.45	0.32
ZH19-CD001	TMG	88.99	0.05	8.84	2.05	0.00	2.08	7.85	44.77	2.20
ZH19-CD002	TMG	80.38	0.04	25.33	7.00	2.20	2.12	8.07	51.10	0.44
ZH19-CD003	TMG	79.42	0.04	26.19	7.79	2.20	2.01	7.75	50.23	0.36

Table 14 Continued.

		Anions (mg/L)					*Cations (mg/L)*			
Sample Name	**Formation**	**Chloride**	**Fluoride**	**Nitrate**	**Sulphate**	**Bicarbonate**	**Calcium**	**Magnesium**	**Sodium**	**Potassium**
ZH19-CD004	TMG	15.42	0.06	0.78	0.97	14.40	2.48	1.92	9.02	2.33
ZH19-CPT002	TMG	30.35	0.02	2.14	3.57	5.61	2.47	2.81	16.99	1.02
ZH19-CPT003	TMG	124.88	0.21	0.35	32.30	9.52	9.59	9.46	71.50	2.79
ZH19-CPT005	TMG	131.88	0.04	0.20	12.15	2.56	1.86	9.12	73.70	1.22
ZH19-CPT006	TMG	159.00	0.03	0.90	19.13	0.00	7.02	11.96	83.82	1.59
ZH19-FH004	TMG	21.59	0.01	12.20	1.05	2.68	1.31	2.26	15.01	0.42
ZH19-FH009	TMG	7.85	0.00	0.26	0.47	1.22	0.11	0.49	4.61	0.06
ZH19-KM001	TMG	46.79	0.01	1.01	6.35	2.20	1.31	3.18	27.53	0.80
ZH19-KM002	TMG	70.52	0.01	0.22	16.09	2.44	2.99	5.52	42.29	1.41
ZH19-KM003	TMG	56.07	0.00	31.29	26.84	7.81	6.19	3.00	46.30	6.22
ZH19-NY001	TMG	34.69	0.10	0.01	15.05	51.48	11.25	10.42	18.52	2.86
ZH19-PV002	TMG	11.07	0.01	0.17	0.99	3.29	2.04	0.87	6.95	0.16
ZH19-RV001	TMG	18.58	0.01	2.88	14.27	9.03	6.12	3.75	8.85	2.20
ZH19-SW003	TMG	90.17	0.70		12.03	10.25	7.06	11.13	72.26	2.43
ZH19-TM001	TMG	25.91	0.01	0.48	3.83	0.00	36.24	2.15	14.96	0.58
ZH19-VD004	TMG	42.94	0.01	1.20	2.20	6.47	1.82	2.86	24.38	0.62
ZH19-VD006	TMG	22.08	0.01	0.73	1.55	2.44	0.13	1.25	13.34	0.76
ZH18-FH003	Granite	26.55	0.09	2.71	0.97	34.04	1.86	1.42	10.24	0.63
ZH18-KB002	Granite	30.83	0.32	0.52	3.91	56.61	14.56	3.05	21.18	2.31
ZH18-R001	Granite	44.25	0.11	26.79	4.01	3.17	1.96	3.33	27.89	0.67
ZH19-BK001	Granite	6.64	0.05	0.18	0.98	13.54	2.31	1.37	4.94	0.43
ZH19-FH005	Granite	29.98	0.33	3.26	5.40	15.25	30.21	4.47	24.85	2.08
ZH19-FH006	Granite	7.49	0.02	0.08	0.98	4.64	1.82	0.83	4.89	0.67
ZH19-FH007	Granite	36.52	0.18	11.32	1.63	8.30	7.70	4.86	27.61	1.48
ZH19-FH008	Granite	26.63	0.13	25.39	1.43	8.54	8.70	5.70	24.04	2.93
ZH19-MAL001	Granite	252.86	0.08	7.99	19.75	58.44	17.11	26.41	116.46	6.59
ZH19-W001	Granite	145.15	0.10	15.13	14.55	11.47	7.82	15.92	78.27	6.18
ZH18-DB001	Malmesbury	21.06	0.12	0.18	1.91	22.45	3.62	2.43	13.35	0.28
ZH18-DK001	Malmesbury	142.24	0.51	1.11	17.00	259.98	47.61	25.51	103.16	1.04
ZH18-FH002	Malmesbury	19.45	0.14	0.08	1.94	93.33	18.24	1.74	23.74	3.40
ZH18-PV001	Malmesbury	95.66	0.08	1.28	6.85	110.04	3.72	8.46	54.51	2.22
ZH18-SV001	Malmesbury	30.36	0.12	0.01	6.32	28.79	8.30	2.28	17.93	0.24
ZH19-MB001	Malmesbury	172.01	0.08	0.03	29.41	242.05	10.66	12.31	109.06	3.49
ZH19-PAA001	Malmesbury	119.96	0.71	0.02	1.04	113.09	6.63	3.77	95.79	0.43
ZH19-RBK001	Malmesbury	129.85	0.09	5.69	22.02	103.46	55.04	14.14	54.59	0.79

APPENDIX II

Table 15 – Inorganic and organic content of dissolved carbon in groundwater samples.

Sample Name	Aquifer	TC	TOC	IC	$\delta^{13}C$
		mg/L	*mg/L*	*mg/L*	*‰*
ZH18-SW001	Alluvial	1.79	0.02	1.76	**-15.7**
ZH18-SW002	Alluvial	4.29	0.90	3.39	**-10.1**
ZH19-CPT001	Alluvial	2.73	1.55	1.19	**-9.5**
ZH19-CPT004	Alluvial	3.43	1.23	2.20	**-10.7**
ZH19-KR001	Alluvial	25.32	7.56	17.76	**-10.7**
ZH19-STB001	Alluvial	5.44	0.41	5.03	**-15.9**
ZH19-STB002	Alluvial				**-12.1**
ZH18-ROB001	Witteberg	99.47	3.67	96.80	**-5.2**
ZH18-BD001	Bokkeveld	29.36	1.44	29.92	**-6.7**
ZH18-C001	Bokkeveld	10.33	3.62	6.72	**-1.5**
ZH18-MON001	Bokkeveld	10.31	0.38	9.93	**-13.6**
ZH19-CAL001	Bokkeveld	5.59	0.01	5.59	**-18.3**
ZH19-CAL002	Bokkeveld	10.89	0.28	10.61	**-12.7**
ZH19-VD005	Bokkeveld	28.24	1.43	26.81	**-10.0**
ZH18-BD002	TMG	0.67	-0.04	0.71	**-12.9**
ZH18-C002	TMG	2.04	1.33	0.71	**-15.2**
ZH18-DB002	TMG	0.69	0.00	0.69	**-13.8**
ZH18-DB003	TMG	0.83	0.16	0.67	**-13.7**
ZH18-DB004	TMG	1.07	0.41	0.66	**-14.9**
ZH18-DD001	TMG	2.26	0.97	1.29	**-13.8**
ZH18-DD002	TMG	2.30	0.43	1.86	**-12.0**
ZH18-FH001	TMG	1.56	0.70	0.86	**-11.5**
ZH18-GRB001	TMG	10.47	9.77	0.70	**-17.5**
ZH18-KB001	TMG	3.60	0.56	3.04	**-14.7**
ZH18-VD001	TMG	1.40	0.51	0.90	**-13.5**
ZH18-VD002	TMG	0.63	-0.07	0.70	**-12.4**
ZH18-VD003	TMG	1.06	-0.13	1.19	**-12.0**
ZH19-BK002	TMG	0.69	-0.01	0.70	**-20.7**
ZH19-CD001	TMG	1.39	0.72	0.67	**-13.6**
ZH19-CD002	TMG	4.79	1.07	3.72	**-18.5**
ZH19-CD003	TMG	1.34	0.59	0.75	**-18.7**
ZH19-CD004	TMG	2.24	-0.10	2.34	**-17.5**
ZH19-CPT002	TMG	1.51	0.03	1.48	**-15.3**

Table 15 Continued.

Sample Name	Aquifer	TC	TOC	IC	$\delta^{13}C$
		mg/L	*mg/L*	*mg/L*	*‰*
ZH19-CPT003	TMG	4.48	2.69	1.79	**-12.2**
ZH19-CPT005	TMG	0.76	0.11	0.65	**-16.5**
ZH19-CPT006	TMG	1.53	0.88	0.65	**-14.5**
ZH19-FH004	TMG	2.18	1.19	0.98	**-16.0**
ZH19-FH009	TMG	0.51	-0.17	0.67	**-15.2**
ZH19-KM001	TMG	0.99	0.21	0.78	**-16.4**
ZH19-KM002	TMG	2.28	1.20	1.08	**-16.5**
ZH19-KM003	TMG	3.67	0.99	2.68	**-11.9**
ZH19-NY001	TMG	9.97	1.57	8.40	**-18.2**
ZH19-PV002	TMG	0.88	0.16	0.72	**-17.6**
ZH19-RV001	TMG	3.03	0.22	2.81	**-17.0**
ZH19-SW003	TMG	15.43	0.81	14.62	**-15.4**
ZH19-TM001	TMG	13.59	12.92	0.67	**-19.2**
ZH19-VD004	TMG	0.79	-0.22	1.01	**-18.7**
ZH19-VD006	TMG	0.54	-0.15	0.70	**-18.8**
ZH18-FH003	Granite	5.90	0.28	5.62	**-12.4**
ZH18-KB002	Granite	9.41	0.18	10.22	**-13.4**
ZH18-R001	Granite	1.02	0.37	0.65	**-14.6**
ZH19-BK001	Granite	1.91	-0.36	2.26	**-18.3**
ZH19-FH005	Granite	17.21	0.65	16.57	**-17.0**
ZH19-FH006	Granite	3.68	2.28	1.40	**-15.1**
ZH19-FH007	Granite	6.49	0.17	6.31	**-17.4**
ZH19-FH008	Granite	7.44	0.06	7.38	**-17.9**
ZH19-MAL001	Granite	6.15	0.79	5.36	**-14.4**
ZH19-W001	Granite	4.75	1.02	3.73	**-12.1**
ZH18-DB001	Malmesbury	3.75	0.01	3.74	**-12.0**
ZH18-DK001	Malmesbury	49.43	2.67	47.76	**-14.7**
ZH18-FH002	Malmesbury	17.49	0.68	16.81	**-17.2**
ZH18-PV001	Malmesbury	4.20	0.10	4.09	**-14.7**
ZH18-SV001	Malmesbury	5.89	1.30	4.59	**-25.5**
ZH19-MB001	Malmesbury	41.69	1.75	39.94	**-11.1**
ZH19-PAA001	Malmesbury	12.92	1.05	11.88	**-19.9**
ZH19-RBK001	Malmesbury	19.32	0.50	18.82	**-11.4**

APPENDIX III

Dissolution of silica in groundwater to produce silicic acid and subsequently H_3O^+ (Bleam, 2016):

$$SiO_2\,(s) + 2\,H_2O\,(l) \leftrightarrow H_4SiO_4\,(aq)$$

$$H_4SiO_4\,(aq) + H_2O\,(l) \leftrightarrow H_3O^+\,(aq) + H_3SiO_4^-\,(aq)$$

APPENDIX IV

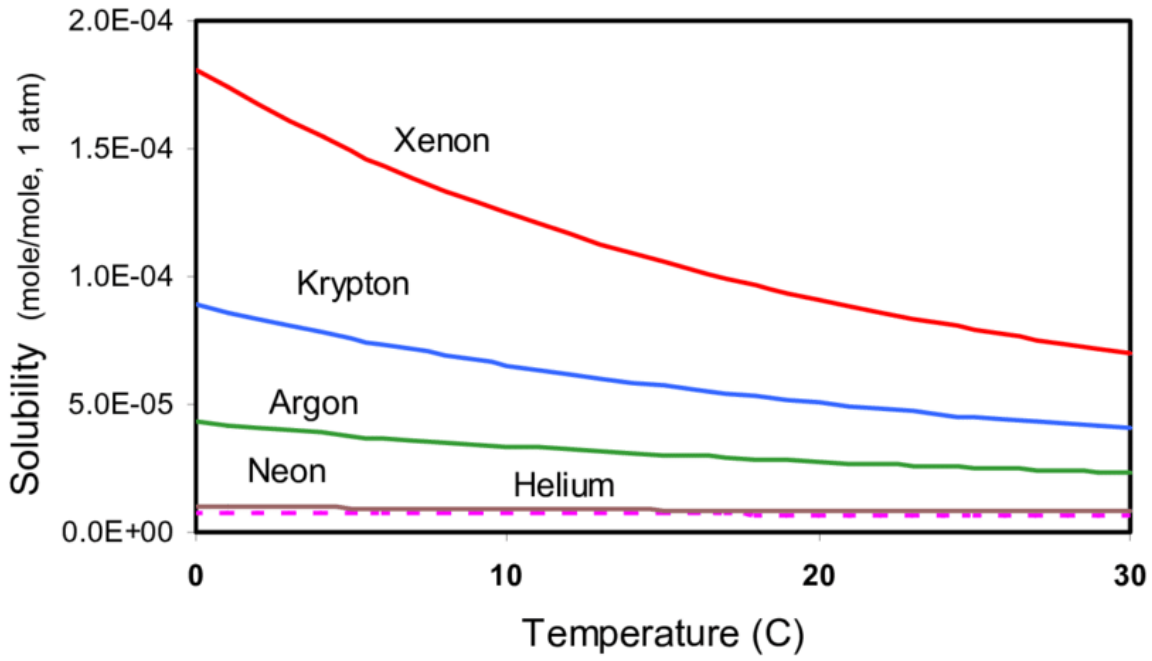

Figure 50 – Noble gas solubility as a function of temperature (Moran et al., 2004).